



Universitat Autònoma de Barcelona

PhD Thesis

PHOTONIC DEVICES BASED ON HYBRID ORGANIC-INORGANIC XEROGEL POLYMERS

Ester Carregal Romero

Directors

Dr. Andreu Llobera Adán

Dr. César Fernández Sánchez

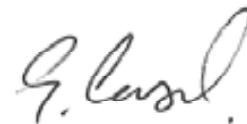
Estudis de Doctorat en Ciència de Materials

Departament de Química, Facultat de Ciències

2012

Memòria presentada per aspirar al grau de Doctor per

ESTER CARREGAL ROMERO



Vist i plau

Directors

DR. CÉSAR FERNÁNDEZ SÁNCHEZ

DR. ANDREU LLOBERA ADÁN



Tutor

DR. JULIÁN ALONSO CHAMARRO



Bellaterra, 29 de setembre 2012

SUMMARY

The aim of the work included in this PhD Thesis was the development of new strategies for the simple and low-cost fabrication of polymeric photonic components and their integration in photonic lab-on-chip (PhLoC) devices. For that, tailor-made silicon based hybrid organic-inorganic polymeric materials were developed by the sol-gel technology and patterned using simple and cost-effective microfabrication techniques. Different monomers were carefully chosen and included in several sol-gel polymer formulations. These molecules influenced not only the physicochemical properties of the resulting materials such as their flexibility, porosity or hydrophobicity but also tuned their optical properties such as transparency or refractive index. Also, the developed materials were easily doped with colored and fluorescent dyes in order to modulate their spectral properties. Patterning of the resulting hybrid polymer was carried out using simple and cost-effective non-photolithographic approaches included in the so-called soft lithography techniques. Working with these materials and applying simple patterning processes enabled the fabrication of photonic components, which could be integrated in lab-on-chip systems in order to develop compact analytical tools with the potential to be applied in decentralized studies for environmental monitoring or point-of-care diagnostics.

The manuscript is divided into seven chapters. In Chapter I, a general introduction to the main concepts for better understanding the sol-gel technology, the synthesis of organic-inorganic hybrid materials and their application in optics and photonics. A description of the different techniques applied for the patterning of these materials is also given to end up with the introduction of the lab-on-chip (LoC) concept and the PhLoC approach, which includes different components, related to micro-optics and integrated optics. This chapter is followed by the definition of the objectives and five more chapters that extensively explain the experimental work carried out and thoroughly describe the experimental results achieved. As a final chapter, Chapter VIII highlights the main conclusions drawn from this work.

Chapter III is focused on the design and synthesis of two different fluorophore doped hybrid materials and their patterning by micromolding in capillaries soft lithographic technique. An exhaustive physicochemical characterization of materials, and their spectral response was carried out. The one-step processing of these materials, showing different geometries and aspect ratios was successfully carried out, and in turn their excellent optical performance demonstrated. Additionally, this chapter demonstrates that this type of materials is robust and highly suitable for the fabrication of disposable solid-state light emitting devices, and by extension, other photonic components for integrated optics. In the following experimental chapters, the fabrication and optical assessment of specific polymeric photonic components, which were then integrated in two different PhLoCs is presented. Chapter IV shows the

fabrication, characterization and implementation in a glass-PDMS PhLoC, of different colored dye-doped hybrid polymeric micro-filters whose absorbance behavior covers different wavelength ranges of the visible spectrum. Chapter V shows the design, fabrication and performance of a fluorophore-doped polymeric blue-light emitter fabricated following the experimental procedures described in previous chapters. Chapter VI describes the work carried out on the integration of this emitter in another glass/ PDMS PhLoC device, which was further applied as a biosensor approach for the detection of a model target analyte. Chapter VII explores other hybrid materials based on quantum dot doped xerogel matrices, as well as an alternative micro-/nanofabrication technique, the thermal nanoimprint lithography, for the patterning of the hybrid polymers presented in the previous chapters.

RESUMEN

El objetivo del trabajo incluido en esta Tesis Doctoral es el desarrollo de nuevas estrategias para la fabricación sencilla y de bajo costo de componentes fotónicos poliméricos y su integración en dispositivos fotónicos lab-on-chip (PhLoC). Para ello, se desarrollaron materiales poliméricos híbridos orgánicos-inorgánicos con un esqueleto de óxido de silicio, mediante la tecnología sol-gel, y se fabricaron microestructuras de estos materiales usando técnicas de microfabricación sencillas y de bajo coste. Diferentes monómeros fueron elegidos seleccionados e incluidos en varias formulaciones sol-gel. Estas moléculas modulan no sólo las propiedades físico-químicas de los materiales resultantes, tales como su flexibilidad, porosidad o hidrofobicidad, sino también sus propiedades ópticas tales como la transparencia o el índice de refracción. Asimismo, los materiales desarrollados fueron dopados con moléculas colorantes y fluorescentes con el fin de controlar sus propiedades espectrales. El microestructurado del material híbrido resultante se llevó a cabo usando técnicas no fotolitográficas incluidas en las llamadas técnicas de litografía blanda (del inglés soft lithography). Trabajando con estos materiales y aplicando sencillos procesos de fabricación, se desarrollaron componentes fotónicos poliméricos, los cuales pueden integrarse en dispositivos lab-on-chip con el fin de desarrollar herramientas de análisis compactas con el potencial de ser aplicadas en estudios descentralizados para el control medioambiental o diagnóstico precoz de enfermedades.

El manuscrito se divide en siete capítulos. En el capítulo I, se realiza una introducción general a los conceptos principales necesarios para una mejor comprensión de la tecnología sol-gel, la síntesis de materiales híbridos orgánicos-inorgánicos y su aplicación en óptica y la fotónica. Igualmente, se describen las diferentes técnicas aplicadas para el microestructurado de estos materiales y, para finalizar, se introducen los dispositivos lab-on-chip (LOC) y el concepto de PhLoC, que incluye componentes diferentes, relacionados con la microóptica y la óptica integrada. Este capítulo va seguido de la definición de los objetivos más otros cinco capítulos que muestran el trabajo experimental llevado a cabo y describen los resultados experimentales obtenidos. Como último capítulo, en el capítulo VIII se destacan las principales conclusiones extraídas de este trabajo.

El capítulo III se centra en el diseño y la síntesis de dos materiales híbridos dopados con fluoróforos y su microestructurado mediante una técnica de litografía blanda denominada micromodelado en capilares. Se realizó una caracterización fisicoquímica exhaustiva de los materiales resultantes y de su respuesta espectral. Se realizó el procesado en un solo paso de microestructuras de estos materiales, con diferentes geometrías y relaciones de aspecto y, a su vez se demostraron sus excelentes

propiedades ópticas. Además, este capítulo muestra que estos materiales son robustos y muy adecuados para la fabricación de emisores de luz de estado sólido desechables, y de otros componentes fotónicos para óptica integrada. En los capítulos experimentales siguientes, se recoge la evaluación óptica de componentes poliméricos fotónicos, y su posterior integración en dos dispositivos PhLoC diferentes. El capítulo IV muestra la fabricación, caracterización e implementación en un PhLoC basado en estructuras PDMS vidrio, de diferentes microfiltros fabricados con los materiales híbridos dopados con colorantes que absorben en diferentes zonas del espectro visible. El capítulo IV presenta el diseño, la fabricación y el funcionamiento de un emisor de luz azul fabricado empleado un material híbrido sol-gel dopado con un fluoróforo y siguiendo los procedimientos experimentales descritos en los capítulos anteriores. El capítulo VI describe el trabajo realizado en la integración de este emisor en otro dispositivo PhLoC fabricado en PDMS y vidrio, el cual se aplicó posteriormente en la fabricación de un biosensor para la detección de un analito modelo. El capítulo VII explora otros materiales híbridos basados en matrices de xerogel dopados con puntos cuánticos, así como una técnica de micro-/nanofabricación alternativa, la litografía por nanoimpresión térmica, para el estructuramiento de los polímeros híbridos presentados en los capítulos anteriores.

RESUM

L'objectiu del treball inclòs en aquesta Tesi Doctoral és el desenvolupament de noves estratègies per a la fabricació senzilla i de baix cost de components fotònics polimèrics i la seva integració en dispositius lab-on-chip fotònics (PhLoC). Per a això, es van desenvolupar materials polimèrics híbrids orgànics-inorgànics amb un esquelet d'òxid de silici, mitjançant la tecnologia sol-gel, i es van fabricar microestructures d'aquests materials usant tècniques de microfabricació senzilles i de baix cost. Diferents monòmers van ser triats seleccionats i inclosos en diverses formulacions sol-gel. Aquestes molècules modulen no només les propietats físic-químiques dels materials resultants, tals com la seva flexibilitat, porositat o hidrofobicitat, sinó també les seves propietats òptiques tals com la transparència o l'índex de refracció. Així mateix, els materials desenvolupats van ser dopats amb molècules colorants i fluorescents amb la finalitat de controlar les seves propietats espectrals. El microestructurat del material híbrid resultant es va dur a terme usant tècniques no fotolitogràfiques incloses en les trucades tècniques de litografia tova (de l'anglès soft lithography). Treballant amb aquests materials i aplicant senzills processos de fabricació, es van desenvolupar components fotònics polimèrics, els quals poden integrar-se en dispositius lab-on-chip amb la finalitat de desenvolupar eines d'anàlisis compactes amb el potencial de ser aplicades en estudis descentralitzats per al control mediambiental o diagnòstic precoç de malalties.

El manuscrit es divideix en set capítols. En el capítol I, es realitza una introducció general als conceptes principals necessaris per a una millor comprensió de la tecnologia sol-gel, la síntesi de materials híbrids orgànics-inorgànics i la seva aplicació en òptica i la fotònica. Igualment, es descriuen les diferents tècniques aplicades pel microestructurat d'aquests materials i, per finalitzar, s'introdueixen els dispositius lab-on-chip (LoC) i el concepte de PhLoC, que inclou components diferents, relacionats amb la micro-òptica i l'òptica integrada. Aquest capítol va seguit de cinc capítols més que mostren el treball experimental dut a terme i descriuen els resultats experimentals obtinguts. Com a últim capítol, en el capítol VII es destaquen les principals conclusions extretes d'aquest treball.

El capítol III se centra en el disseny i la síntesi de dos materials híbrids dopats amb fluoròfors i el seu microestructurat mitjançant una tècnica de litografia tova denominada micromodelat en capil·lars. Es va realitzar una caracterització fisicoquímica exhaustiva dels materials resultants i de la seva resposta espectral. Es va realitzar el processament en un sol pas de microestructures d'aquests materials, amb diferents geometries i relacions d'aspecte i, al seu torn es van demostrar les seves excel·lents propietats òptiques. A més, aquest capítol mostra que aquests materials són robusts i molt adequats per a la fabricació d'emissors de llum d'estat sòlid d'un sol

ús, i d'altres components fotònics per a òptica integrada. En els capítols experimentals següents, es recull l'avaluació òptica de components polimèrics fotònics, i la seva posterior integració en dos dispositius PhLoC diferents. El capítol III mostra la fabricació, caracterització i implementació en un PhLoC basat en estructures *PDMS vidre, de diferents microfiltres fabricats amb els materials híbrids dopats amb colorants que absorbeixen en diferents zones de l'espectre visible. El capítol V presenta el disseny, la fabricació i el funcionament d'un emissor de llum blava fabricat emprant un material híbrid sol-gel dopat amb un fluoròfor i seguint els procediments experimentals descrits en els capítols anteriors. El capítol VI descriu el treball realitzat en la integració d'aquest emissor en un altre dispositiu PhLoC fabricat en PDMS i vidre, el qual es va aplicar posteriorment en la fabricació d'un biosensor per a la detecció d'un analit model. El capítol VII explora altres materials híbrids basats en matrius de xerogel dopats amb punts quàntics, així com una tècnica de *micro-/nanofabricació alternativa, la litografia per nanoimpresió tèrmica, per a l'estructurat dels polímers híbrids presentats en els capítols anteriors.

CONTENTS

CHAPTER I

GENERAL CONCEPTS

1.1 The sol-gel technology	1
1.1.1. The sol-gel chemical process	1
1.1.2. Type of materials	4
1.1.3. Applications	6
1.2 Hybrid organic-inorganic materials	7
1.2.1 Historical overview	7
1.2.2 Silicon based hybrid organic-inorganic materials	8
1.2.3 Materials for optics and photonics	11
1.3 Micro/ nanofabrication techniques	12
1.3.1 Photolithography	13
1.3.2 Soft lithography	15
1.3.3 Micromolding in Capillaries (MIMIC)	19
1.4 Lab-on-chip	20
1.4.1 General concepts	20
1.4.2 Photonic lab-on-chip	21
1.4.3 Micro-optics & integrated optics	22
References	25

CHAPTER II

OBJECTIVES	31
-------------------	-----------

CHAPTER III

ONE-STEP SOFT-LITHOGRAPHIC PATTERNING OF HYBRID XEROGEL MATERIALS APPLIED FOR THE FABRICATION OF PHOTONIC COMPONENTS

3.1 Summary	32
3.2 Introduction	34
3.3 Experimental section	
3.3.1 Materials	34
3.3.2 Fluorophore doped synthesis	35

3.3.3	Fabrication of masters and stamps	36
3.3.4	Fabrication of microstructures by MIMIC	36
3.3.5	Material characterization	37
3.4	Results and discussion	
3.4.1	Synthesis and structural characterization of the xerogel material	38
3.4.2	Characterization of the xerogel microstructures	43
3.4.3	Optical characterization	44
3.5	Conclusions	47
	References	48

CHAPTER IV

DEVELOPMENT AND INTEGRATION OF XEROGEL ABSORBANCE MICROFILTERS

4.1	Summary	49
4.2	Introduction	49
4.3	Design of the test microstructure	51
4.4	Fabrication	52
4.5	Material and structural characterization	53
4.6	Spectral analysis	55
4.7	Integration of the filters into a PhLoC	60
4.8	Conclusions	64
	References	64
	Appendix	66

CHAPTER V

SOLID STATE LIGHT EMITTER BASED ON FLUOROPHORE-DOPED XEROGEL MATERIAL

5.1	Summary	71
5.2	Introduction	71
5.3	Fabrication	72
5.4	Spectral response of Atto-doped xerogel waveguides	74
5.5	Design of the solid state light emitter	74
5.6	Material and structural characterization	76
5.7	Mapping emission intensity	79
5.8	Conclusions	81

References	81
<u>CHAPTER VI</u>	
INTEGRATION OF A DOPED XEROGEL SOLID STATE LIGHT EMITTER INTO A LAB-ON-CHIP DEVICE	
6.1 Summary	83
6.2 Introduction	83
6.3 Experimental section	
6.3.1 Materials	85
6.3.2 Design	85
6.3.3 Fabrication	86
6.3.4 Enzyme immobilization	87
6.3.5 Absorbance measurements protocol	87
6.4 Analytical performance of the PhLoC	87
6.5 Conclusions	88
References	92
<u>CHAPTER VII</u>	
OTHER DOPED SILICON-BASED POLYMERIC MATERIALS AND FABRICATION TECHNIQUES EXPLORED	
7.1 Quantum-dots doped hybrid organic-inorganic polymer	
7.1.1 Introduction	94
7.1.2 Experimental details	95
7.1.3 Characterization	96
7.1.4 Conclusions	99
References	100
7.2 Xerogel waveguides fabricated by Nano Imprint Lithography (NIL)	
7.2.1 Introduction	101
7.2.2 Experimental details	102
7.2.3 Characterization	104
7.2.4 Conclusions	107
References	107
CONCLUDING REMARKS	108

Chapter I

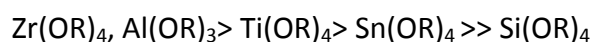
GENERAL CONCEPTS

1.1 THE SOL-GEL TECHNOLOGY

1.1.1 The sol-gel chemical process

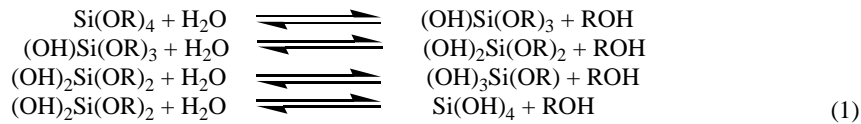
The so-called sol-gel methodology is a low-temperature chemical synthesis technique for glass-like materials and ceramics.^[1] A *sol* is a dispersion of colloidal (submicrometer) particles in a liquid; a gel is a rigid interconnected network of polymeric chains with submicrometer size pores.^[2] In general, the precursors are mixed with water and co-solvents (usually methanol or ethanol); hydrolysis and polycondensation reactions start to take place and a progressive densification of the mixture is achieved until a *sol* is formed. After drying and curing a polymeric rigid material is achieved.

The precursors are in the form $M(OH)_n$ and/or $M(OR)_n$, where $M = Si, Ti, Sn, Zr, Al, B...$ etc., which represent the network-forming element, $R = (C_xH_{2x+1})$ is an alkyl group and n is the number of groups that can be attached to the metal. Hydrolysis and polycondensation can be accelerated by employing an appropriate catalyst, either an acid or a basis. For non-silicate metal alkoxides, generally no catalyst is needed because they are very reactive. The sequence of reactivity is expressed as follows:^[3-4]

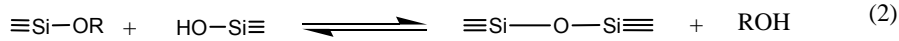


As depicted above, the reaction is divided in two steps: hydrolysis of metal alkoxides to produce hydroxyl groups, followed by polycondensation of hydroxyl and residual alkoxy groups to form a polymeric three-dimensional network. Working with silicon alkoxides as the example: silanol groups ($\equiv Si-OH$) are generated by hydrolysis reactions in hydroalcoholic solutions usually containing an acid or basic catalyst. Polycondensation reactions involving these groups give rise to siloxane bonds ($\equiv Si-O-Si \equiv$); alcohol and water are generated as sub-products and remain in the network pores. Once the first hydrolysis reaction takes place, the subsequent hydrolysis and polycondensation reactions simultaneously occur. The viscosity of the mixture is progressively increasing and when sufficient interconnected siloxane bonds are formed in a region, they respond cooperatively as colloidal particles. The general scheme is represented in Scheme 1.

Hydrolysis



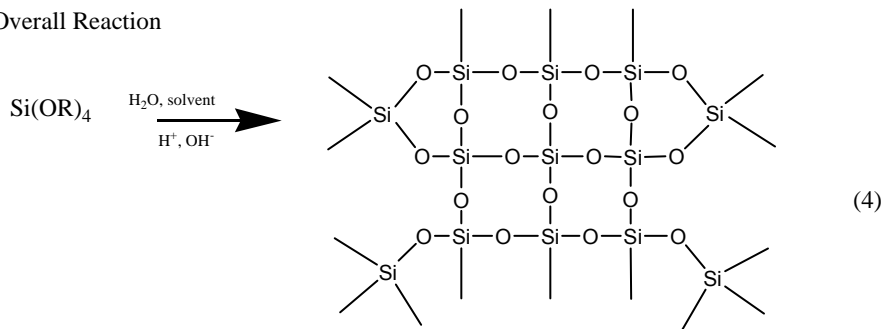
Alcohol Condensation (Alcoxolation)



Water Condensation (Oxolation)



Overall Reaction



Scheme 1. General scheme of hydrolysis and polycondensation reactions for a silicate alcoxide.

Both, hydrolysis and condensation reactions occur by a nucleophilic substitution (S_N) mechanism, which involve three steps: nucleophilic addition (A_N), proton transfer within the transition states, and removal of the protonated species as either alcohol or water. Kinetics of hydrolysis/ polycondensation reactions depends on the nature of the precursors and R ratio ($R = [\text{H}_2\text{O}] / [\text{M}(\text{OR})_4]$) among other variables such as working conditions that include the use of catalysts, solvents and temperature.^[1] The size of the *sol* particles and the crosslinking within the particles (i.e., density) strongly depend upon the pH and the nature of the catalyst. So the structure and morphology of the consequent matrix is consequently influenced. Under basic catalysis conditions, the overall reaction rate is determined by the hydrolysis step. Thus, dense, microporous materials, in the form of colloidal aggregates with low degree of crosslinking, are obtained. Conversely, under an acidic environment, the hydrolysis rate is high relative to condensation reactions, so more linear polymer-like species are formed during the initial mixing step of the sol-gel process. This leads to mesoporous materials conformed by long, linear, highly cross-linked polymeric chains.^[5] Besides the pH of the mixture, the length and nature of the alkoxy group (i.e., nature of the precursor) can also influence the hydrolysis and condensation reactions via steric effects or leaving-group stability. For example, tetramethoxysilane (TMOS) is more reactive than tetraethoxysilane (TEOS). The nature of the solvent and [precursor]/ [solvent] ratio are also important. The ratio influences the pore size and the volume of the solvent

molecules influences gelation kinetics; the more voluminous the molecule is the more gelation time is required.

The transformation from a *sol* to a gel constitutes the gelation process. Gelation occurs when the colloidal units that constitute the sol link each other to form a three-dimensional network. At this point, viscosity increases sharply, and solvents and sub-products generated during previous stages are entrapped into the matrix pores. A *sol* becomes a gel when it can support a stress elastically.^[6] This is typically defined as the gelation point or gelation time, t_{gel} . Depending on sol-gel process conditions (pH, alkoxide precursor, $[H_2O]/[M(OR)_4]$ ratio, etc) gelation can take place in seconds, minutes, days or even months. In Fig. 1 the *sol* to gel transition is shown.

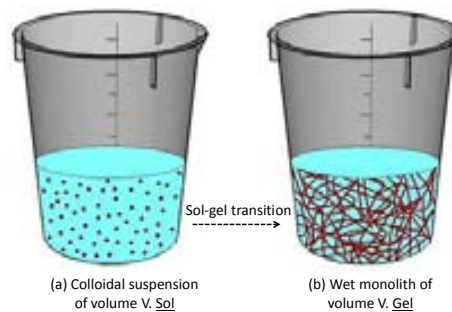
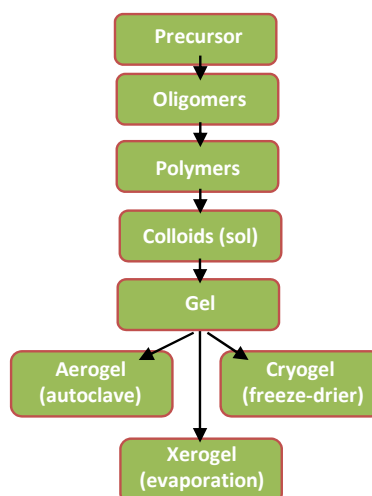


Figure 1. Gelation process (a)Sol (b) Gel

During the next sol-gel process step, namely drying, the liquid is removed from the pores. The drying mechanism strongly influences the structure of the resulting material.^[7] This last step may either conserve or dramatically alter the properties obtained in the previous aggregation states. If the wet gel is dried by evaporation a xerogel type material is produced, aerogels are produced by supercritical drying and cryogels by freeze-drying. The mechanisms governing the different drying processes and the characteristics of the corresponding materials are discussed in the next section. For completeness, a scheme of the whole sol-gel process is shown in Scheme 2.



Scheme 2. General overview of the sol-gel chemical process

1.1.2 Type of Materials

In this subsection, a brief introduction of the most significant properties of the materials obtained by sol-gel technique using different drying mechanism.

1.1.2.1 Xerogel type materials

Xerogel type materials result from drying a wet gel at atmospheric pressure, either at ambient conditions or under controlled temperature. There are three stages for drying:^[6]

- # **Stage I: Deformation.** The lost of volume is equal to the volume of the evaporated liquid. Large capillary forces induced by liquid-vapour surfaces deform the network and the shrinkage can be considerable. The largest change in volume, weight, density and structure occurs during this stage which ends when the shrinkage ceases.

- # **Stage II: Critical point.** As the network resistance increases, the radius of the meniscus is reduced. At the critical point the contact angle approaches zero and the radius of the meniscus equals the radius of the pore. Then, the network cannot compress any further and the pores begin to empty. The liquid flows to the surface by capillary stress gradient where evaporation occurs.

- # **Stage III: Equilibrium.** The remaining liquid can escape only by evaporation from within the pores. There are no further dimensional changes but just a slow progressive loss of weight until equilibrium is reached.

The microstructure of xerogels is very sensitive to the synthesis route applied for the preparation of the gel. Thus, the pore size and the final density of the material are mainly governed by the initial gel structure (polymer nodule/pore sizes, network stiffness), which is a consequence of the synthesis conditions (pH, *R* ratio...). Xerogels are normally dense materials with low specific areas containing micropores, but different approaches to increase pore sizes and also avoid cracking due to shrinkage have been developed. To obtain high surface area and porous materials, "drying control chemical additives" (DCCA) such as surfactants, formamide, glycerol, oxalic acid and tetramethyl ammonium hydroxide are employed. The role of these additives is to reduce the capillary pressure and thus increase the pore radius and material uniformity.^[8] DCCAs also minimize the differential drying shrinkage (Figure 2)

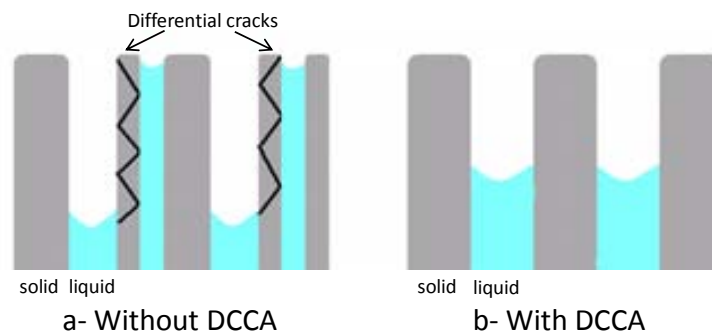


Figure 2. Effect of formamide on the pore size distribution of gels. After Hench^[9]

Xerogel type materials general features are:

- # Commonly, they are dense materials. Nevertheless, pore size and pore volume can be increased by the addition of DCCAs, or by different drying strategies like solvent exchange.
- # They can be prepared in many different forms such as monoliths (adopting the shape of the container), thin films, fibers, powder, particles... depending on the intended final application.
- # They present mechanical resistance to deformation, minimum swelling in aqueous or organic solutions and they are electro-, optical- and chemically stable (inert).
- # Mild synthesis conditions allow the incorporation of chemical species such as organic compounds, enzymes or even particles while preserving their functionality. In this context, xerogel type materials can act as inert solid hosting matrices.
- # They can be molecularly imprinted. Commonly, the molecularly imprinted polymers (MIP) reported in the literature are based on organic polymers. Silica-based xerogels have enabled the application of this technology to the imprinting of hydrophilic molecules and the use of an aqueous media for the synthesis of MIPs.

1.1.2.2 Aerogel and cryogel type materials

To preserve the original pore texture of the wet gel it can be dried either under supercritical conditions or by freeze-drying. In principle, with these techniques no shrinkage occurs.

Before supercritical drying, water is exchanged with a solvent with lower surface tension, for example, acetone or cyclohexane. This technique consists of heating the wet gel in a closed container, so that the pressure and temperature exceed the critical values, T_c and P_c . The solvent in the pores becomes a supercritical fluid with null surface tension. The resulting material is called aerogel.^[10] Another way to avoid liquid-

vapour surfaces is to use freeze-drying. After freezing, the solvent is removed by sublimation under low pressure and a cryogel is obtained.^[11]

Characteristics of aerogels and cryogels are very similar:

- # They are extremely porous materials with high specific surface area and very low bulk density.
- # Monoliths and powders are easily fabricated (but not other forms).
- # They show good thermal, electrical and acoustic insulation properties.
- # They are highly brittle and swell in contact with liquids.

Although these techniques lead to the largest pore texture range in sol-gel materials, they are not easy to apply at an industrial level: they are expensive and needs pre-treatment of gels (solvent exchange for aerogels),^[12] and are difficult to handle due to their brittleness.

1.1.3 Applications

Sol-gel processing methods, first used historically for decorative and constructional materials, were extensively developed during the last three decades for a wide range of applications. Nowadays, they are reaching their full potential, enabling the preparation of new generations of advanced materials not easily accessible by other methods and are extending even further their range of applications. Still, they are widely applied to their initial purpose; many examples of coatings fabricated with sol-gel materials can be found, either from laboratory research or commercially available, with much different functionality: decorative, anticorrosion, antireflection, antisoiling, adhesion-promotion, conductive, and biocompatible coatings. The sol-gel approach offers the possibility of coating large and/or curved substrates using simple deposition techniques (spin coating, dip coating, and spray coating).

These materials can be tailored to be transparent over a wide wavelength range and to have an adequate refractive index. Moreover, they can be molded into many different shapes, even at the micro/nanoscale, showing smooth facets with no cracks. These features make them very attractive for the fabrication of low-cost micro-optical and photonic components such as waveguides,^[13] diffraction gratings^[14] or microlenses.^[15] Doping these materials with optically passive/active organic molecules (i.e., dyes, fluorophores, etc.) further increases their potential for a great variety of functions including laser action,^[16] photoluminescence,^[17] photochemical hole burning,^[18] photochromism,^[19] and NLO (non-linear optics).^[20]

The possibility of the entrapment of chemical species even from biological origin within a porous network, which means still being accessible to a solution, opens the door for the fabrication of chemical sensors and biosensors. Some examples of sol-gel-based chemical sensors are absorbance pH sensors by entrapped pH sensitive dyes,^[21-22] dissolved oxygen sensors based on fluorescence quenching^[23-24] or metal ion sol-gel

monolithic-like sensors.^[25] Examples of encapsulation of enzymes for the fabrication of biosensors^[26-27] and other bio-applications such as bioreactors^[28-29] can be found in the literature. Additionally to enzymes, many diverse biological entities had been successfully entrapped within sol-gel materials such as algae,^[30] cells,^[31] bacteria,^[32] and antibodies.^[33] The main problem encountered with the encapsulation of such different species was their possible diffusion out of the solid matrix with time, albeit leaching is not a problem for disposable sensors. For continuous monitoring purposes, entrapment efficiency can be improved by covalently attaching the sensing species to the rigid network. For bio-applications, additional issues are related with denaturation of the entrapped biological molecules, although different studies show that it can be avoided by optimizing the sol-gel process using additives, biocompatible alcohols and/or specific precursors.^[34]

Other interesting sol-gel materials have been developed for the fabrication of catalysts,^[35-36] membranes,^[37] electronic,^[38] and electrochromic^[39] materials or ceramics^[40] among others.

1.2 HYBRID ORGANIC-INORGANIC MATERIALS

Organic-inorganic hybrids can be fabricated by sol-gel technology and are materials that combine the merits of inorganic glasses and organic polymers. Both small organic moieties and polymeric/oligomeric species can be either physically entrapped in the inorganic network (class I) and/or chemically bonded to the monomer structure (class II) to produce organic-inorganic hybrid network structures.^[41] Mild processing conditions of the sol-gel method allow producing these materials at temperatures under which the organic components will not be degraded.

1.2.1. Historical overview

These type of materials have received different names, from “ceramers” (by Wilkes *et. al.*^[42]), “Ormosils” to “Ormocers” (by Schmidt *et. al.*^[43]) or simply hybrid organic-inorganic materials. However, albeit all these names referred to synthetic materials, nature has been fabricating them over the last five hundred million years. Some examples of natural organic-inorganic hybrids are crustacean carapaces, mollusk shells and bone and teeth tissues in vertebrates.^[44] There are also several examples of man-made hybrid materials since time immemorial: Egyptian inks, green bodies of china ceramics, Maya blue pigment, prehistoric frescos, etc.^[45] Maya blue is a good example of the interesting and powerful characteristics of hybrid materials. Ancient Maya fresco paintings are characterized by bright blue colors that have been miraculously preserved (see Fig. 3). This pigment is composed by blue indigo natural dye encapsulated within a mineral known as palygorskite.^[46] It combines the color of the organic dye with the resistance of the inorganic hosting mineral, which had made these frescos to withstand twelve centuries of jungle climate and environment (rainfall

is often more than 250 mm a year; relative humidity between 77 and 88%; temperatures between 24°C and 34°C) with almost no discoloration.



Figure 3. Image of a Maya warrior from Bonampak archeological site, (Mexico). After Gómez-Romero.^[46]

From an industrial point of view, man-made hybrid materials appeared during the 1950s. At Dow Corning Corporation (Midland MI, USA), a series of phenylsilsesquioxane/alkylsilsesquioxane copolymers of low molecular weight and high hydroxyl functionality were produced. They were (and still are) employed as weather-resistance coatings used for example for naval aircraft.^[47] Other examples of early industrial applications of this family of materials can be found in the field of paints and coating technologies.^[48] In those days, they were not known as “hybrids”, since the concept of “hybrid organic-inorganic materials” was coined at the eighties with the expansion of the concept of *chimie douce*^[49] (soft chemistry) pioneered by Jacques Livage one decade before.^[50] Since then, the study of functional hybrid materials and nanocomposites has been a research area of increasing interest yielding innovative advanced materials with applications in many different fields such as catalysis, sensing and biosensing, optics and photonics, photovoltaic and fuel cells technology, and microelectronics.

1.2.2 Silicate-based hybrid organic-inorganic materials

The family of hybrid organic-inorganic polymers based on a silicon oxide (siloxane) backbone is the most widely studied and implemented. As mentioned above, hybrid organic-inorganic materials can be divided into two main classes.

- # **Class I.** Organic molecules, prepolymers or even polymers embedded in an inorganic matrix. Hydrolysis and polycondensation reactions of the silicon alcoxides take place in the presence of organic compounds. Thus,

the rigid inorganic network is formed trapping inside the organic components. Interaction between both phases is only due to weak bonds, that is Van der Waals forces and hydrogen bonds.

- # **Class II.** The inorganic and organic compounds are connected by covalent bonds. Organic groups can be bonded to an inorganic siloxane network as network modifiers or network formers. The precursors of silicate-based hybrid polymers are organo-substituted silanes of general formula $R'_n \text{Si}(\text{OR})_{4-n}$, where R' is an organic moiety. If R' is a non hydrolyzable group bonded to silicon atoms (Si-C), it will have a network modifying effect. For example, the inclusion of $-\text{CH}_3$ groups give rise to a less cross-linked and more hydrophobic network. However, if R' can react with itself (e. g., R' contains a methacryl group) or additional components, it will act as network forming (see Fig. 4); the result will be two networks (organic, inorganic) intimately interconnected. In Table 1 some examples of network formers and modifiers are included. The organic part is the responsible of the physical properties of the hybrid material, i.e. mechanical integrity, hydrophobicity, refractive index, electrochemical behavior, etc.

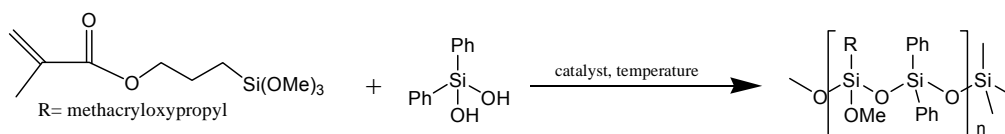


Figure 4. Formation of a class II organic-inorganic hybrid polymer.

Examples of class I are dyes or biomolecules entrapped into porous silicate-based sol-gel matrices.^[51-52] There are many different families of class II hybrids with very dissimilar structure and chemical composition, some of them are shown in Figure 5. The simplest class II hybrids are these formed by organo- modified silane precursors, where a terminal group is bonded to the silicon atom (Fig. 5 (a) and (b)). Another family of hybrids is formed by the arylene-, alkylene- and phenylene- bridged polymers, one example is shown in Fig. 5 (c). The polyhedral oligomeric silsesquioxanes (POSS)^[53] are another family of hybrids; a monomeric precursor is shown in Fig. 5 (d), where R is a non-reactive terminal group and Y is network forming group. And yet another family is the one formed for the so-called “star gels”,^[54] Fig. 5 (e). These are formed from polyfunctional network precursors with a number of flexible arms radiating from an atomic, linear or cyclic core and terminating in trialkoxysilane groups.

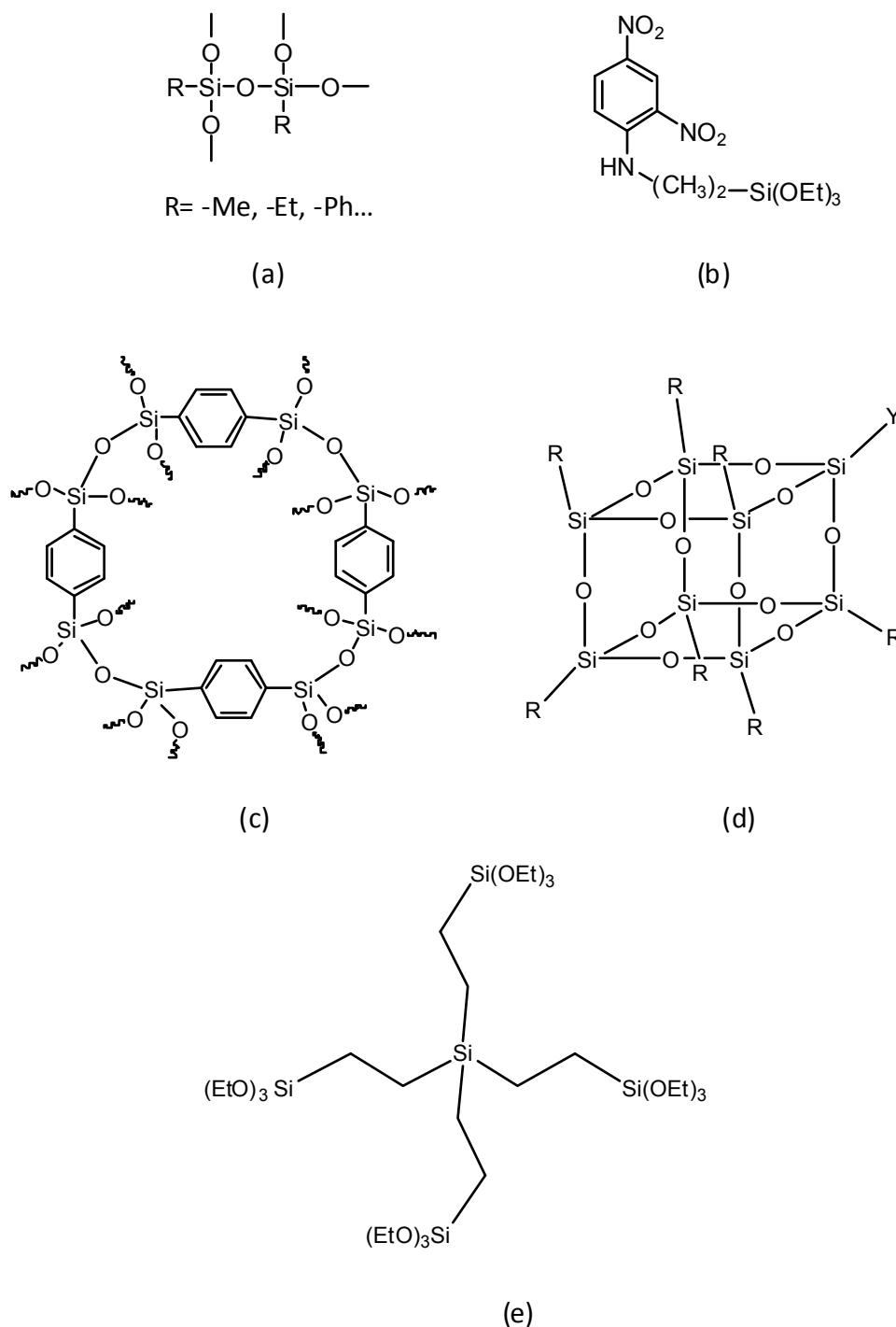


Figure 5. Examples of class II hybrid organic-inorganic materials : (a) R= organic terminal group, (b) triethoxysilylpropyl 2,4-dinitrophenylamine (TDP), (c) phenylene-bridged polymer, (d) polyhedral oligomeric silsesquioxane (POSS) monomeric precursor, where R is a non-reactive end group and Y is a polymerizable group and (e) "star gel".

One of the most attractive features of these materials is the wide spectrum of possibilities concerning composition, synthetic routes and potential applications. Much of their appeal lies in the high versatility of the material processing, which is compatible with microfabrication processes.

Hybrid organic-inorganic materials science allows to obtain many different compounds with very different properties can be obtained by a careful selection of the monomers and synthetic routes. One of the main advantages of these materials is the versatility of the material processing. Depending on the chemical composition the material can be either optically or thermally structured. In the first case, either standard UV-lithography^[55-56] or the more promising two-photon absorption polymerization (TPA) have successfully been applied for the development of two dimensional pattern and more complex structures, respectively. With the later method organic-inorganic hybrid polymers are polymerized with nanosecond laser pulses, this technology allows to directly writing arbitrary structures in three-dimensions into the hybrid polymer with a resolution of down to 100 nm or even below.^[57] Some examples of TPA manufactured microstructures are shown in Fig. 6.

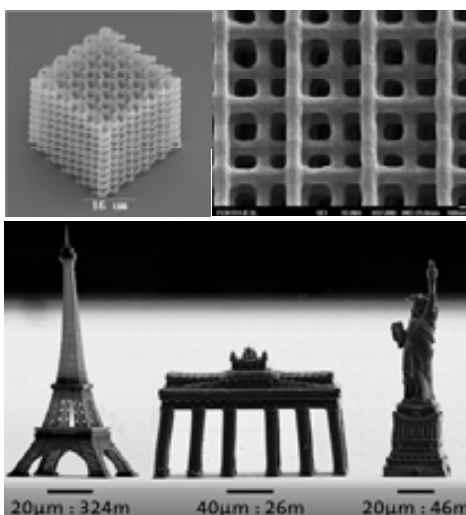


Figure 6. Different organic-inorganic polymeric microstructures made by TPA.

When photopolymerizable functionalities are not present in the material chemical composition, sol-gel microstructures can still be obtained by thermally controlled processes and other lithographic techniques such as soft lithography^[58] or nanoimprint lithography.^[59] Some of these techniques will be explained in detail in subsequent sections of this chapter.

1.2.3 Hybrid materials for optics and photonics

The sol-gel methodology has been explored as a low-cost, low-temperature route to fabricate optical components. Among the different sol-gel materials described above, organic-inorganic hybrids can be tailored to be transparent over a wide wavelength range and to have an adequate refractive index. Moreover, they can be molded into many different shapes, even at the micro- and nanoscale, showing crack-free smooth facets. These features make them very attractive for the fabrication of low-cost micro-optical and photonic components. Doping these materials with

optically passive or active organic molecules, such as dyes and fluorophores, respectively, further increases their potential for a great variety of functions.

The applications of organic-inorganic hybrids in optics cover a wide spectrum ranging from decorative colored coatings to sophisticated nanostructured composites for photonics. Regarding their functionality, these materials can be divided in two major categories: optically passive and optically active hybrid sol-gel matrices depending on whether their interaction with light induces changes in their physical properties or not. Some examples of applications are listed in Table 1.

Table 1. Examples of different applications of organic-inorganic hybrid materials for optics and photonics.

Organic-inorganic hybrid	Type*	Application	Ref.
GPTMS doped with TiO ₂ nanocrystals	P	High refractive index material for antireflective coatings	[60]
TEOS:MMA:MPMS doped with commercial red dye	P	Red colored transparent coating	[61]
TEOS: P123 block copolymer doped with spirooxazine/ spiropyran	A	Photochromic hybrid for fast optical switches	[62]
MTEOS doped with an indolyfulgide	A	Photochromic hybrid for optical data storage	[63]
Silica: P123 block copolymer doped with Rh6G fluorophore	A	Hybrid solid-state laser-dye material	[64]
MTMOS:PhTMOS:TMOS doped with HRP enzyme	A	Full-field photonic biosensor for H ₂ O ₂ detection	[26]
GPTMS	P	Fabrication of microlenses arrays	[65]
TMOS: MPTMS	A	Films for thermo-optical devices	[66]

* P= passive, A= active.

TEOS:tetraethyl orthosilicate, GPTMS:(3-glycidylxypropyl) trimethoxysilane,MMA:methyl methacrylate, MPMS: 3-(trimethoxysilyl) propyl methacrylate, MTEOS:methyltriethoxysilane, Rh6G: rhodamine 6G, MTMOS: methyltrimethoxysilane, PhTMOS: phenyltrimethoxysilane, TMOS: trimethyl orthosilicate, HRP: horseradish peroxidase, MPTMS: (3-mercaptopropyl) trimethoxysilane.

1.3 MICRO/ NANOFABRICATION TECHNIQUES

Nowadays, there is a clear tendency to miniaturization of analytical devices, which allowed the integration of a large number of components in a minute space. Smaller dimensions involve more components per device, lower cost, and higher yield with lower energy consumption and/or portability.

1.3.1 Photolithography

Most of the developments in microelectronics and microfabrication are based on the use of photolithographic steps. Photolithography is based on a projection-printing system in which the image of a pattern is transferred (via reduction and/or projection) onto a thin film of a light-sensitive substance known as photoresist through a high numerical aperture lens system. The basic process consists in several steps, which are illustrated in Fig. 7, and will be explained below.^[67]

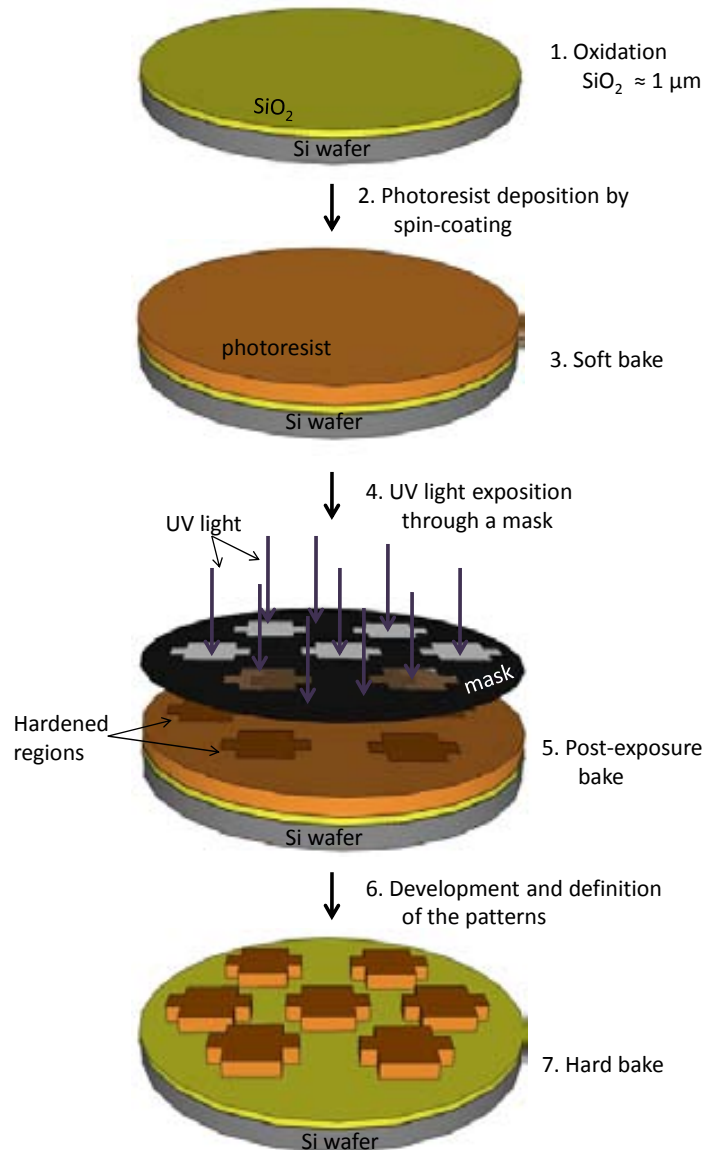


Figure 7. Example of a conventional photolithographic process for negative photoresists. Here, an oxidized Si wafer is applied. Process steps included soft bake, exposure, post-exposure bake, development and hard bake. Steps 1 through 7 are explained in the text.

In a conventional photolithographic process, the silicon wafer is cleaned to eliminate possible organic contamination and then, a common step is to grow or deposit a slab layer of the required material (i.e. oxidation of a silicon wafer a furnace at temperatures between 900 and 1150°C, in steam or in a humidified oxygen stream

atmosphere obtain stoichiometric SiO₂, see Fig. 7.1). Afterward, a thin layer of an organic polymer, a photoresist sensitive to UV radiation, is spun on the oxide surface by spin-coating (Fig. 7.2). A resist can be either positive or negative. A photoresist is considered positive when the photochemical reactions during exposure weaken the polymer by rupture of the main and side polymeric chains, and the exposed resist becomes more soluble in developing solutions. Conversely, as illustrated in Fig. 7, a negative photoresist becomes insoluble in organic or water-based developers upon UV exposure by either the formation of a more crosslinked polymer or by the formation of new insoluble products. After spin-coating, the resist still contains up a high percentage of solvents so the wafer is soft baked (75-100°C, 10 min) to remove solvents and to promote adhesion of the resist layer to the wafer. After that, the resist-coated wafer is transferred to some type of illumination or exposure system (typically a mask aligner) where it is aligned with the features on the mask and is illuminated with UV light (Fig. 7.4). A mask is a nearly optically flat glass or quartz plate with an absorber pattern metal (e.g., a chromium layer). The absorber pattern on the mask is opaque to UV light, whereas glass and quartz are transparent. Often (especially with chemically-amplified resists), the reactions initiated during exposure may not have run to completion. For that, in some cases a post-exposure bake has to be carried out to enhance the reactions or induce new ones (Fig. 7.5). Development step transforms the latent resist image formed during exposure into a relief image. During this process, selective dissolution of resist takes place (Fig. 7.6). Finally, an optional baking step can be done after the development to remove residual solvents and to promote interfacial adhesion of the resist. It is called hard bake because it occurs at higher temperatures and longer times than the soft and post-exposure bakes (2h at 120°C in inert atmosphere).

The resolution R of this technique is limited by optical diffraction according to the Rayleigh equation (Eq. 1), where λ is the wavelength of the exposure light, NA is the numerical aperture of the lenses system and k_1 is a constant that depends on the photoresist.

$$R = k_1 \lambda / NA$$

Equation 1

Although the theoretical limit is about $\lambda/2$, the minimum feature size that can be obtained by photolithography is approximately the wavelength of the light used. From Eq. 1, resolution can be improved by either reducing the irradiation wavelength or increasing the numerical aperture of the lenses. Improvement in resolution has followed the first alternative achieving minimum feature sizes down to 100 nm. So, advanced photolithographic techniques, known as next-generation lithographies (NGL), include extreme UV (EUV) lithography, soft X-ray lithography, electron-beam writing, focused ion beam writing, proximal-probe lithography, and UV-thermal nanoimprint lithography (NIL).^[67]

Despite the effort and success in the continuous shrinking of the feature sizes to the nanoscale, these techniques have severe limitations. They are expensive (especially NGL techniques); they are not suitable for patterning non-planar substrates; they are poorly suited for introducing chemical functionalities. To overcome these drawbacks new non-photolithographic microfabrication techniques have been developed such as the set of techniques known as soft lithography.

1.3.2 Soft lithography

Many different soft lithographic techniques have been developed, the most applied ones being: microcontact printing (μ CP), replica molding (REM), microtransfer molding (μ TM), embossing and micromolding in capillaries (MIMIC).

Soft lithography, pioneered by Whitesides *et al.*,^[68] include well-known parallel non-photolithographic approaches. Generally they consist in a double replication: firstly, a master is fabricated by photolithography or micromachining; secondly, this master is replicated (generally using an elastomeric material) and a mold that is the negative of the pattern on the master, is obtained. The master can be reused many times, which reduces production costs, as will be explained in detail below. A scheme of the main steps of this technique is depicted in Fig. 8.

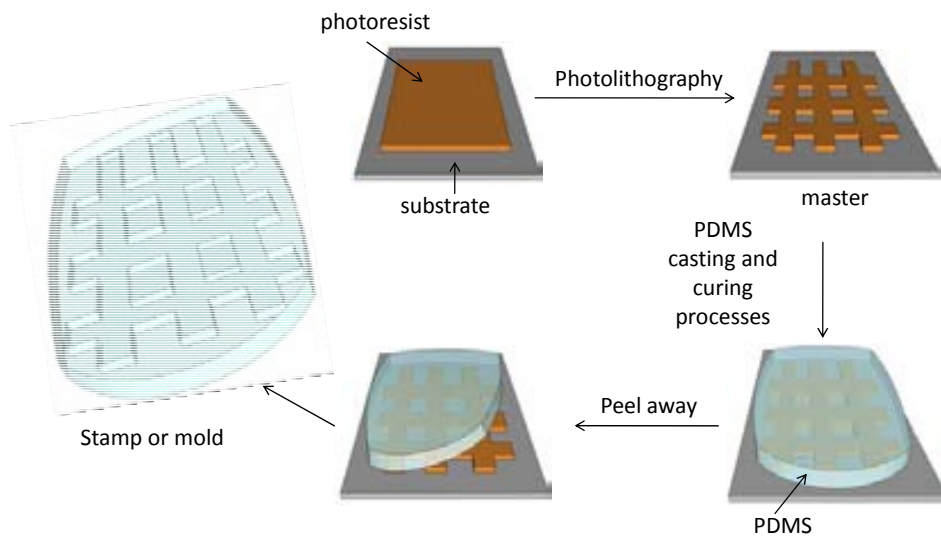


Figure 8. Schematic procedure for the fabrication of a PDMS mold for soft lithography.

One of the competitive advantages of these techniques is related to their compatibility with a wide range of substrates and materials. The term “soft” comes from that each of these techniques makes use of an elastomeric mold or stamp to transfer the pattern fabricated on the master to a substrate. Table 2 shows a comparison between both photolithography and soft lithography techniques.

Table 2. Comparison of photolithography to soft lithography.^[68]

	Photolithography	Soft Lithography
Definition of patterns	Rigid photomask	Elastomeric stamp
Materials that can be directly patterned	Photoresists SAMs [‡]	Photoresists SAMs [‡] Polymers (epoxy, PU, PMMA, ABS, CA, PS, PE, PVC) [*] Polymer precursors (of carbon materials and ceramics) Polymer beads Conducting polymers Colloidal materials Sol-gel materials Organic and organic salts Biological macromolecules

[‡]SAMs: self-assembled monolayers.

^{*}PU: polyurethane, PMMA: poly(methyl methacrylate), ABS: poly (acrylonitrile-butadiene-styrene, CA: cellulose acetate, PS: polystyrene, PE: polyethylene, PVC: poly (vinyl chloride).

By far, the most employed elastomer is poly(dimethylsiloxane) (PDMS). PDMS conforms to the substrate surface over relatively large areas; it is deformable enough to achieve conformal contact on curved substrates, even at the micrometer scale; and it is easily released, even from complex and fragile patterns defined on the master. It is chemically inert, homogeneous, isotropic, optically transparent (UV-NIR), non-hygroscopic, thermally stable, and permeable to gases. Moreover, the PDMS surface can easily be chemically modified in order to achieve appropriate interfacial interactions with different materials. An example of a process to chemically modified PDMS surface is shown in Fig. 9.

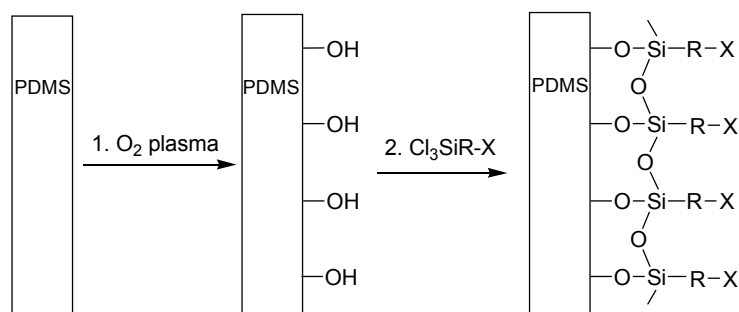


Figure 9. Schematic process to chemically modified PDMS surface: 1. O₂ plasma treatment generates superficial hydroxyl moieties, 2. Reaction with silyl chloride vapor. Interfacial properties can be tailored by selecting different X terminal groups.

However, PDMS as well other elastomers, show some technical problems (mainly associated to the small Young's Modulus) that have to be taken into account when designing complex microstructures. Adhesion, gravity and capillary forces can make a structure to collapse and produce defects while transferring patterns. Figure 10 resumes some of the main issues, that is pairing, sagging and shrinking. Pairing occurs when the aspect ratio of the features are too large, so the PDMS microstructures fall under their own weight and collapse, as in Fig. 10 (a). Similarly, when the aspect ratio is too low, as in Fig. 10 (b), the relief structures are not able to withstand the compressive forces typical of the adhesion of stamp and substrate, causing sagging. Finally, under the more conventional synthesis conditions, PDMS shrinks by a factor of 1% upon curing, as in Fig. 10 (c); thereby not conserving the exact dimensions of the patterns on the master during the replication step. Figure 11 schematically explains the principles of some of these techniques. MIMIC will be explained in detail in the next section.

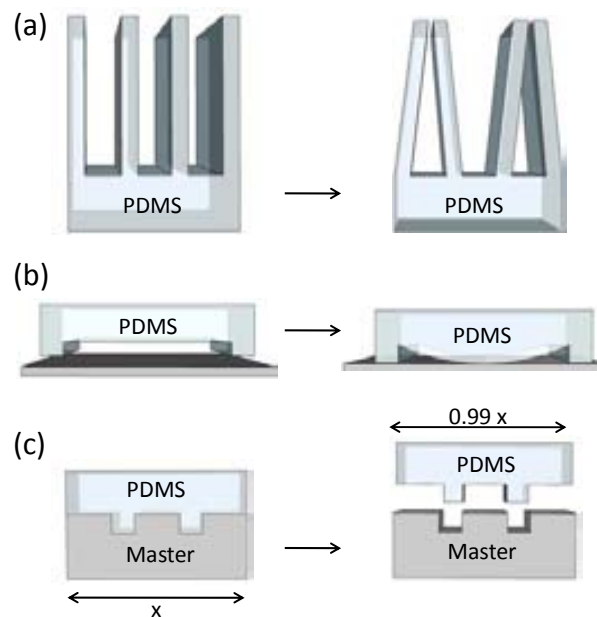


Figure 10. Schematic illustration of possible deformations of microstructures defined on PDMS molds: (a) pairing, (b) sagging and (c) shrinking.

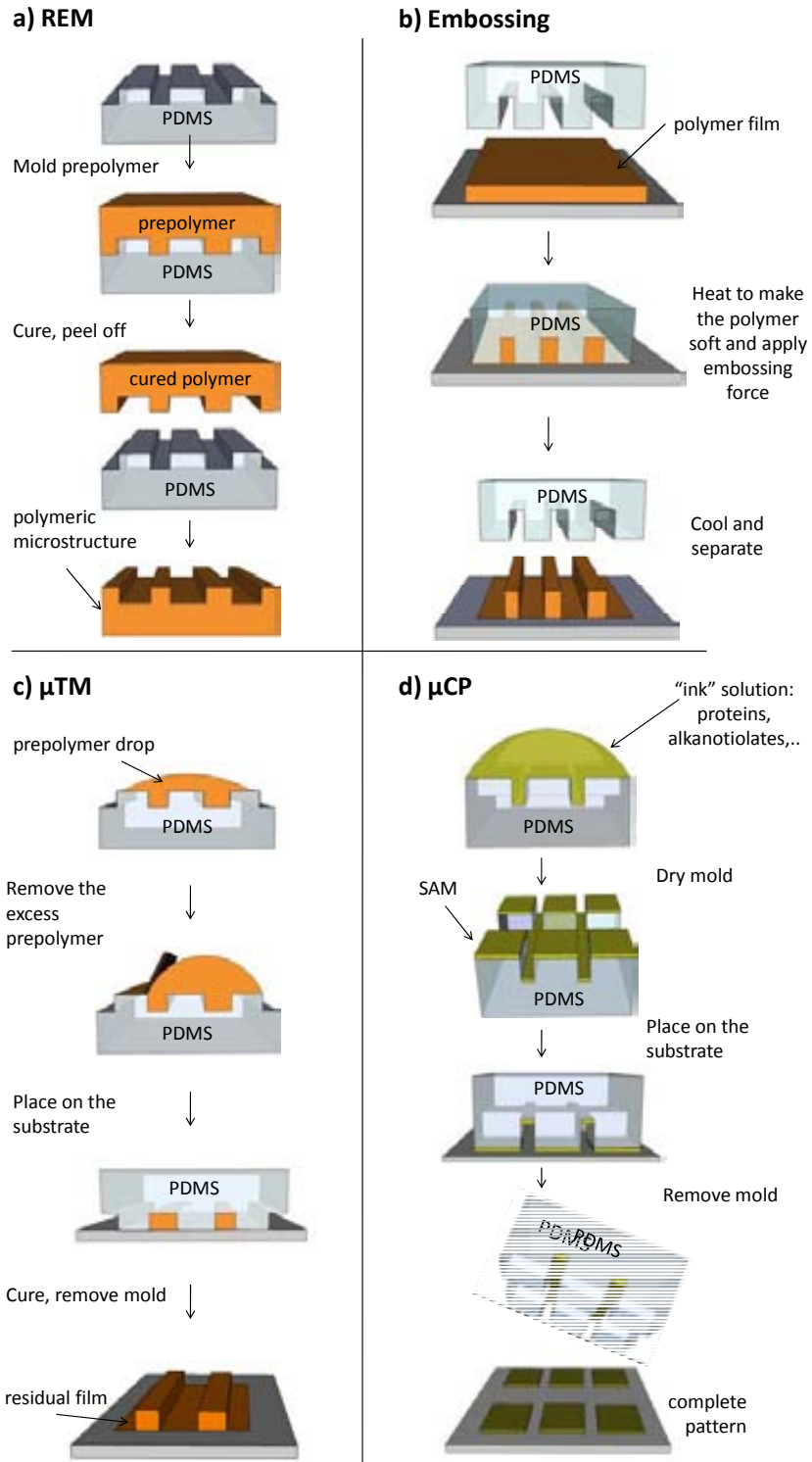


Figure 11. Schematic illustration of the working principles of different soft lithographic techniques: (a) replica molding, (b) embossing, (c) microtransfer molding, and (d) microcontact printing.

Some of the major advantages of soft lithography are the following.^[68]

- # Patterning of nonplanar surfaces.
- # Generation and replication of 3D topologies or structures even in a multilayer configuration are possible.

- # No diffraction limit; features as small as 30 nm have been fabricated.^[69]
- # Compatibility with many different materials (see Table 2).
- # Applicability to the patterning of large surface areas.
- # Cost-effectiveness, simplicity and short processing times.

The main disadvantages are related with the limitations of the elastomeric molds, described above (see Fig. 10), and residual layers generated in some of the techniques, see Fig. 11 (b) and (c).

1.3.3 Micromolding in Capillaries

In MIMIC a network of continuous channels are formed by conformal contact between a solid support and an elastomeric mold whose surface had been patterned with a relief structure having micrometer-scale dimensions. When a low-viscosity prepolymer liquid solution is put at one end of these channels filling occurs naturally by capillary forces. Once the microchannels are fully filled, the polymer can be cured by UV light or temperature, depending on its nature. The mold is then removed and the polymeric microstructures are eventually released.^[70]

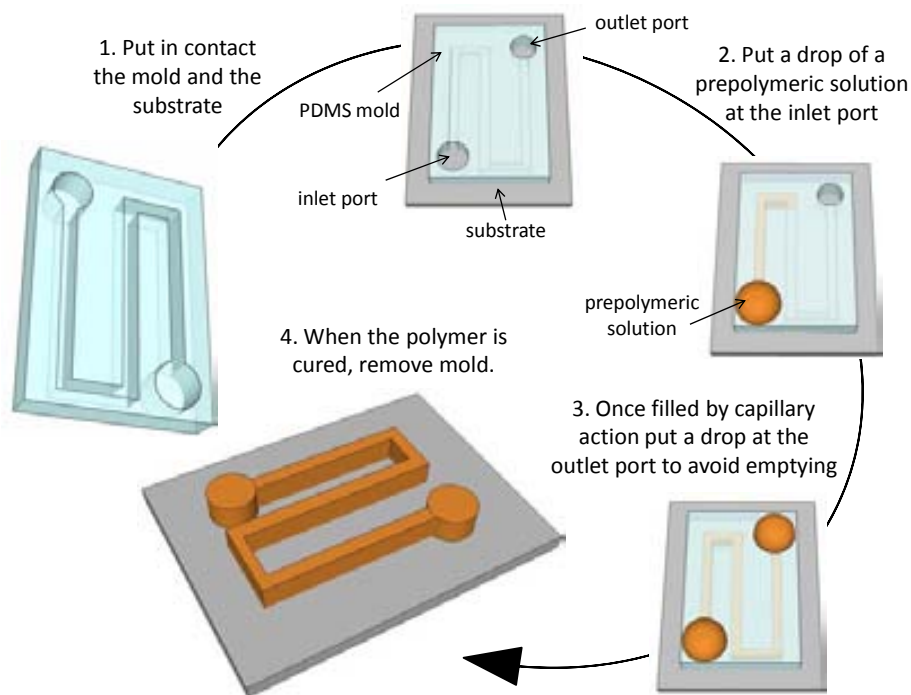


Figure 12. Schematic illustration of a micromolding in capillaries process.

Capillary filling is a well-known process. The filling rate is determined by the surface tension γ and viscosity η of the liquid, the radius of the capillary R , and the length of the filled section of the capillary z .^[71] The rate of filling is proportional to the cross-sectional dimension of the capillary and inversely proportional to the length of

filled capillary and the viscosity of the liquid. So the rate of filling decreases as the capillary fills or when a more viscous liquid is used.

$$\frac{dz}{dt} = \frac{R\gamma_{LV}\cos\theta}{4\eta z} = \frac{R(\gamma_{SV} - \gamma_{SL})}{4\eta z} \quad (2)$$

(γ_{LV} , γ_{SV} and γ_{SL} are liquid-vapor, solid-vapor and solid-liquid free energies)

MIMIC presents some limitations that should be considered. Hydraulically connected network of capillaries are necessary so it is not possible to pattern isolated structures. The rate of filling over large distances (>1cm) and small capillary cross-sections (< 1 μ m) decreases significantly, making this technique of not practical use for some types of structures. However, this technique is remarkable for its simplicity, cost effectiveness, compatibility with a variety of materials in addition to polymers (ceramic precursors, polymer beads, biological macromolecules...), and its fidelity in transferring the patterns from the mold to the surface to be patterned.

1.4 LAB-ON-CHIP

1.4.1 General concepts

Manz and co-workers^[72] introduced in 1990 the concept of micro total analysis systems (μ TAS), also known as lab-on-chips (LoC). It consists in the miniaturization and integration of different laboratory processes in a single chip. A LoC is expected to enable to perform one or more analytical function(s) such as chemical separation, dilution, mixing and analysis. Originally, it was thought that the most significant benefit of these LoCs devices would be the analytical improvements associated with the scaling down of the size: faster response times, improved selectivity, higher sensitivity and portability. Nowadays, research into miniaturization is primarily driven by the need to reduce fabrication costs by minimizing the consumption of expensive reagents and by increasing throughput and automation together with the decrease in sample, reagent and waste volumes, as well as price. Since this concept was first described, many research groups have put a great effort in developing LoC approaches^[73] applied in many different fields such as clinical diagnosis,^[74] genomics,^[75] cellomics^[76] and environmental monitoring.^[77]

The development of LoCs is an interdisciplinary field that has been favored by the enormous development in three main areas: microfluidics, microfabrication techniques and materials science. Microfluidics is the science of designing and manufacturing devices which can channel very small fluid flows, in the microliter/nanoliter range. Over the years it has evolved from the initial microchannels and reservoirs fabricated by standard photolithography on silicon or glass wafers to more complex microfluidic components such as valves,^[78] pumps,^[79] pressure systems,^[80] and mixers^[81] fabricated in a variety of materials.

The LoC concept would never have reached the current maturity without the development of polymeric materials. Polycarbonate (PC),^[82] poly (methyl methacrylate),^[83] and especially PDMS^[84] have been widely applied to the fabrication of low-cost LoC devices. Polymeric LoCs fabricated by simple and inexpensive microfabrication techniques, such as the above mentioned soft lithography, have allowed fulfilling the low-cost assumption without compromising their performance, thus opening the door to the development of disposable devices.

As an example of a LoC system an integrated nanoliter-scale nucleic acid bioprocessor for DNA Sanger sequencing^[85] is shown in Figure 13. The reported LOC integrates all three Sanger sequencing steps, thermal cycling, sample purification and capillary electrophoresis in a single device.

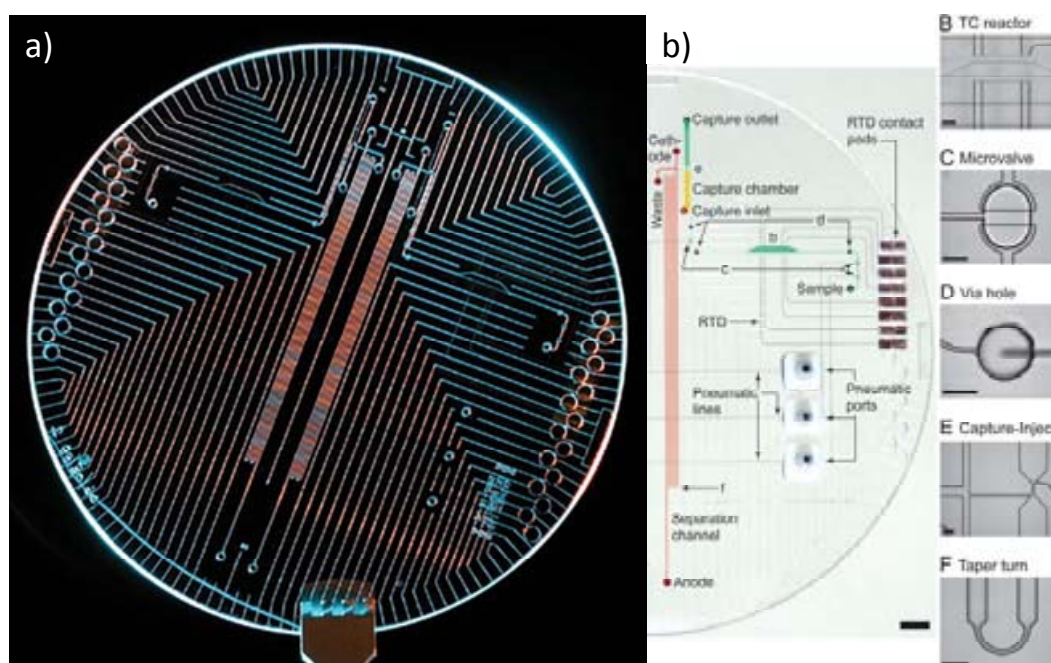


Figure 13. (a) Photograph of the microdevice showing two complete nucleic acid processing systems. (b) Bioprocessor components. Colors indicate the location of sequencing reagent (green), capture gel (yellow), separation gel (red), and pneumatic channels (blue), (Scale bar, 5 mm). B–F correspond to the following component microphotographs: (B) A 250-nl thermal cycling reactor with RTDs (Scale bar, 1 mm), (C) A 5-nl displacement volume microvalve, (D) A 500-µm-diameter via hole, (E) Capture chamber and cross injector, (F) A 65-µm-wide tapered turn, (Scale bars, 300 µm). Images extracted from Ref. [85].

1.4.2 Photonic lab-on-chip

When miniaturizing sensing systems, detection issues have to be taken into account. One of the main premises regarding the selection of the detection method for microfluidic devices is the required sensitivity. Optical detection has so far presented the highest sensitivity in LoC devices, moreover, such configuration presents additional advantages as compared with its counterparts^[86] (electrochemical, mass spectroscopy...) such as immunity to electromagnetic interferences, higher robustness,

multiplexed detection in a single system and simpler handling. Photonic lab-on-chips (PhLoCs) use light as the interrogation mechanism. There are different working principles in which PhLoCs can be based on. Phase and wavelength changes are known to provide with the highest sensitivity. Nevertheless, they are also prone to have more interference from small fluctuations^[87]. Therefore, Intensity-based detection methods are generally the selected option by many researchers, and examples of such are fluorescence,^[88] absorbance,^[89] and scattering.^[90] Fluorescence detection is the most common analytical optical method in chemistry and biochemistry and also the most widely applied so far in miniaturized analytical devices.^[91]

PhLoCs have successfully been applied to the detection and quantification of different chemical and biological species such as glucose,^[92] nucleic acids,^[93] and cells^[94] and capable to achieve limits of detection as low as in the picomolar range.^[93] As an example, Fig. 13 shows a picture of a PhLoC (extensively described in ref [94]) with application in cell cultures analysis. This PDMS/glass-based optofluidic system shows a high degree of monolithic integration, since it comprises self-alignment systems for adequate positioning of optical fibers, lenses, focusing mirrors, and a microfluidic channel.

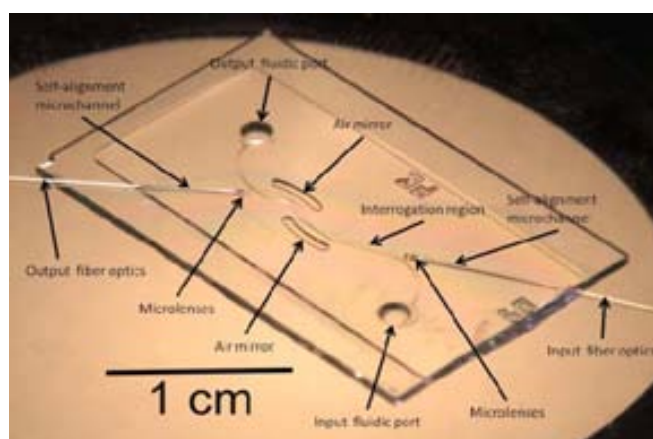


Figure 13. Picture of a glass/PDMS based PhLoC for cell analysis.^[94]

1.4.3 Integrated optics and micro-optics

In addition to sensitivity, another crucial factor that affects the choice of the detection method for a LoC is scalability to smaller dimensions. There is a developing interest to implement optical components into microfluidic devices, possible due to the availability of new nano-/microtechnological tools and materials. Nowadays, two configurations have been used: integrated optics and micro-optics. Such a classification emphasizes the different nature of the photonic components. In integrated optics, light remains confined in a waveguiding structure, being only able to interact with the analyte through evanescent field or by defining specific interaction

regions. Conversely, micro-optical elements such as filters, diffraction gratings, lenses, emitters, and mirrors arise from the miniaturization of optical elements while preserving the functionality of their bulky counterparts.

In the case of PhLoC with integrated optical components, the systems normally comprise one or several waveguides that are in plane with microfluidic channels used to transport excitation light to them, a microfluidic interrogation region and finally, the readout.^[95-96] Micro-optics elements such as air mirrors, microlenses and prisms in PhLoCs primarily take in advantage of the excellent optical and structural properties of PDMS to define them monolithically integrated in or in the vicinity of the interrogation region,^[84, 97] (see also the device shown in Fig. 13).^[94] All these elements are used to direct and focus excitation light onto the microfluidic channel where detection takes place with significant improvement on the analytical performance. For example, it has been demonstrated that the use of PDMS hollow prisms and air mirrors produce an enhancement of the response on absorbance detection and then an improvement in the limit of detection (LOD).^[97] It is also possible to obtain microlenses showing advanced characteristics, as can be correcting the astigmatism of a micro-optical system^[98] while still employing low-cost polymeric materials (e.g. PDMS, epoxy-based photoresists) and simple microfabrication techniques.

When a PhLoC systems works in fluorescence detection regime, optical filtering is often required due to the difficulty to discriminate between the excitation and emission signals. The more accepted filtering configurations suitable to be implemented in PhLoC platforms are based on interferometric and absorbance-based approaches.^[99] Interferometric filters consist in alternating layers of high- and low-refractive-index materials. In spite of these filters showing high absorbance levels they suffer from serious drawbacks: absorption depends on the angle of the incidence light,^[100] expensive and complicated fabrication. These effects hamper its integration into PhLoC. Conversely, the most promising low-cost approaches rely on absorbance filtering. Absorbance filters are generally fabricated with polymeric matrices containing a chromophore^[101] or a bandgap material,^[102] which have high absorption at the excitation wavelength but low absorption at the emission wavelength. Several attempts successfully integrated in PhLoCs have been reported for this configuration.^[103-104]

Moving on this direction most of the effort has been focused in the integration of (organic) light emitting diodes, (O)LEDs.^[105-109] Although their good performance these devices are normally based on a multilayer configuration which implied complicated fabrication and alignment issues. In contrast, when the photonic system and the light source are defined in the same technological process, the components are inherently self-aligned. Steps towards this approach have already been given, e. g., Baslev et. al.^[110] presented the integration of multiple photonic components including an

optofluidic dye laser and embedded photodiodes into a PhLoC system. Liquid light sources are undoubtedly interesting, but are solvent-sensitive and may experience fast ageing.

Heterogeneous integration of several optical/microfluidic components has already been demonstrated. Some examples of this PhLoCs are listed in Table 3, where the integrated optical and micro-optical elements as well the analytical features of the device are highlighted. The way to achieve a truly PhLoC independent from bulky external elements is to develop highly integrated devices. Despite of their good performance, these microsystems are at the proof-of-concept level, revealing that this new scientific area is still in its infancy. Nevertheless, these examples draw attention to the potential of this field and establish the path to follow for the next years in PhLoC research.

Table 3. Analytical performance of PhLoC microfluidic systems with integrated optical components.^[111]

Optical detection	Micro-optical and integrated optical components	Analyte	LOD*	Ref.
Absorbance	Waveguide	Crystal Violet	0.54 μ M	[112]
Absorbance (Ab), fluorescence (Fl)	Array of waveguides	Alexa Fluor 633 dye	1 μ M (Ab), 10 nM (Fl)	[113]
Absorbance	Liquid dye laser, waveguides, cuvettes, photodiodes	Xylenol Orange	-	[110]
Fluorescence	Microlens	Cy5	3.3 nM	[114]
Fluorescence	Multiple-2D planar microlenses	Fluorescent dyes	-	[115]
Fluorescence	Passband filters	Rhodamine B	-	[103]
Fluorescence	OLEDs [‡]	Fluorescein	1 μ M	[106]
Fluorescence	Blue LED [‡] , CdS filter, silicon photodiode	Fluorescein	0.12 μ M	[116]
Fluorescence	Silicon photodiode, filters	Fluorescein	17 nM	[117]
Chemiluminescence	Photodiode	DNA	0.9 nM	[118]
Refractive index	2D photonic crystal lattice waveguide	Air, methanol, isopropanol	-	[119]

*LOD= limit of detection, [‡](O)LED= (organic) light emitting diode

References

1. Hench, L.L. and J.K. West, *THE SOL-GEL PROCESS*. Chemical Reviews, 1990. **90**(1): p. 33-72.
2. Flory, P.J., *Principles of Polymer Chemistry*. 1953, Ithaca: Cornell University Press.
3. Ribot, F., P. Toledano, and C. Sanchez, *HYDROLYSIS CONDENSATION PROCESS OF BETA-DIKETONATES-MODIFIED CERIUM(IV) ISOPROPOXIDE*. Chemistry of Materials, 1991. **3**(4): p. 759-764.
4. Bradley, D.C., Mehrotra, R. C., Gaur, D. P., *Metal Alcoxides*. 1978, London: Academic.
5. Prassas, M., Hench, L. L., , *In Ultrastructure Processing of Ceramics, Glasses and Composites*. 1984, New York: Wiley.
6. Brinker, J., Sherer, G., *Sol-Gel Science*. 1989, New York: Academic Press.
7. Kalinin, S.V., et al., *Influence of the drying technique on the structure of silica gels*. Journal of Sol-Gel Science and Technology, 1999. **15**(1): p. 31-35.
8. Uchida, N., et al., *CHEMICAL EFFECTS OF DCCA TO THE SOL-GEL REACTION PROCESS*. Journal of Materials Science, 1994. **29**(19): p. 5188-5192.
9. Hench, L.L., Ulrich, D. R., *Science of Ceramic Chemical Processing*. 1986, New York: Wiley.
10. Pierre, A.C. and G.M. Pajonk, *Chemistry of aerogels and their applications*. Chemical Reviews, 2002. **102**(11): p. 4243-4265.
11. Pajonk, G.M., et al., *FROM SOL-GEL TO AEROGELS AND CRYOGELS*. Journal of Non-Crystalline Solids, 1990. **121**(1-3): p. 66-67.
12. Job, N., et al., *Carbon aerogels, cryogels and xerogels: Influence of the drying method on the textural properties of porous carbon materials*. Carbon, 2005. **43**(12): p. 2481-2494.
13. Llobera, A., et al., *Fluorophore-doped xerogel antiresonant reflecting optical waveguides*. Optics Express, 2011. **19**(6): p. 5026-5039.
14. Tohge, N., et al., *Fabrication of two-dimensional gratings using photosensitive gel films and their characterization*. Journal of Sol-Gel Science and Technology, 2003. **26**(1-3): p. 903-907.
15. Zhang, X.H., et al., *Fabrication of micro-lens arrays built in photosensitive hybrid films by UV-cured imprinting technique*. Journal of Sol-Gel Science and Technology, 2011. **60**(1): p. 71-80.
16. Deshpande, A.V. and U. Kumar, *Efficient lasing action from Rhodamine-110 (Rh-110) impregnated sol-gel silica samples prepared by dip method*. Journal of Luminescence, 2010. **130**(5): p. 839-844.
17. Qiao, Y., et al., *Photoluminescent Lanthanide-Doped Silica Nanotubes: Sol-Gel Transcription from Functional Template*. Journal of Physical Chemistry C, 2011. **115**(15): p. 7323-7330.
18. Tani, T., et al., *PHOTOCHEMICAL HOLE-BURNING STUDY OF 1,4-DIHYDROXYANTHRAQUINONE DOPED IN AMORPHOUS SILICA PREPARED BY ALCOHOLATE METHOD*. Journal of Applied Physics, 1985. **58**(9): p. 3559-3565.
19. Levy, D., S. Einhorn, and D. Avnir, *APPLICATIONS OF THE SOL-GEL PROCESS FOR THE PREPARATION OF PHOTOCHROMIC INFORMATION-RECORDING MATERIALS - SYNTHESIS, PROPERTIES, MECHANISMS*. Journal of Non-Crystalline Solids, 1989. **113**(2-3): p. 137-145.
20. Chaumel, F., H.W. Jiang, and A. Kakkar, *Sol-gel materials for second-order nonlinear optics*. Chemistry of Materials, 2001. **13**(10): p. 3389-3395.
21. El-Nahhal, I.M., S.M. Zourab, and N.M. El-Ashgar, *Encapsulation of phenolphthalein pH-indicator into a sol-gel matrix*. Journal of Dispersion Science and Technology, 2001. **22**(6): p. 583-590.

22. Zaggout, F.R., A.E.-F.A. Qarraman, and S.M. Zourab, *Behavior of immobilized Alizarin Red S into sol-gel matrix as pH sensor*. *Materials Letters*, 2007. **61**(19-20): p. 4192-4195.
23. McDonagh, C.M., et al., *Optical sol-gel-based dissolved oxygen sensor: Progress towards a commercial instrument*. *Journal of Sol-Gel Science and Technology*, 1998. **13**(1-3): p. 207-211.
24. Estella, J., et al., *Fabrication and performance evaluation of highly sensitive hybrid sol-gel-derived oxygen sensor films based on a fluorinated precursor*. *Analytica Chimica Acta*, 2010. **666**(1-2): p. 83-90.
25. Carrington, N.A., et al., *Optical determination of Cr(VI) using regenerable, functionalized sol-gel monoliths*. *Analytica Chimica Acta*, 2007. **581**(2): p. 232-240.
26. Llobera, A., et al., *Full-field photonic biosensors based on tunable bio-doped sol-gel glasses*. *Lab on a Chip*, 2008. **8**(7): p. 1185-1190.
27. Frenkel-Mullerad, H. and D. Avnir, *Sol-gel materials as efficient enzyme protectors: Preserving the activity of phosphatases under extreme pH conditions*. *Journal of the American Chemical Society*, 2005. **127**(22): p. 8077-8081.
28. Ferrer, M.L., et al., *High operational stability in peroxidase-catalyzed non-aqueous sulfoxidations by encapsulation within sol-gel glasses*. *Journal of Molecular Catalysis B-Enzymatic*, 2004. **27**(2-3): p. 107-111.
29. Kato, M., et al., *Monolithic bioreactor immobilizing trypsin for high-throughput analysis*. *Analytical Chemistry*, 2005. **77**(6): p. 1813-1818.
30. Darder, M., et al., *Algae-silica systems as functional hybrid materials*. *Journal of Materials Chemistry*. **20**(42): p. 9362-9369.
31. Chia, S.Y., et al., *Patterned hexagonal arrays of living cells in sol-gel silica films*. *Journal of the American Chemical Society*, 2000. **122**(27): p. 6488-6489.
32. Ferrer, M.L., et al., *Biocompatible sol-gel route for encapsulation of living bacteria in organically modified silica matrixes*. *Chemistry of Materials*, 2003. **15**(19): p. 3614-3618.
33. Liang, R.P., H.D. Qiu, and P.X. Cai, *A novel amperometric immunosensor based on three-dimensional sol-gel network and nanoparticle self-assemble technique*. *Analytica Chimica Acta*, 2005. **534**(2): p. 223-229.
34. Avnir, D., et al., *Recent bio-applications of sol-gel materials*. *Journal of Materials Chemistry*, 2006. **16**(11): p. 1013-1030.
35. Ito, S., et al., *Mesoporous aluminosilicate-catalyzed allylation of carbonyl compounds and acetals*. *Tetrahedron*. **67**(11): p. 2081-2089.
36. Maschmeyer, T., et al., *HETEROGENEOUS CATALYSTS OBTAINED BY GRAFTING METALLOCENE COMPLEXES ONTO MESOPOROUS SILICA*. *Nature*, 1995. **378**(6553): p. 159-162.
37. Lee, J.H., et al., *Synthesis and microstructure of silica-doped alumina composite membrane by sol-gel process*. *Journal of Materials Science Letters*, 1999. **18**(17): p. 1367-1369.
38. Schwartz, R.W., *Chemical solution deposition of perovskite thin films*. *Chemistry of Materials*, 1997. **9**(11): p. 2325-2340.
39. Nagarajan, S., V. Raman, and N. Rajendran, *Synthesis and electrochemical characterization of porous niobium oxide coated 316L SS for orthopedic applications*. *Materials Chemistry and Physics*. **119**(3): p. 363-366.
40. Mark, J.E., *Hybrid organic-inorganic composites containing mixed-oxide ceramics and high-temperature polymers*. *Journal of Macromolecular Science-Pure and Applied Chemistry*, 1996. **A33**(12): p. 2005-2012.
41. Wen, J.Y. and G.L. Wilkes, *Organic/inorganic hybrid network materials by the sol-gel approach*. *Chemistry of Materials*, 1996. **8**(8): p. 1667-1681.

42. Huang, H.H., B. Orler, and G.L. Wilkes, *CERAMERS - HYBRID MATERIALS INCORPORATING POLYMERIC OLIGOMERIC SPECIES WITH INORGANIC GLASSES BY A SOL-GEL PROCESS .2. EFFECT OF ACID CONTENT ON THE FINAL PROPERTIES*. Polymer Bulletin, 1985. **14**(6): p. 557-564.
43. Schmidt, H., *NEW TYPE OF NON-CRYSTALLINE SOLIDS BETWEEN INORGANIC AND ORGANIC MATERIALS*. Journal of Non-Crystalline Solids, 1985. **73**(1-3): p. 681-691.
44. Sanchez, C., H. Arribart, and M.M.G. Guille, *Biomimetism and bioinspiration as tools for the design of innovative materials and systems*. Nature Materials, 2005. **4**(4): p. 277-288.
45. Sanchez, C., et al., *Applications of hybrid organic-inorganic nanocomposites*. Journal of Materials Chemistry, 2005. **15**(35-36): p. 3559-3592.
46. Gomez-Romero, P. and C. Sanchez, *Hybrid materials. Functional properties. From Maya Blue to 21st century materials*. New Journal of Chemistry, 2005. **29**(1): p. 57-58.
47. Warrick, E., *Forty years of firsts*. 1990, New York: McGraw-Hill.
48. Arkles, B., *Commercial applications of sol-gel-derived hybrid materials*. Mrs Bulletin, 2001. **26**(5): p. 402-+.
49. Sanchez, C., et al., *"Chimie douce": A land of opportunities for the designed construction of functional inorganic and hybrid organic-inorganic nanomaterials*. Comptes Rendus Chimie, 2010. **13**(1-2): p. 3-39.
50. Livage, J., M. Henry, and C. Sanchez, *SOL-GEL CHEMISTRY OF TRANSITION-METAL OXIDES*. Progress in Solid State Chemistry, 1988. **18**(4): p. 259-341.
51. Lebeau, B., et al., *OPTICAL-PROPERTIES OF A NEAR-INFRARED DYE-LASER INCORPORATED INSIDE SOL-GEL MATRICES*. Chemical Physics Letters, 1993. **206**(1-4): p. 15-20.
52. Gornowich, D.B. and G.J. Blanchard, *Enhancement of Enzyme Activity by Confinement in an Inverse Opal Structure*. Journal of Physical Chemistry C, 2012. **116**(22): p. 12165-12171.
53. Laine, R.M. and M.F. Roll, *Polyhedral Phenylsilsesquioxanes*. Macromolecules. **44**(5): p. 1073-1109.
54. Sharp, K.G. and M.J. Michalczyk, *Star gels: New hybrid network materials from polyfunctional single component precursors*. Journal of Sol-Gel Science and Technology, 1997. **8**(1-3): p. 541-546.
55. Bredol, M. and M. Schem, *Microstructured UV-sensitive luminescent sol-gel layers*. Optical Materials, 2004. **27**(3): p. 521-525.
56. Houbertz, R., et al., *Inorganic-organic hybrid materials for application in optical devices*. Thin Solid Films, 2003. **442**(1-2): p. 194-200.
57. Houbertz, R., *Laser interaction in sol-gel based materials - 3-D lithography for photonic applications*. Applied Surface Science, 2005. **247**(1-4): p. 504-512.
58. Fernandez-Sanchez, C., et al., *Patterning high-aspect-ratio sol-gel structures by microtransfer molding*. Chemistry of Materials, 2008. **20**(8): p. 2662-2668.
59. Guo, L.J., *Nanoimprint lithography: Methods and material requirements*. Advanced Materials, 2007. **19**(4): p. 495-513.
60. Liu, Y., et al., *High refractive index organic-inorganic hybrid coatings with TiO₂ nanocrystals*. Colloids and Surfaces a-Physicochemical and Engineering Aspects, 2008. **328**(1-3): p. 67-72.
61. Almaral-Sanchez, J.L., et al., *Red colored transparent PMMA-SiO₂ hybrid films*. Journal of Physics and Chemistry of Solids, 2005. **66**(10): p. 1660-1667.
62. Wirnsberger, G., et al., *Fast response photochromic mesostructures*. Advanced Materials, 2000. **12**(19): p. 1450-1454.
63. Biteau, J., et al., *Photochromism of an indolyfulgide trapped in a hybrid sol-gel matrix*. Chemistry Letters, 1998(4): p. 359-360.

64. Yang, P.D., et al., *Mirrorless lasing from mesostructured waveguides patterned by soft lithography*. *Science*, 2000. **287**(5452): p. 465-467.
65. Della Giustina, G., et al., *Electron beam lithography of hybrid sol-gel negative resist*. *Microelectronic Engineering*, 2009. **86**(4-6): p. 745-748.
66. Moujoud, A., et al., *Thermally stable optical characteristics of sol-gel hybrid material films*. *Applied Physics Letters*, 2006. **88**(10).
67. Madou, M.J., *Fundamentals of microfabrication. The science of miniaturization*. second edition ed, ed. C. Press. 2002.
68. Xia, Y.N. and G.M. Whitesides, *Soft lithography*. *Angewandte Chemie-International Edition*, 1998. **37**(5): p. 551-575.
69. Xia, Y.N., et al., *Complex optical surfaces formed by replica molding against elastomeric masters*. *Science*, 1996. **273**(5273): p. 347-349.
70. Kim, E., Y.N. Xia, and G.M. Whitesides, *POLYMER MICROSTRUCTURES FORMED BY MOLDING IN CAPILLARIES*. *Nature*, 1995. **376**(6541): p. 581-584.
71. Washburn, E.W., *The dynamics of capillary flow*. *Physical Review*, 1921. **17**(3): p. 273-283.
72. Manz, A., N. Graber, and H.M. Widmer, *MINIATURIZED TOTAL CHEMICAL-ANALYSIS SYSTEMS - A NOVEL CONCEPT FOR CHEMICAL SENSING*. *Sensors and Actuators B-Chemical*, 1990. **1**(1-6): p. 244-248.
73. West, J., et al., *Micro total analysis systems: Latest achievements*. *Analytical Chemistry*, 2008. **80**(12): p. 4403-4419.
74. Figeys, D. and D. Pinto, *Lab-on-a-chip: A revolution in biological and medical sciences*. *Analytical Chemistry*, 2000. **72**(9): p. 330A-335A.
75. Schmalzing, D., et al., *DNA sequencing on microfabricated electrophoretic devices*. *Analytical Chemistry*, 1998. **70**(11): p. 2303-2310.
76. Andersson, H. and A. van den Berg, *Microfluidic devices for cellomics: a review*. *Sensors and Actuators B-Chemical*, 2003. **92**(3): p. 315-325.
77. Abu-Hatab, N.A., et al., *Multiplexed microfluidic surface-enhanced Raman spectroscopy*. *Applied Spectroscopy*, 2007. **61**(10): p. 1116-1122.
78. Hitzbleck, M., et al., *Capillary soft valves for microfluidics*. *Lab on a Chip*. **12**(11): p. 1972-1978.
79. Kim, J., et al., *Lifting Gate Polydimethylsiloxane Microvalves and Pumps for Microfluidic Control*. *Analytical Chemistry*. **84**(4): p. 2067-2071.
80. Hiraoka, M., et al., *Miniature conductive polymer actuators for high pressure generation in lab on chip systems*. *Sensors and Actuators a-Physical*. **177**: p. 23-29.
81. Park, J.M., K.D. Seo, and T.H. Kwon, *A chaotic micromixer using obstruction-pairs*. *Journal of Micromechanics and Microengineering*. **20**(1).
82. Gamby, J., et al., *Polycarbonate microchannel network with carpet of Gold NanoWires as SERS-active device*. *Lab on a Chip*, 2009. **9**(12): p. 1806-1808.
83. Mathur, A., et al., *Characterisation of PMMA microfluidic channels and devices fabricated by hot embossing and sealed by direct bonding*. *Current Applied Physics*, 2009. **9**(6): p. 1199-1202.
84. Llobera, A., R. Wilke, and S. Buttgenbach, *Poly(dimethylsiloxane) hollow Abbe prism with microlenses for detection based on absorption and refractive index shift*. *Lab on a Chip*, 2004. **4**(1): p. 24-27.
85. Blazej, R.G., P. Kumaresan, and R.A. Mathies, *Microfabricated bioprocessor for integrated nanoliter-scale Sanger DNA sequencing*. *Proceedings of the National Academy of Sciences of the United States of America*, 2006. **103**(19): p. 7240-7245.
86. Flusberg, B.A., et al., *Fiber-optic fluorescence imaging*. *Nature Methods*, 2005. **2**(12): p. 941-950.

87. Salvade, Y. and R. Dandliker, *Limitations of interferometry due to the flicker noise of laser diodes*. Journal of the Optical Society of America a-Optics Image Science and Vision, 2000. **17**(5): p. 927-932.
88. Greif, D., et al., *Single cell analysis in full body quartz glass chips with native UV laser-induced fluorescence detection*. Journal of Chromatography A, 2008. **1206**(1): p. 83-88.
89. Dasgupta, P.K., et al., *High-sensitivity gas sensors based on gas-permeable liquid core waveguides and long-path absorbance detection*. Analytical Chemistry, 1998. **70**(22): p. 4661-4669.
90. Wang, Z., et al., *Measurements of scattered light on a microchip flow cytometer with integrated polymer based optical elements*. Lab on a Chip, 2004. **4**(4): p. 372-377.
91. Mogensen, K.B. and J.P. Kutter, *Optical detection in microfluidic systems*. Electrophoresis, 2009. **30**: p. S92-S100.
92. Srinivasan, V., V.K. Pamula, and R.B. Fair, *Droplet-based microfluidic lab-on-a-chip for glucose detection*. Analytica Chimica Acta, 2004. **507**(1): p. 145-150.
93. Qavi, A.J. and R.C. Bailey, *Multiplexed Detection and Label-Free Quantitation of MicroRNAs Using Arrays of Silicon Photonic Microring Resonators*. Angewandte Chemie-International Edition. **49**(27): p. 4608-4611.
94. Vila-Planas, J., et al., *Cell analysis using a multiple internal reflection photonic lab-on-a-chip*. Nature Protocols, 2011. **6**(10): p. 1642-1655.
95. Puyol, M., et al., *Improved integrated waveguide absorbance optodes for ion-selective sensing*. Analytical Chemistry, 2002. **74**(14): p. 3354-3361.
96. Ruano, J.M., et al., *Design and fabrication of a silica on silicon integrated optical biochip as a fluorescence microarray platform*. Biosensors & Bioelectronics, 2003. **18**(2-3): p. 175-184.
97. Llobera, A., R. Wilke, and S. Buettgenbach, *Enhancement of the response of poly(dimethylsiloxane) hollow prisms through air mirrors for absorbance-based sensing*. Talanta, 2008. **75**(2): p. 473-479.
98. Lee, S.-Y., et al., *Microlens with tunable-astigmatism*. IEEE Photonics Technology Letters, 2007. **19**(17-20): p. 1383-1385.
99. Dandin, M., P. Abshire, and E. Smela, *Optical filtering technologies for integrated fluorescence sensors*. Lab on a Chip, 2007. **7**(8): p. 955-977.
100. Macleod, H.A., ed. *Thin Film Optical Filters*. 2001, Institute of Physics Publishing: London.
101. Chabinyk, M.L., et al., *An integrated fluorescence detection system in poly(dimethylsiloxane) for microfluidic applications*. Analytical Chemistry, 2001. **73**(18): p. 4491-4498.
102. Mahan, A.H., et al., *On the influence of short and medium range order on the material band gap in hydrogenated amorphous silicon*. Journal of Applied Physics, 2004. **96**(7): p. 3818-3826.
103. Llobera, A., et al., *Monolithic PDMS passband filters for fluorescence detection*. Lab on a Chip, 2010. **10**(15): p. 1987-1992.
104. Yamazaki, M., et al., *Non-emissive colour filters for fluorescence detection*. Lab on a Chip, 2011. **11**(7): p. 1228-1233.
105. Pais, A., et al., *High-sensitivity, disposable lab-on-a-chip with thin-film organic electronics for fluorescence detection*. Lab on a Chip, 2008. **8**(5): p. 794-800.
106. Edel, J.B., et al., *Thin-film polymer light emitting diodes as integrated excitation sources for microscale capillary electrophoresis*. Lab on a Chip, 2004. **4**(2): p. 136-140.
107. Miyaki, K., et al., *Fabrication of an integrated PDMS microchip incorporating an LED-induced fluorescence device*. Analytical and Bioanalytical Chemistry, 2005. **382**(3): p. 810-816.
108. Yao, B., et al., *A microfluidic device using a green organic light emitting diode as an integrated excitation source*. Lab on a Chip, 2005. **5**(10): p. 1041-1047.

109. Liu, R., et al., *Organic Light-Emitting Diode Sensing Platform: Challenges and Solutions*. *Advanced Functional Materials*, 2011. **21**(24): p. 4744-4753.
110. Balslev, S., et al., *Lab-on-a-chip with integrated optical transducers*. *Lab on a Chip*, 2006. **6**(2): p. 213-217.
111. Kuswandi, B., et al., *Optical sensing systems for microfluidic devices: A review*. *Analytica Chimica Acta*, 2007. **601**(2): p. 141-155.
112. Duggan, M.P., T. McCreedy, and J.W. Aylott, *A non-invasive analysis method for on-chip spectrophotometric detection using liquid-core waveguiding within a 3D architecture*. *Analyst*, 2003. **128**(11): p. 1336-1340.
113. Malic, L. and A.G. Kirk, *Integrated miniaturized optical detection platform for fluorescence and absorption spectroscopy*. *Sensors and Actuators a-Physical*, 2007. **135**(2): p. 515-524.
114. Roulet, J.C., et al., *Performance of an integrated microoptical system for fluorescence detection in microfluidic systems*. *Analytical Chemistry*, 2002. **74**(14): p. 3400-3407.
115. Seo, J. and L.P. Lee, *Disposable integrated microfluidics with self-aligned planar microlenses*. *Sensors and Actuators B-Chemical*, 2004. **99**(2-3): p. 615-622.
116. Chediak, J.A., et al., *Heterogeneous integration of CdS filters with GaN LEDs for fluorescence detection microsystems*. *Sensors and Actuators a-Physical*, 2004. **111**(1): p. 1-7.
117. Kamei, T., et al., *Integrated hydrogenated amorphous Si photodiode detector for microfluidic bioanalytical devices*. *Analytical Chemistry*, 2003. **75**(20): p. 5300-5305.
118. Namasivayam, V., et al., *Advances in on-chip photodetection for applications in miniaturized genetic analysis systems*. *Journal of Micromechanics and Microengineering*, 2004. **14**(1): p. 81-90.
119. Loncar, M., A. Scherer, and Y.M. Qiu, *Photonic crystal laser sources for chemical detection*. *Applied Physics Letters*, 2003. **82**(26): p. 4648-4650.

Chapter II

OBJECTIVES

The aim of the work included in this PhD Thesis was two-folded.

1. Development of new strategies for the simple and low-cost fabrication of photonic components based on hybrid xerogel polymers. and their integration in photonic lab-on-chip (PhLoC) devices.
2. Integration of , such photonic components in photonic lab-on-chip devices (PhLoC), which could be further implemented in compact analytical tools with the potential to be applied in decentralized studies for environmental monitoring or point-of-care diagnostics.

To achieve the above mentioned objectives the following specific issues have been defined:

- Development of different tailor-made silicon based hybrid organic-inorganic polymeric materials by sol-gel technology. Careful selection of different monomers to be included in several sol-gel polymer formulations and the experimental conditions for their synthesis in order to tune the specific properties of the resulting polymeric materials. This also includes the study of different doping agents, from colored and fluorescent dyes to quantum-dots in order to modulate the spectral properties of the xerogel materials.
- Use of simple and cost-effective microfabrication techniques for patterning of the resulting hybrid polymers. Different approaches included in the so-called soft lithography techniques can be explored together with other nanofabrication techniques such as nanoimprint lithography.
- Design and fabrication of different micro-optical (filters and solid state emitters) and integrated optical (waveguides) photonic components. Characterization of their optical properties (losses, spectral response).
- Integratation of the developed photonic components into PhLoC systems. Evaluation of the analytical performance of these systems with model analytes. Development of a biosensor approach to extend the applicability of the developed strategies.

Chapter III

ONE-STEP SOFT-LITHOGRAPHIC PATTERNING OF HYBRID XEROGEL MATERIALS APPLIED TO THE FABRICATION OF PHOTONIC COMPONENTS

The work contained in this chapter has been reported in one paper entitled “*One-step patterning of hybrid xerogel materials for the fabrication of disposable solid-state light emitters*” by Ester Carregal-Romero, Andreu Llobera, Victor J. Cadarso, Margarita Darder, Pilar Aranda, Carlos Domínguez, Eduardo Ruiz-Hitzky, and César Fernández-Sánchez, ACS Applied Materials & Interfaces, in press, DOI: 10.1021/am3014696.

3.1 SUMMARY

The one-step room temperature micropatterning of a fluorophore-doped xerogel material on silicon oxide substrates is reported. The organo-alkoxysilane precursors and organic fluorescent dyes as well as the polymerization experimental conditions were tailored in order to obtain a highly homogenous transparent material suitable for photonic applications. A thorough structural characterization was carried out by FT-infrared spectroscopy, ²⁹Si-magnetic nuclear resonance, thermal gravimetric analysis, N₂ adsorption BET porosimetry and confocal microscopy. These studies revealed a stable non-porous highly cross-linked polymer network containing evenly dispersed fluorescent molecules.

Xerogel microstructures having thicknesses between 4-80 μm, height-to-width ratios between 0.04 and 4 and showing different geometries, from well arrays to waveguides, were patterned in a single step by micromolding in capillaries (MIMIC) soft lithographic technique. The reliability of the replication process was tested by bright field optical microscopy and scanning electron microscopy (SEM) that show the close fidelity of the microstructures to the applied mold.

The optical performance of the developed material was demonstrated by fabricating waveguides and evaluating their corresponding spectral response, obtaining absorption bands, at the expected excitation wavelengths of the corresponding fluorescent dyes and gain due to photonic reemission (fluorescence) at their corresponding dye emission wavelengths. The hybrid xerogel material and the application of the simple fabrication technology presented herein can be directly applied to the development of cost-effective photonic components, as could be light

emitters, to be readily integrated in single-use lab on chip devices and other polymeric microsystems.

3.2 INTRODUCTION

The excellent properties of luminescent dye-doped sol-gel materials for the fabrication of solid-state light emitters have been clearly shown in excellent reviews by Sánchez^[1] and Lebeau.^[2] Dye-doped hybrid materials exhibit amplified luminescent emission at different wavelength ranges depending on the material transparency (no scattering losses), stability (aging), density (negligible optical inhomogeneity) and mechanical resistance. They should also provide the adequate environment to retain the luminescent quantum yield of the dye (lack of aggregation) and to prevent its degradation. In order to fulfill all these requirements, thorough empiric studies focused on the optimization of the hybrid xerogel matrix, the choice of the appropriate dye and the interaction dye/matrix have to be carried out.^[3, 4]

Lasing performance of hybrid sol-gel materials doped with dyes either embedded or bound to the polymer network have been demonstrated, with the latter showing higher dye loading and thus improved performance in terms of luminescent intensity and dye degradation.^[5] However, the preparation of these materials is more laborious and is limited to dyes that could covalently react with the sol-gel matrix or required initial chemical modification of these molecules in order to get such interaction. Keeping in mind all these studies, this work shows the simple development of a tailor-made hybrid material doped with organic fluorophore dyes and its thorough characterization in order to demonstrate its suitability for the easy and cost-effective fabrication of disposable solid-state light emitters. The presented material shows the above-mentioned requirements with the added advantage of being easily synthesized and processed as microstructures of different geometries by a single-step non-photolithographic approach without altering its material physicochemical properties and optical performance.

Combining a fluorophore-doped organic-inorganic sol-gel material, thermally cured at room temperature, with the micromolding in capillaries soft lithographic technique, high quality optical microstructures can be easily fabricated in a single-step. Related previously reported approaches make use of rather complicated material synthesis approaches or photolithographic techniques, which, although may show improved performance, make the fabrication more expensive and/or difficult to implement with other optical components.^[6-8]

3.3 EXPERIMENTAL DETAILS

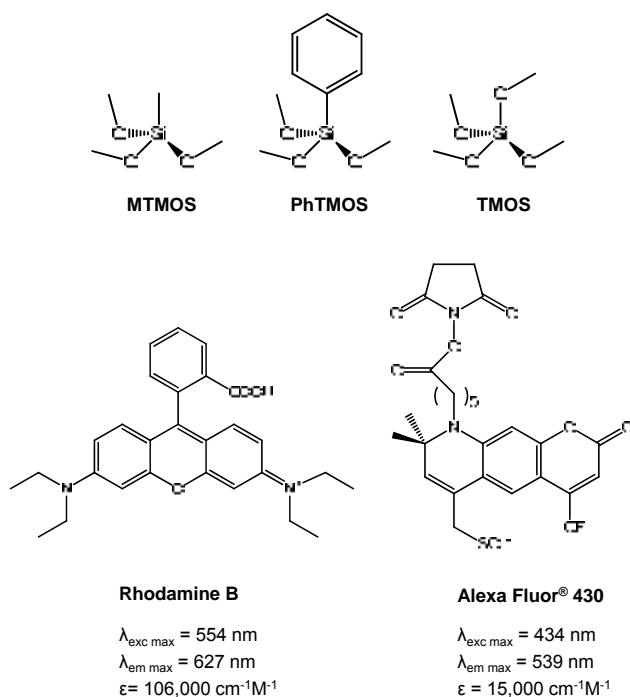
3.3.1 Materials

Tetramethoxysilane (TMOS), methyltrimethoxysilane (MTMOS), phenyltrimethoxysilane (PhTMOS) and Rhodamine B were purchased from Sigma-Aldrich Química S.A. (Spain) and used as received. Alexa Fluor® 430 carboxylic acid succinimidyl ester (Alexa) was purchased from Invitrogen (California, USA). SU-8 2005 and SU-8 2025 photocurable polymers and propylene glycol ether acetate (PGMEA) developer were from Microresist Technology GmbH (Berlin, Germany). Sylgard 184 elastomer kit was from Dow Corning Corp, (Midland, MI). All other chemicals were of reagent grade and used as received.

3.3.2 Fluorophore-doped sol-gel synthesis

The *sol* solution was prepared in a fume cupboard under clean room conditions. Some 615 μL of MTMOS, 60 μL of TMOS and 75 μL of PhTMOS were mixed in a disposable plastic beaker, under constant stirring. Then, 2750 μL of DI water were added dropwise. These volumes gave a 10:1:1 MTMOS:PhTMOS:TMOS and 1:30 silanes:water molar ratios. No catalyst was added. Molecular structures of the different components are depicted in scheme 1. The resulting mixture was gently stirred overnight, at room temperature, until a 30 % weight loss was achieved. Then, 100 μL of this *sol* solution was mixed with 30 μL of an aqueous solution containing either Alexa or Rhodamine B fluorophores in a concentration range from 10^{-5} M to 10^{-3} M, and vigorously stirred in a vortex. The resulting mixtures were homogenous, and at this point they were ready for the patterning process.

Scheme 1. Silane precursors and dye chemical structures.



3.3.3 Fabrication of masters and stamps

Masters were fabricated with the SU-8 2005 and 2025 negative photoresists by one photolithographic process.⁵⁸ A 4-in Si wafer ((100), 525 μm thick) on to which a 400 nm- thick SiO_2 was thermally grown, was cleaned with *Piranha* solution (fuming H_2SO_4 : 30% H_2O_2 , 3:1 v/v). Then, a layer of SU-8 2005 or 2025 resins was deposited by spin-coating under different rotation speed and time conditions in order to obtain the required thicknesses. SU-8 was used for thicknesses between 4 and 25 μm , whereas SU-8 2025 was used for thicker layers. Following a bake at 95° C for 1 h to evaporate the excess of solvent, the SU-8 was exposed to UV light through a mask. A post-exposure bake at 95°C for 15 min was then carried out before developing the SU-8 in propylene glycol methyl ether acetate (PGMEA) that eventually revealed the masters.

The polydimethylsiloxane (PDMS) elastomer was used for the fabrication of the molds. The pre-polymeric solution was prepared by mixing the Sylgard 184 elastomer with the curing agent (10:1, v/v). Then, the mixture was carefully poured onto the SU-8 master to cover its entire area. Air bubbles that may have been generated during the PDMS mixing and pouring process were removed under vacuum. Finally the PDMS was cured at 80° C for 30 min in a hot-plate. The resulting mold was peeled off the master with the aid of tweezers and stored in a closed container under clean room facilities until use.

3.3.4 Fabrication of xerogel microstructures by Micromolding in Capillaries (MIMIC)

The polymer patterning was carried out on either thermally grown SiO_2/Si or glass substrates having areas between 1-1.5 cm^2 . A previous cleaning step was done by immersion in *Piranha* solution for 30 min. After a rinsing step with DI water and ethanol the substrates were dried under a N_2 stream and then activated by immersion in $\text{NH}_4:\text{H}_2\text{O}_2:\text{H}_2\text{O}$ (1:1:5 v:v:v) solution for 10 min. This treatment improved the adherence between the exposed silanol groups in the sol-gel polymer matrix with the thus activated silanol groups of the substrate. Then, the PDMS mold was placed on the substrate to establish conformal contact. Different microstructures were defined in the PDMS molds having heights from 4 μm to 80 μm and showing different geometries and configurations. Two different MIMIC approaches were carried out. The conventional process made use of molds containing microstructures in the form of channels with opens at both ends that appear at the edge of the mold. The alternative one included the implementation of inlets and outlets on the top surface of the mold. When the former was applied, thick residual layers of the xerogel material were formed at both sides of the structures resulting from the excess of the *sol* solution used to fill the structures. By contrast, the excess of *sol* solution in the latter approach appear on top of the PDMS, which, once cured, could be torn off when removing the PDMS mold. This process enables the good definition of the different facets of the structures, which

is important when fabricating photonic components. In both fabrication processes, a drop of fluorophore-doped sol-gel *sol* solution was placed at one end of the open microchannels, which were completely filled by capillary action. Then, the PDMS/substrate system was left undisturbed under clean room conditions (21° C, atmospheric pressure) for at least two days to allow the polymer to gel and dry. Once the doped xerogel was formed, the PDMS stamp was peeled off with the aid of tweezers and the microstructures were released.

3.3.5 Material characterization

The following studies were carried out with non-doped and 10^{-3} M Rhodamine B doped xerogel materials, unless stated otherwise. The latter corresponds to the material with the highest content of the fluorophore (7000:1 silane:fluorophore molar ratio in the *sol* solution), which was chosen in order to assess the strongest influence that the doping agent might have on the xerogel structure. This fluorophore content corresponds to about 0.36 wt % Rhodamine B concentration in the final solid, which was estimated assuming that the monomers fully hydrolyzed and condense to generate the polymer network and the 30% weight loss in the preparation of the *sol* solution was related to the evaporation of methanol, coming from the hydrolysis process of such monomers, and water. FT-infrared spectroscopy (FT-IR; Bruker IFS 66v/S spectrophotometer), ^{29}Si single-pulse (SP) solid state magic angle spinning nuclear magnetic resonance (MAS-NMR; Bruker Avance 400 spectrometer), thermogravimetric analysis (TG-DTA, Seiko SSC/5200), N_2 adsorption BET porosimetry (Micromeritics ASAP 2010 analyzer) and confocal microscopy studies (Leica TCS SP2 confocal microscope equipped including a HC PL APO CS 10.0x UV objective with a 0.40 numerical aperture and a diode UV 405 nm laser as light source) were carried out in order to elucidate the structural properties of the resulting doped polymer matrix. For the ^{29}Si -MAS NMR analysis, the xerogel materials were obtained in bulk, grinded and sieved to get a particle size below 150 μm . Then they were spun at 10 kHz and spectrometer frequency was set to 79.49 MHz Chemical shift values were referenced to tetramethylsilane (TMS). Spectra were recorded using a single-pulse sequence of 5 μs pulse time and 5 s waiting between accumulations until approximately 1200 accumulations were reached. For the FTIR study, the samples in powder form were prepared as pellets after dilution in KBr, and the spectra were recorded from 4000 to 400 cm^{-1} with 2 cm^{-1} resolution. TG-DTA analysis was carried out under dynamic air atmosphere (flux of 100 mL/min) from room temperature to 850°C at 10 °C/min heating rate. Textural properties were analyzed by N_2 adsorption/desorption experiments performed at 77 K after outgassing the samples at 393 K overnight. The specific total surface area and the average pore diameter were calculated by applying the Brunauer–Emmett–Teller (BET) and the Horvath–Kawazoe methods, respectively. Confocal microscopy analysis was carried out with fluorophore-doped polymer microstructures fabricated as described above. The scanned area was 600x600 μm

(width x length) and pictures were taken every 0.5 μm in depth with a resolution of 8 bits. Up to 50 pictures were taken depending of the thickness of the microstructures. The projections of the picture series were generated with Leica LAS AF software. The isosurface module of Imaris v. 6.1.0 software (Bitplane; Zürich, Switzerland) was used to reconstitute the 3-D models.

3.3.6 Characterization of the xerogel microstructures

Bright field optical, fluorescence (Leica MZFLIII microscope) and scanning electron microscopy (SEM, Zeiss LEO1530 Gemini) images were performed to test the quality of the patterning process. Optical characterization of waveguide microstructures was carried out mounting the chip in a vacuum chuck to ensure a fixed position. Two 230 μm multimode fiber optics (Thorlabs Inc., Dachau, Germany) were employed for coupling the light in the structures and collecting it. The fiber optics were aligned with the waveguide facets with the help of micropositioners. This was possible by fabricating the waveguides using silicon chips with a defined recessed area at both edges. Different light sources were used depending on the fluorophore. When Alexa was applied, a blue LED light was used as light source whereas for Rhodamine B a broadband halogen lamp (HL-2000, Ocean Optics, Dunedin, FL, USA) was used. Light collection was recorded with a microspectrometer (QE 65000-FL microspectrometer, Ocean Optics, Dunedin, FL, USA), unless stated otherwise. In order to assess the effect of the fluorophore doping component, measurements were recorded with both fluorophore-doped and non-doped (reference) xerogel waveguides.

3.4 RESULTS AND DISCUSSIONS

3.4.1 Synthesis and structural characterization of the xerogel material

The doped hybrid organic-inorganic xerogel was synthesized by the sol-gel technology using MTMOS, PhTMOS and TMOS as liquid alkoxide precursors and H_2O as solvent with no catalysts.⁷ MTMOS monomer was responsible for the mechanical integrity of the resulting material, also preventing the formations of cracks, fractures or defects in the surface of the material during the drying process. Additionally, it provided a strong hydrophobic character that was balanced with the presence of TMOS monomer. The role of PhTMOS is the modulation of the refractive index, which is directly related to the concentration of this monomer.⁵⁹ Two different fluorophore organic molecules were chosen, based on their absorption / emission bands, Stoke shift and proven photostability. Both Alexa Fluor[®] 430 and Rhodamine B have been fully characterized and showed high photostability, with Alexa showing a large Stokes shift.

The preparation process of the *sol* solution was reproducible by keeping the room conditions (clean room facilities) and the stirring speed constant. The weight loss step of the *sol* solution was carried out in order to partly remove the water used to dissolve

the silane monomers and to enable the methanol generated during the hydrolysis of the monomer methoxy groups to evaporate. In a previous work by our group,²¹ it was observed that this step was required in order to get a *sol* solution with the required viscosity to carry out the soft lithographic patterning process and to guarantee that no loss of dimensions of the resulting polymer structures with respect to those in the mold took place during the polymerization process.

²⁹Si-MNR provides useful information about the chemical environment surrounding the Si atoms within the polymeric network. From the presented spectra shown in Fig. 1(A), Q³ = XO-Si-(OSi)₃ signal at -101.2 ppm is ascribed to Si atoms coming from the TMOS precursor, which formed three siloxane (Si-O-Si) bonds and contain either a methoxy group or a silanol group. This signal is barely observed because of the low content of TMOS in the xerogel composition. Tⁿ= R-Si-(OSi)_n signals correspond to MTMOS and PhTMOS, which are capable to form up to three siloxane bonds, as occurs in other related systems¹⁰⁻¹¹. The chemical shifts (T² -56 ppm, T³ -65 ppm), which are typical of sol-gel silicon-based polymers,⁶⁰ are quite similar in both doped and non-doped samples. The signal at -71 ppm could also be attributed to a T³ signal coming from Si atoms bound to aromatic moieties that appear to shift from the characteristic signal recorded when just silicon atoms bound to aliphatic groups are present in the polymer matrix.⁶¹ This signal is less intense than the one at -65 ppm and is in accordance with the PhTMOS to MTMOS molar ratios in the material composition. A slight difference in the relative T³/T² areas for both materials was observed. This data provides information about the degree of condensation of the polymeric network. For the non-doped xerogel, relative areas of 49/51 were calculated, which means that 49 % and 51 % of the Si atoms from the organotrimethoxysilanes are forming three and two siloxane bonds, respectively. The Rhodamine B-doped xerogel showed 45/55 relative values, which means that the presence of the fluorophore molecule partially impeded the formation of siloxane bonds leading to a polymer with a slightly lower cross-linked degree. This effect caused for the inclusion of molecules into polysiloxane matrices is well-known and was previously observed for the entrapment of enzymes^{21,62} and dye molecules⁶³ into similar polymeric cages. However, this fact affects neither the macroscopic integrity of the polymeric microstructures nor their physicochemical and optical properties, as will be shown below.

FT-IR spectra (see Fig. 1(B)) showed the characteristic bands between 1200 and 900 cm⁻¹ wavenumber for the stretching vibrations of Si-O bonds of the polysiloxane backbone, free silanol groups and Si-OCH₃ groups that were not be hydrolyzed during the polymerization process, for both samples. Also, a broad band in the region of 3500 cm⁻¹ due to the stretching vibrations of -OH groups of Si-OH moieties is clearly visible. Both materials also showed a weak band around 1600 cm⁻¹ corresponding to deformation vibrations of remaining water molecules within the polymer matrix. Other

bands that appear in both spectra are characteristic of bending and stretching vibrations of C-H, Si-C and Si-CH₃ groups, as described elsewhere¹⁰⁻¹¹. It can be stated that spectra of both non-doped and doped xerogel materials did not show dissimilarities that could be ascribed to the formation of different bonds due to the inclusion of the fluorophore during the polymerization process and therefore, it did not appear to affect the polymer structure. Additionally, characteristic bands for Rhodamine B that should appear between 1650 and 1750 cm⁻¹, related to the vibrations of the carbonyl group containing carboxylic moieties cannot be observed in the FTIR spectrum of the doped xerogel matrix, even though the material with the highest loading of the doping agent was analyzed. The reason could be the very low content of the fluorophore in the material (7000:1 Rhodamine B:silanes), which cannot be detected by this spectroscopic technique.

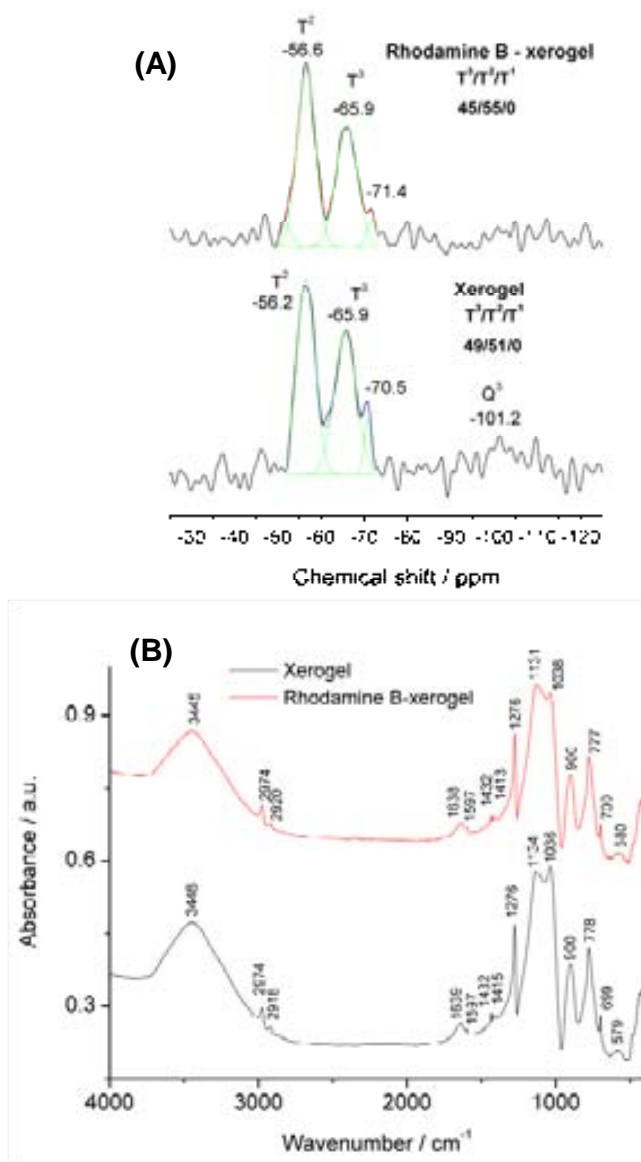


Figure 1. (A) ²⁹Si-NMR and (B) FT-IR spectra of both non-doped and Rhodamine B doped xerogels.

TG-DTA analysis was carried out in order to analyze the strength of the interactions between the fluorophore molecule and the xerogel network. Fig 2 shows the TG-DTA curves corresponding to the raw xerogel and Rhodamine-doped xerogel. The two samples showed a weight loss around 100°C of 2.2-2.7 % corresponding to the complete removal of the remaining water entrapped in the matrix pores. A further weight loss of 6.0 -6.5 % occurred for both xerogel and Rhodamine B-xerogel samples between 200-250° C related to the combustion of aromatic structures and cleavage of C-C bonds. That means that this material withstands temperatures up to 200° C. At this point the organic components in the polymer, phenyl and methyl groups started to degrade. The weight loss observed between 500–800 °C (about 15% in both materials) can be attributed to the oxidation of pyrolytic products formed in the incomplete combustion of the organic moieties at previous stages, which remain entrapped within the dense polysiloxane matrix.⁶⁴ Although both TG curves are quite similar, a remarkable difference can be observed in the DTA curves over that temperature range. The non-doped xerogel only shows an exothermic peak centered at 562 °C, while the fluorophore-doped material shows an additional sharp and intense exothermic peak at a lower temperature of 516 °C, together with the one at 563 °C. This splitting in several decomposition stages may be related to the presence of diverse structural environments in the doped xerogel. Thus, the doped xerogel material with a lower content of Si atoms surrounded by three siloxane bonds, as determined from the ²⁹Si NMR spectra, may contain regions with a lower condensation degree, where the removal of the entrapped pyrolytic residues may be easier to occur. A similar behavior was observed in related systems of ionophore-doped MAPTS/TMOS matrixes.⁶⁵

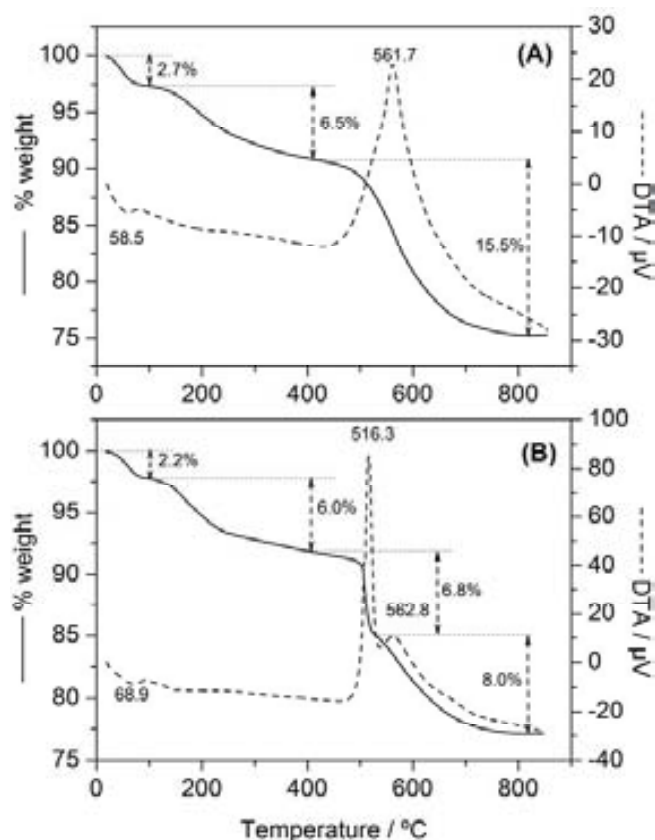


Figure 2. Thermogravimetric (solid line) and differential thermal analyses (dashed line) of, (A) non-doped and, (B) Rhodamine B doped xerogel materials.

N_2 adsorption BET porosimetry study was carried out with non-doped and Rhodamine B-doped sol-gel materials. A very low specific surface area around $2 \text{ m}^2/\text{g}$ was measured for both samples that indicate a high degree of condensation and low porosity. The pore size is around 10 \AA , which means that the polymer is essentially microporous. These results indicate that these materials are highly dense and therefore, fluorophore leaching from the polymeric network can be neglected.

Confocal microscopy was carried out in order to test the dispersion of the fluorophores within the polymeric matrix. Alexa-doped xerogel waveguides were scanned in this study. 3D reconstructions of the microstructures were made, as described in the experimental section, and results recorded with $100 \text{ }\mu\text{m}$ -wide Alexa-doped waveguide structures are shown in Fig. 3(A). Similar fluorescence intensity along the structures can be observed. Also, different emission spectra at nine arbitrary points of the microstructures were also recorded and shown in Fig. 3(B). The mean values for the maximum fluorescence emission intensity and wavelength were 201 ± 18 (8% coefficient of variation, number of spectra =9) and $514 \pm 1 \text{ nm}$ respectively. These results are a good indication of the homogeneous dispersion of the fluorophores into the host matrix that is of key importance to control the optical properties of the resulting material.

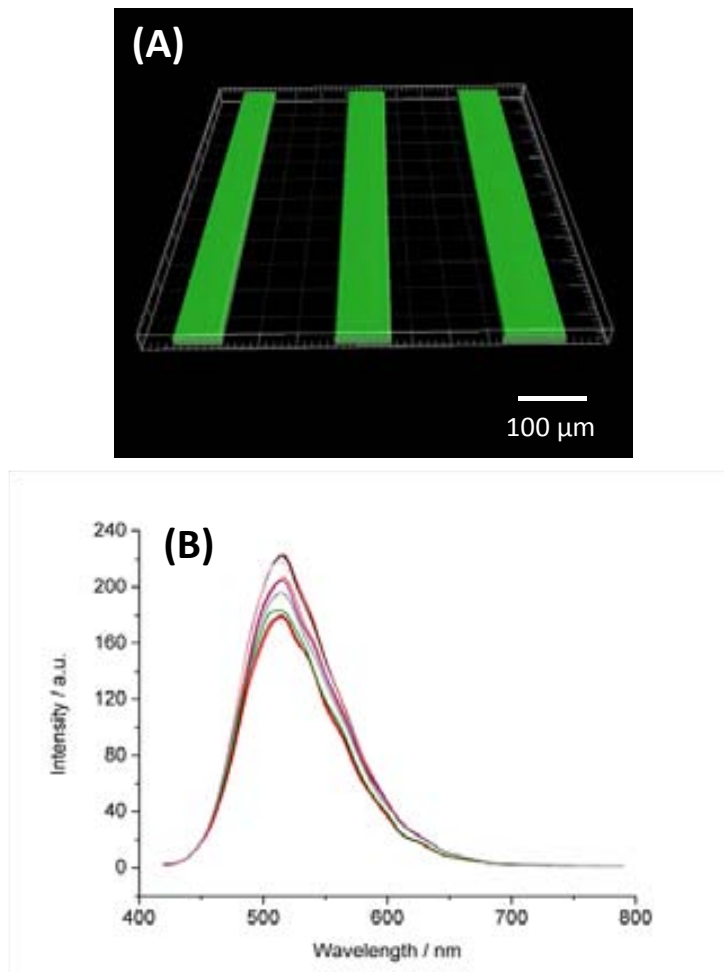


Figure 3. Optical characterization by confocal microscopy. (A) 3D reconstruction of the fluorescence intensity of Alexa-doped xerogel waveguides. (B) Emission spectra recorded at nine points of the waveguides.

3.4.3 Characterization of the xerogel microstructures

The quality of the microstructures in terms of uniformity, lack of surface defects and reliability of the replica from the PDMS mold was tested by optical, fluorescence and scanning electron microscopy. As mentioned above, the microfabrication process applied in this work combined with the tailored xerogel material allowed the definition of structures with different geometries and sizes, with heights ranging from 4 μm to 80 μm. In order to get a high yield in the fabrication of the xerogel patterns, all the process was carried out in a controlled environment, under clean room conditions, as pointed out above.

In Fig. 4, different bright field optical and fluorescence microscopy images of fluorophore-doped xerogel microstructures are depicted. Rhodamine B-doped xerogel 80 μm-high waveguides showing widths between 20-100 μm (A, E) and other 20 μm-high 1x4 multimode interference coupler (MMI) photonic structures (B, F) were fabricated as well as Alexa-doped xerogel 20-μm high mode converter like patterns (C, G) and 4-μm high curved waveguides (D, H). These images highlight the versatility of the presented material and the microfabrication approach. Also, the inclusion of the fluorophores did not appear to affect the replication

process of the xerogel microstructures. The SEM images in Fig. 5 show a highly accurate reproduction of the patterns in the PDMS mold. It also evidences that the material is smooth and crack free thus making it a suitable candidate for photonic applications.

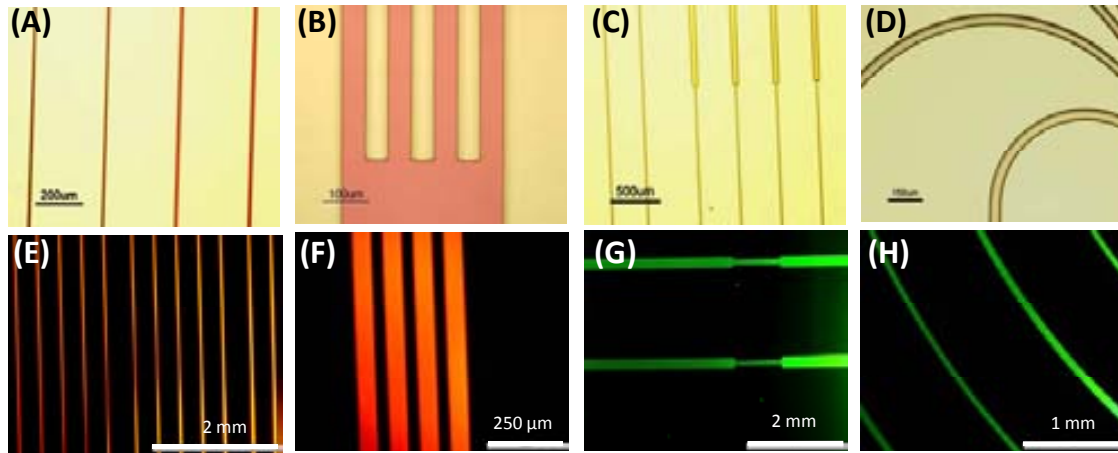


Figure 4. (A-D) Bright field optical and, (E-H) fluorescence images of microstructures fabricated using the Rhodamine B (A, B, E, F) and Alexa Fluor (C, D, G, H) -doped xerogel materials. The brighter areas in images G and H come from the residual light emitted by the thick layers of the material created at the sides of the microstructures during the MIMIC fabrication process.

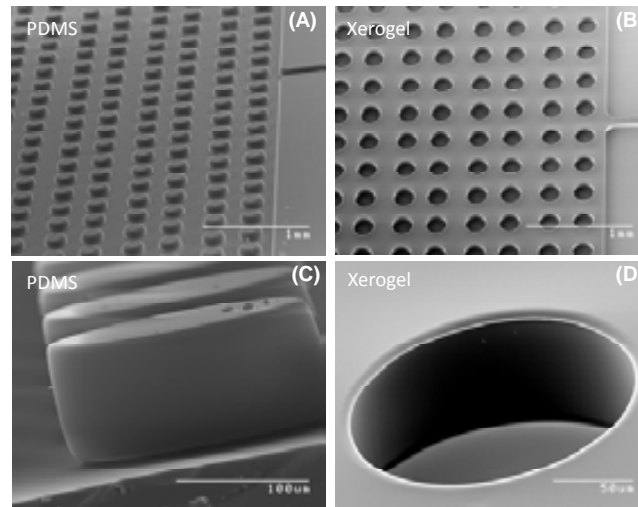


Figure 5. SEM images of the PDMS molds and the xerogel replicas. (a) Array of PDMS pillars, 80 μm high x 200 μm wide; (b) array of microwells of the same dimensions xerogel being the replica of the former mold; (c), (d) detailed images of PDMS micropillars and xerogel microwell. Samples were firstly sputtered with a 30-nm thick gold layer to avoid charging effects.

3.4.4 Optical characterization of the xerogel material and performance of waveguide microstructures.

In order to demonstrate the potential of this xerogel material and the fabrication approach presented herein for the development of photonic components, an evaluation of the xerogel optical properties and a

subsequent characterization of optical waveguides manufactured by MIMIC were carried out. A study of the material transparency was carried out with the non-doped xerogel material prepared as a 2 mm-thick monolith and using a spectrophotometer. Transmittance (T) values were recorded between 200-800 nm, with the %T being between 94 % at 300 nm (97 % at 400 nm) and 99 % at 800 nm and steadily decaying to 10 % below 300 nm. These results evidenced that this material is transparent over the entire visible spectra and extends to the near UV and near-IR regions.

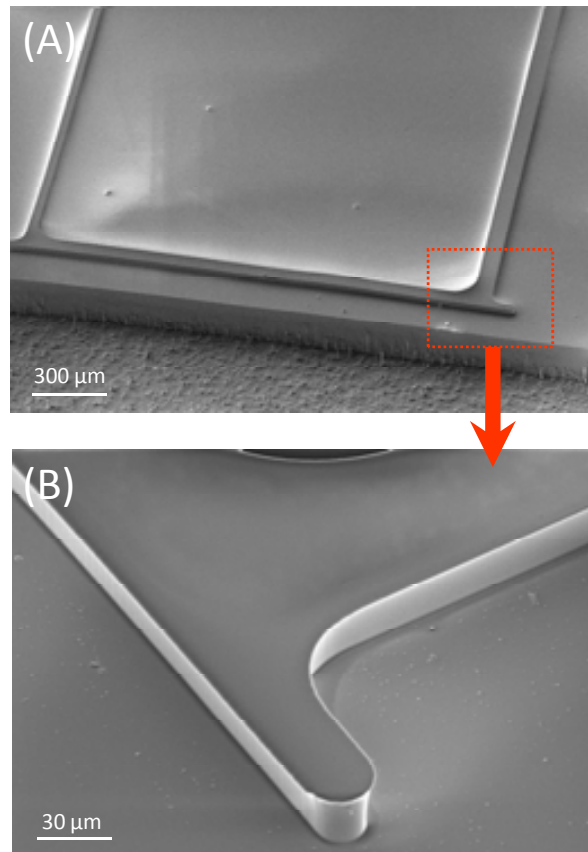


Figure 6. SEM images of the fabricated waveguides (A), and close-up view of the facet end (B).

Finally, the optical behavior of doped xerogel waveguides was studied. Using the second approach of the MIMIC process described in the experimental section, the waveguide facets are defined in the mold so that the cleaving process could be neglected. Thus, waveguides with perfectly defined dimensions were fabricated on $1.5 \times 1 \text{ cm}^2$ Si chips coated with a 2 μm -thick thermally grown SiO_2 layer, all of them being 35 μm high, 1.5 cm long. Five different waveguides were defined on the same chip having widths of 20 , 60 , 100 , 150 and 200 μm . These were fabricated using the non-doped xerogel as well as the Rhodamine B- doped and the Alexa Fluor-doped xerogel materials. SEM images in Figure 6 shows the good definition of both the waveguides and their corresponding facets. It can also be observed that a dead-end channel was defined at the outer waveguide side, with the aim of ensuring that the unstable meniscus that might be formed on the vertices of the channels were

completely filled by capillary action. All of them were optically characterized using the set-up described in the experimental section. Figure 7(A) shows two waveguides fabricated with the doped xerogel material pumping light. In both cases, the output light coming from the waveguide is clearly observed. This light was imaged by replacing the output fiber with a CCD camera (Pixelfly 200 XS VGA PCO AG, Germany) and is shown in Figure 7(B), which also evidenced the good confinement of the light propagating inside these structures.

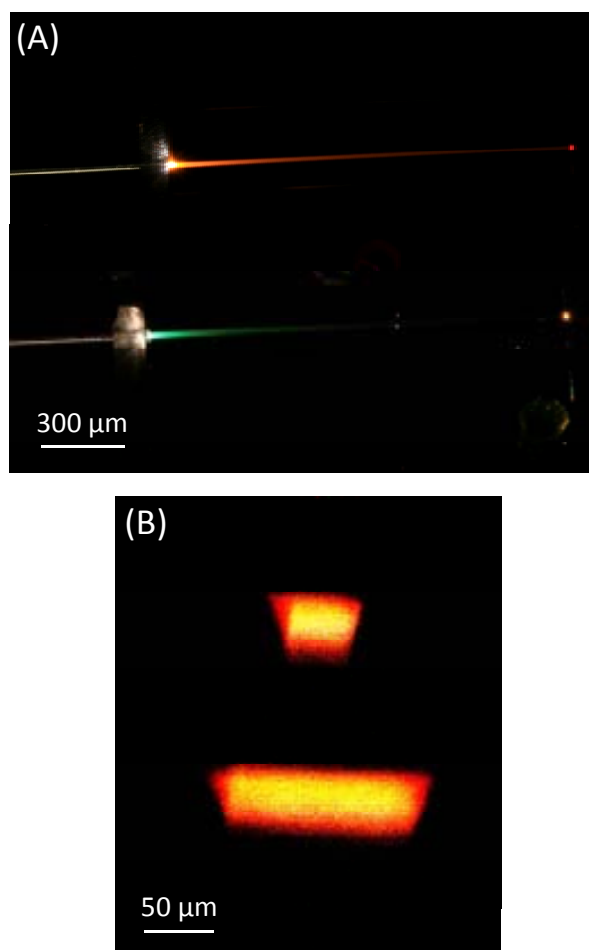


Figure 7. (A) Photograph of 60 μm-wide 100 μM Rhodamine B-doped xerogel and 150 μm-wide 100 μM Alexa -doped xerogel waveguides pumping light. (B) Output light recorded with both waveguides.

Fig. 8(A) shows the spectra recorded with a 200 μm-wide, 10^{-4} M Rhodamine B doped xerogel waveguide and its non-doped counterpart. A strong absorption between 550-600 nm and a significant reemission above 600 nm are observed. These wavelengths match with the maximum absorption/emission of Rhodamine B ($\lambda_{\text{absorption}} = 554$ nm, $\lambda_{\text{emission}} = 627$ nm). In Fig. 8(B) the signal at lower wavelengths corresponds to the recorded output light from the excitation blue LED recorded at the end of the non-doped xerogel waveguide. At higher wavelengths the emission band of Alexa ($\lambda_{\text{absorption}} = 434$ nm, $\lambda_{\text{emission}} = 539$ nm) is clearly visible. The same tests were carried out with the

waveguides showing different widths on a chip, and showed that the emission intensity was proportional to the waveguide cross-sectional area.

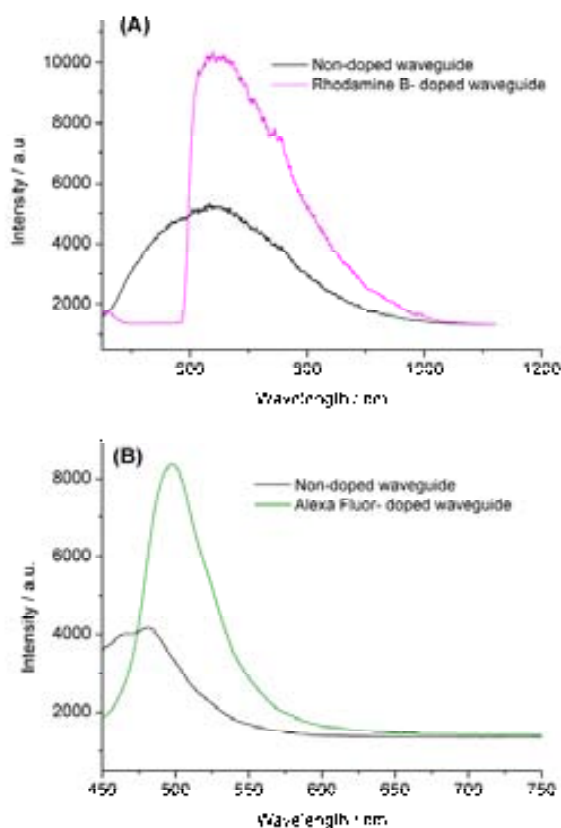


Figure 8. Spectral responses of 200 μm -wide non-doped xerogel and 10^{-4} M fluorophore-doped xerogel waveguides. (A) Rhodamine B and, (B) Alexa.

3.5 CONCLUSIONS

A simple approach for the low-cost fabrication of polymeric photonic components based on fluorophore-doped hybrid organic-inorganic polymers was developed. A thorough characterization of the material has been carried out demonstrating its good structural and optical properties. Different microstructures were fabricated by micromolding in capillaries soft lithography technique with high repeatability, reproducibility and reliability in the replication of the desired dimensions. Waveguides with different dimensions were easily fabricated and optically characterized. From the results shown in this work, it can be anticipated that this material and the proposed patterning process are a suitable approach for the fabrication of disposable photonic devices. Work is in progress in order to implement fluorophore-doped xerogel solid state light emitters in low-cost photonic lab on chip systems.

References

1. Sanchez, C., et al., *Optical properties of functional hybrid organic-inorganic nanocomposites*. *Advanced Materials*, 2003. **15**(23): p. 1969-1994.
2. Lebeau, B. and P. Innocenzi, *Hybrid materials for optics and photonics*. *Chemical Society Reviews*, 2011. **40**(2): p. 886-906.
3. Reisfeld, R., et al., *Solid-state lasers based on inorganic-organic hybrid materials obtained by combined sol-gel polymer technology*. *Polymers for Advanced Technologies*, 2004. **15**(6): p. 291-301.
4. Sanchez, C., et al., "*Chimie douce*": *A land of opportunities for the designed construction of functional inorganic and hybrid organic-inorganic nanomaterials*. *Comptes Rendus Chimie*, 2010. **13**(1-2): p. 3-39.
5. Seifert, A., et al., *Synthesis of dye functionalized xerogels via nucleophilic aromatic substitution of fluoro aromatic compounds with aminosilanes*. *Journal of Sol-Gel Science and Technology*, 2010. **53**(2): p. 328-341.
6. Yang, P.D., et al., *Mirrorless lasing from mesostructured waveguides patterned by soft lithography*. *Science*, 2000. **287**(5452): p. 465-467.
7. Wirnsberger, G., et al., *Patterned block-copolymer-silica mesostructures as host media for the laser dye rhodamine 6G*. *Journal of Physical Chemistry B*, 2001. **105**(27): p. 6307-6313.
8. Brusatin, G. and G. Della Giustina, *Hybrid organic-inorganic sol-gel materials for micro and nanofabrication*. *Journal of Sol-Gel Science and Technology*, 2011. **60**(3): p. 299-314.

Chapter IV

XEROGEL ABORBANCE MICRO-FILTERS

The work contained in this chapter has been reported in one paper entitled "*Development and integration of xerogel polymeric absorbance micro-filters into lab-on-chip systems*" [Ester Carregal-Romero, César Fernández-Sánchez, Alma Eguizabal, Stefanie Demming, Stephanus Büttgenbach, and Andreu Llobera, Optic Express, accepted.

4.1 SUMMARY

This work reports on the implementation of different optical micro-filters based on a hybrid organic-inorganic polymeric material synthesized by the sol-gel process. This xerogel has been dye-doped so as to selectively modify the spectral response of the polymeric material. Microstructures containing eight different filter widths were fabricated in polydimethylsiloxane (PDMS), bonded to glass substrates and filled with the corresponding dye doped polymeric material by a soft lithography approach. The filtering capacity as a function of dye concentration and filter width was studied and revealed a linear dependence with both parameters, as expected according to the Beer-Lambert law. Relatively sharp stopband regions and zero passband transmittance values were achieved in all cases. Finally, such filters were monolithically integrated into a disposable fluorescence-based photonic lab-on-a-chip (PhLoC) approach. Calibration curves carried out with a model fluorophore target analyte showed an over two-fold increase in sensitivity and a thirty-fold decrease of the limit of detection (LOD) compared with the values recorded using the same PhLoC system but without the polymeric filter structure.

4.2 INTRODUCTION

One of the most common analytical methods (both in micro and macroscale) is the measurement of fluorescence.^[1] Optical filtering is often required in this technique due to the following main reasons. In fluorescence spectroscopy the intensity of the excitation light is typically orders of magnitude larger than the fluorescence light of the fluorophore target molecule. Additionally, the Stokes shift of fluorophore molecules is usually very small, which makes it even more difficult to discriminate between the excitation and emission signals. The more accepted filtering configurations suitable to

perform such discrimination are based on interferometric and absorbance-based approaches.^[2] Interferometric filters consist in alternating layers of high- and low-refractive-index materials. In spite of these filters showing high absorbance levels at the stopband (blocked wavelengths) with sharp bands and zero passband (allowed wavelengths) penalties they suffer from serious drawbacks. First, the absorption depends on the angle of the incidence light.^[3] Second, the thickness of the layers has to be perfectly controlled in order to obtain filtering at the required wavelength, which makes the fabrication an expensive and critical process. When related to the integration of such filters into a PhLoC, these restrictions clearly hamper its integration. Conversely, absorbance filters are generally fabricated with a single layer of a material containing a chromophore^[4] or a band gap material.^[5] In both cases, they are fabricated to show high absorption at the excitation wavelength and low absorption at the fluorescence wavelength of the solution or compound being measured. The performance of such absorbance filters is governed by the Beer-Lambert law and, unlike interferometric filters, their response is independent of the beam incidence angle.^[2] Because of their simplicity, robustness and low cost, these filters are more suitable for being integrated into disposable PhLoCs, although their optical properties are more limited when compared with their interferometric counterparts. The material synthesis and fabrication processes can also be designed to be simple and not time-consuming.

Several attempts have been previously reported for this configuration. Hoffman *et al.*^[6] used a millimeter-thick dye-doped PDMS film as a fluorescence filter. In order to get an adequate dispersion of the dye in the polymer matrix they use toluene, a toxic solvent that has to be completely removed if the system is being used for bio-applications. In a previous work of the group, this problem was overcome^[7] by fabricating PDMS-based filters of varying width using red, green and blue ink directly mixed with the PDMS pre-polymer solution. However, the resulting filters exhibited broad stop band values (ranging from 100 to 150 nm) and non-zero passband values, which limit their applicability. Yamazaki *et al.*^[8] reported colored filters based on a porous titanium oxide film onto which a monolayer of dye molecules was defined. The fabrication involves the sintering of a titania film at 450^o C, which limits their compatibility with polymeric substrates and/or low temperature fabrication methods, making difficult the implementation of these filters into low-cost microsystems. Richard *et al.*^[9] presented an integrated hybrid absorption and interference filter based on a dye doped epoxy-based photoresist, obtaining with the absorption layers high rejection levels at the stopband with short optical path lengths(0.8-2 μm). Nevertheless, these filters can only act like high-pass filters (wavelengths larger than 650 nm) with broad stopband widths (> 250 nm) limiting their applicability in fluorescence detection since most common analytes show emission wavelengths below this value. Moreover, at the optimized maximum dye concentration they did not succeed in developing patterns (e.g. channels), and also the photoresist solvents make

this approach not biocompatible. An alternative absorbance filtering approach that circumvents the drawbacks of those above-mentioned absorbance filter approaches is described in this chapter.

4.3 DESIGN OF THE TEST MICROSTRUCTURE

A 230- μm thick filter test microstructure to be fabricated in PDMS was designed as a single continuous microfluidic system with its width varying downstream. Once filled with the polymeric material, it gives rise to several filter structures with the same dye concentration but varying optical path, as explained below (Figure 1 (a)). One of the major advantages of such structure is that identical experimental conditions are applied in the fabrication of all the filters included in the same microfluidic structure. Then, more reliable comparative studies can be carried out. In order to test the influence of the optical path length in the filtering properties, eight different widths were defined, i.e. 100, 250, 500, 1000, 1500, 2000, 2500 and 3000 μm . The filter channel also included two microfluidic ports at both ends for adequate structure filling with the pre-polymerization solution. Inlet and outlets were designed as holes on the surface of the mold thus avoiding the accumulation of residual material at both sides of the mold. These top holes also reduced the quantity of pre-polymerization solution needed to block the apertures (in order to prevent the emptying of the structure due to shrinkage during drying) due to their small size, circular shape and position. Xerogel materials tend to shrink when they are synthesized due to the loss of volume caused by solvent evaporation. In this context, diamond-shaped widenings were designed at both sides of the filling channel that act as internal pre-polymerization solution reservoirs for re-filling of the filtering channel during the polymerization process and thus preventing the formation of air bubbles that could distort the resulting filter structures. The test structure is completed with self-alignment channels for positioning of the input and output optical fibers at both sides of each filter, together with micro-lenses at the end of every self-alignment channel for correcting the numerical aperture of the used fiber optics and achieve parallel beams.^[10]

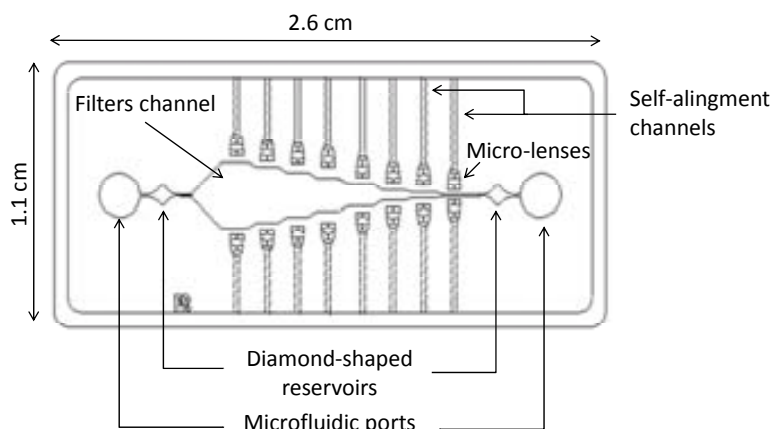


Figure 1. Design of the mask employed to fabricate the test microstructure.

4.4 FABRICATION

4.4.1 Material synthesis

The pre-polymerization solution (*sol*) was prepared by mixing phenyltrimethoxysilane (PhTMOS) monomer (Sigma-Aldrich Química S.A., Spain) with dye aqueous solutions at pH 3 (adjusted with diluted HCl). Four different dye concentrations in the aqueous solution were used: 10, 50, 100 and 200 μ M. The silane:water molar ratio was 1:6. The selected dyes for this study were quinoline yellow (QY), phenol red (PR), methyl orange (MO) and crystal violet (CV) (all of them from Sigma-Aldrich Química S. A., Spain), whose absorbance bands show maximum absorbance values at 420, 515, 530 and 600 nm wavelengths, respectively. These dyes were selected to cover most of the visible spectrum. Except QY, these dyes are pH sensitive, showing different color for the acidic and the basic form. PR color changes from yellow to red (pH, 6.8-8.0), MO from red to orange-yellow (pH 3.1-4.4) and CV from yellow to blue (0.0-1.8). The mixture was gently stirred using a magnet until a homogeneous solution was achieved (this homogenization takes 4h approximately). At this point the resulting *sol* solution was ready for filling the test microstructure.

4.4.2 Fabrication of the test microstructure

The structure from which the eight micro-filters were obtained was fabricated by an adaptation of the micromolding in capillaries (MIMIC) soft lithographic technique. The master was developed using the SU-8 photocurable polymer in a one-step photolithographic process and following a similar process to that described in chapter II. SU-8 2025 (Microresist Technology GmbH, Berlin, Germany) was used to obtain a layer with a thickness of 230 μ m by spin-coating (more detailed description of the photolithography process can be found in ref. [11]). PDMS pre-polymer solution (Sylgard 184 elastomer kit, Dow Corning Corp, Midland, MI) used for the replication of the master was made by mixing the silicon elastomer with the curing agent in a 10:1 ratio (v:v). Then, it was carefully poured over the SU-8 master. Once cured at 80 $^{\circ}$ C for 20 minutes, the PDMS was peeled off the master with the aid of tweezers. The resulting PDMS test structures were irreversibly bonded to glass slides by a conventional oxygen plasma process.^[12] For the sealing, both PDMS and glass surfaces received a plasma treatment. That is, they were placed in a barrel etcher and exposed to oxygen plasma (75 sccm O₂, 85 W, 12s), (300E plasma processor, Tepla, Wettenberg, Germany). The fluidic ports included in the test structures, as described above, were opened and the microstructure was filled with the *sol* solutions. Filling was achieved by capillary forces starting from the side with the largest width, thus avoiding the use of external pumps. The polymer was left to cure and dry at room temperature for 4-5 days. The curing time could be reduced to 1 h by applying a temperature of 80 $^{\circ}$ C,

without observing any alteration of the resulting material structure. The dye-doped xerogel structure was thus formed and the filters were ready to be tested. Figure 2 shows a picture of polymeric micro-filters fabricated in the PDMS test structure using a xerogel polymer doped with a 200 μM CV solution.



Figure 2. Picture of Crystal Violet doped xerogel micro-filters.

4.5 MATERIAL & STRUCTURAL CHARACTERIZATION

In order to give some insight into the resulting doped polymer matrix structure, FT-Infrared Spectroscopy (Tensor 27 FT-IR spectrophotometer including a MKII Golden Gate™ Single Reflection ATR module, Bruker Corporation, Germany), ^{29}Si -Magnetic Nuclear Resonance (^{29}Si -NMR single-pulse (SP) solid state magic angle spinning nuclear magnetic resonance, Bruker Avance 400 spectrometer, Bruker Corporation, Germany) and Scanning Electron Microscopy (SEM) (LEO 1530 Gemini, Carl Zeiss, Oberkochen, Germany) studies were carried out. Measurement of dye-doped and non-doped xerogel refractive indexes was kindly carried out by Metricon Corporation (NY,USA) using the Metricon Model 2010/M Prism Coupler equipment, which determines the refractive index from (m-line) layer modes.^[13]

The material transparency was also tested by collecting light passing through a drop-coated xerogel glass slide. The result of the latter experiment is shown in Fig. 3. As it can be seen, the material is transparent over the entire visible spectrum and near infrared region.

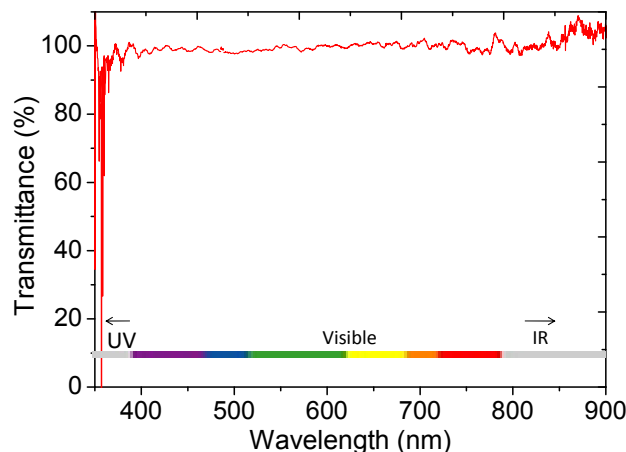


Figure 3. Picture of Crystal Violet doped xerogel micro-filters.

^{29}Si -NMR spectroscopy study provides information about the degree of condensation in the resulting polysiloxane matrix.^[14-15] The number of siloxane bonds that surround each silicon atom is determined from characteristic signals. Si atoms from PhTMOS can only form a maximum of three bonds and are responsible for T^n signals where n is the number of oxygen atoms bonded to silicon and forming siloxane bridges (Si-O-Si) with adjacent silicon atoms. These signals have been widely observed when analyzing xerogel materials with different compositions. Here, the ^{29}Si -NMR spectrum of the non-doped xerogel (Figure. 4) signals at -69.8 ppm and -79.5 ppm were assigned to T^2 and T^3 , respectively. The relative area of the T^3/T^2 signals in this material are 43/57, which indicates a high degree of condensation with 43% of Si atoms involved in three siloxane bonds. The spectrum of the dye-doped (CV) xerogel (Figure. 4) showed the same displacement for the two signals but with different areas. The polycondensation of hydrolyzed PhTMOS seem to be slightly affected by the addition of the CV dye with 49% of Si atoms involved in three siloxane bonds resulting in a more cross-linked structure than the one of the non-doped material. This difference is likely to be related to the acid base nature of the dye, which nonetheless may have a positive influence in the avoidance of dye leaching from the polymer network.

The FT-IR study (Figure. 5) revealed that the incorporation of the dye into the polymer matrix has a negligible effect on the polymeric structural properties. FTIR spectra for both non-doped and dye-doped material show the characteristic and identical bands for the bending and stretching of the Si-O bond (in the zone of 1000 cm^{-1}) as well as characteristic bands ascribed to the phenyl ring (C=C, 1600 cm^{-1} and 1475 cm^{-1} , C-H, $3150\text{-}3050\text{ cm}^{-1}$). If the inclusion of dyes had altered the polymeric process and thus the resulting xerogel composition this would have been reflected in the disappearance and/or formation of bands in the spectra. SEM images were also recorded and showed a smooth and crack-free xerogel material that perfectly replicated the pattern on the PDMS stamp.

The refractive index of both the non-doped and dye-doped xerogel materials, measured at $\lambda = 633\text{ nm}$ was 1.5663 ± 0.0001 ($n = 6$), which again corroborates the negligible effect of the doping process on the xerogel optical and structural properties.

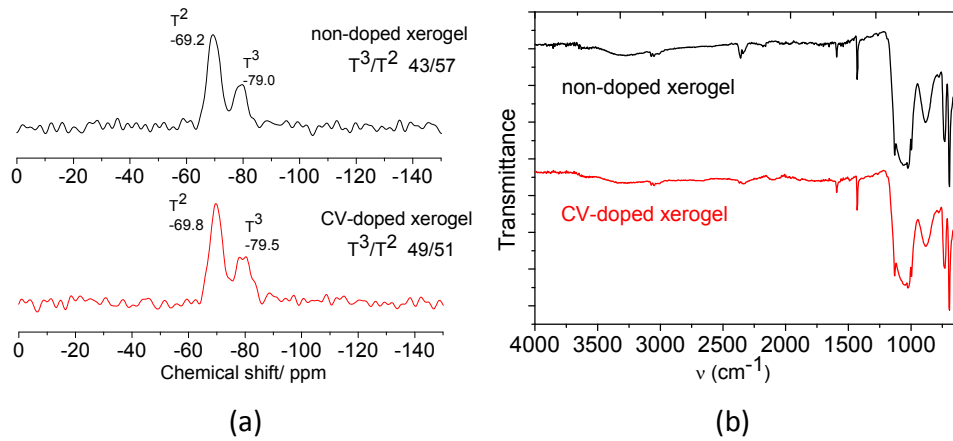


Figure 4. (a) ^{29}Si -MNR Spectra of the non-doped and crystal violet-doped hybrid polymer. (b) FT-Infrared Spectroscopy spectra of the non-doped and dye-doped hybrid polymer.

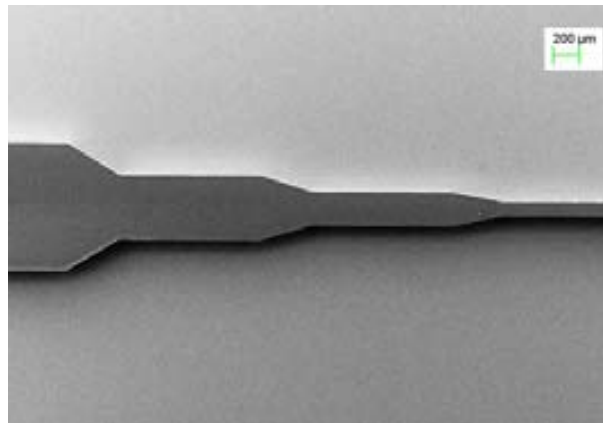


Figure 5. SEM image of 100, 250, 500 and 1000 μm side xerogel microfilters fabricated in the same microstructure.

4.6 SPECTRAL ANALYSIS

The setup for the analysis is shown in Figure 6 and included a broadband halogen lamp as light source (HL-2000, Ocean Optics, Dunedin, FL, USA), two 230 μm diameter multimode optical fibers (Thorlabs Inc., Dachau, Germany) for coupling and collecting the light and a microspectrometer (QE 65000-FL, Ocean Optics, Dunedin, FL, USA). All filters were scanned in a wavelength region between 300 and 1000 nm with an integration time of 50 ms. The non-doped xerogel filter microstructure was fabricated and measured under the same experimental conditions and used as a reference.

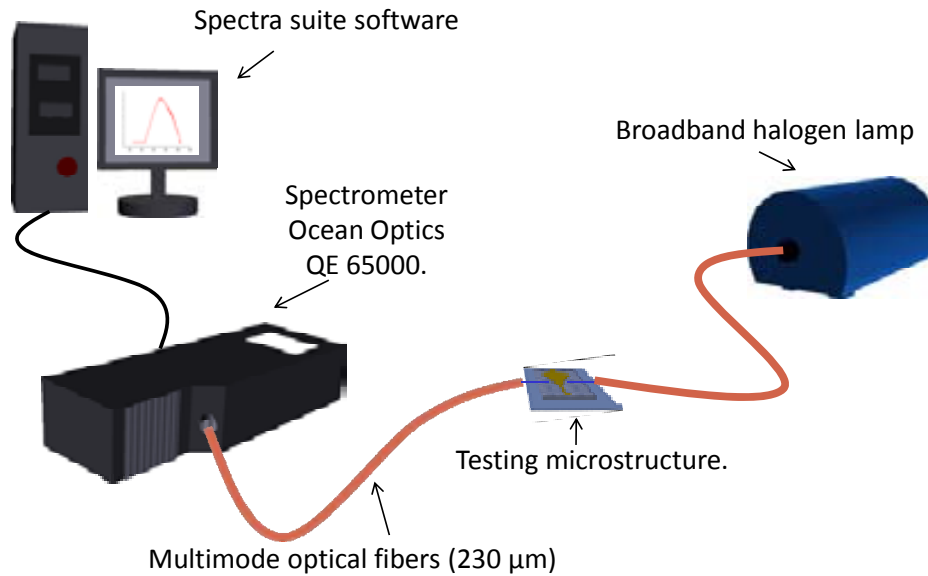


Figure 6. Set up for the optical characterization

Two of the most important parameters to characterize a filter are the rejections levels at the stopband (blocked wavelengths) and the transmission levels at the passband (allowed wavelengths).^[2] Figure 7 illustrates the transmittance values for the 200 μM dye-doped, 3000 μm wide filters. Minimum transmittance values at the stopband vary from -7 dB (for MO) to values below the dynamic range limit of our experimental setup (which was measured to be -26 dB) for CV (see Table 1). In the case of CV-based filters only an estimation of the transmittance can be provided. Here, by fitting the transmittance dependence with the filter width to an exponential decay function, the maximum transmittance values for the 2000, 2500 and 3000 μm-wide filters can be estimated to be -28.7, -30.7 and -31.9 dB, respectively. By comparing these values with the ones recorded in our previous work (where transmittance values at the stopband were between -2 dB and -24 dB), a clear improvement was attained. They also outperformed those ones reported by Yamazaki *et. al.*,^[8] who recorded transmittance values between -6 dB and -20 dB with dye-modified titanium oxide filters. In addition, they are of the same order of magnitude to these reported with dye doped photoresist based filters fabricated by Richard *et. al.*,^[9] which showed values from -5 dB to -32 dB. The state-of-the-art in integrated absorbance-based filters generally includes approaches with broad absorption bands that restrict their applicability to high-pass filters.^[6-9] By contrast, this work reports xerogel-based absorbance microfilters with almost zero passband values (Table 1) and relatively sharp stopbands (Figure.7) . It should be noted that the nature of the dye determined the absorption capacity and the working wavelength, resulting in very different transmittance values for the same dye concentration and filter width.

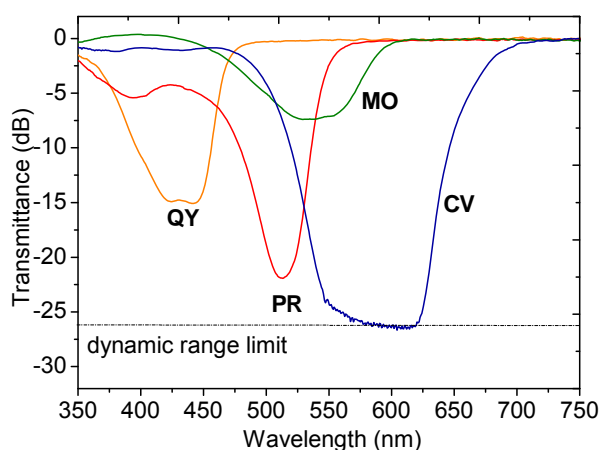


Figure 7. Transmittance vs. wavelength for four different 200 μM dye-doped, 3000 μm wide filters.

Table 1. Stopband and passband transmittance values of the 3000 μm wide filters fabricated with the doped xerogel material (200 μM).

Dye	Stopband		Passband	
	λ [16]	Transmittance [dB]	λ [16]	Transmittance [dB]
Quinoline Yellow	420	-14.7	530	-0.2
Phenol Red	515	-21.8	575	-0.2
Methyl Orange	530	-7.4	650	-0.2
Crystal Violet	600	-31.9*	700	-0.5

* Theoretically estimated value

As previously discussed, the dyes selected in this work covered most of the visible spectrum. Nevertheless, other hydrosoluble dyes could also be incorporated in the same polymeric material, as could be aniline blue (with a maximum absorption wavelength at 620 nm). Specific selection of the dye would basically depend on the required wavelength filtering and application.

The overall dimension of the filter is one of the most important premises from the miniaturization and integration point of view. It is clear that the longer the optical path, the higher the absorption but this assumption goes against integration. This issue can be tackled by increasing the dye concentration for a fixed optical path. Figure 8 illustrates the transmittance values of the filters at the stopband wavelength as a function of filter width and dye concentration. A linear trend is observed in all cases as expected according to the Beer-Lambert law. For filters showing a width of 2000 μm and above, as well as for these containing the highest dye concentration, saturation was reached in all cases. Most importantly, passband values still retain the value close to zero for all the tested filters. This effect can be observed in Tables A1-A4 (see Appendix) that includes the transmittance values at the passband and stopband regions recorded with all the tested structures. These results show that the dyes are

homogeneously dispersed into the xerogel matrix without causing aggregates or phase separation, which may lead to scattering centers, and therefore decrease the transmittance in the passband region, as it was the case in a previous work of our group with ink-doped PDMS.^[7]

Figure 9 (a) shows the recorded transmittance spectra of 3000 μm -wide filters fabricated with the xerogel material doped with different concentrations of PR. The expected decrease in transmittance values at the stopband as the dye concentration increases is observed. Additionally, a secondary stopband, associated with the yellow acidic form of PR can be observed at short wavelengths (close to 450 nm). An almost zero passband value is also shown in Figure. 9 (a), which means that the material exhibits a high transparency at wavelengths above 570 nm. The same study was carried out with these filters fabricated with the xerogel doped with QY, MO and CV and results are shown in Figure. 9 (b-d).

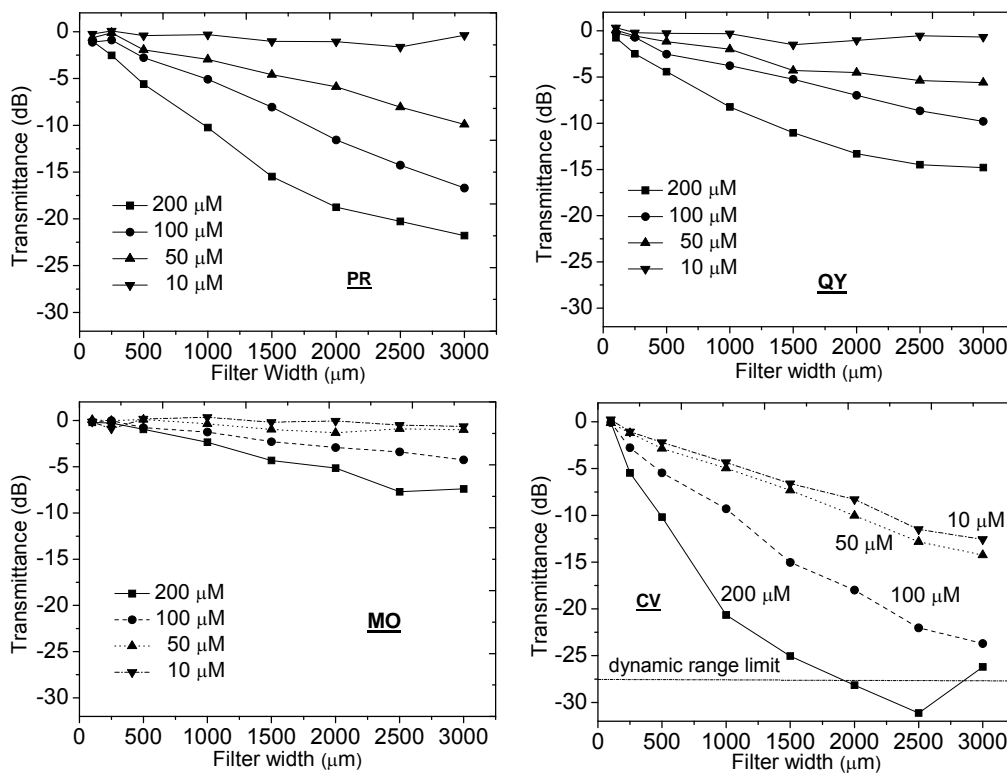


Figure 8. Transmittance as a function of filter width for the phenol red (PR), quinoline yellow (QY), methyl orange (MO), and crystal violet (CV), loaded filters for concentrations ranging between 10 and 200 μM .

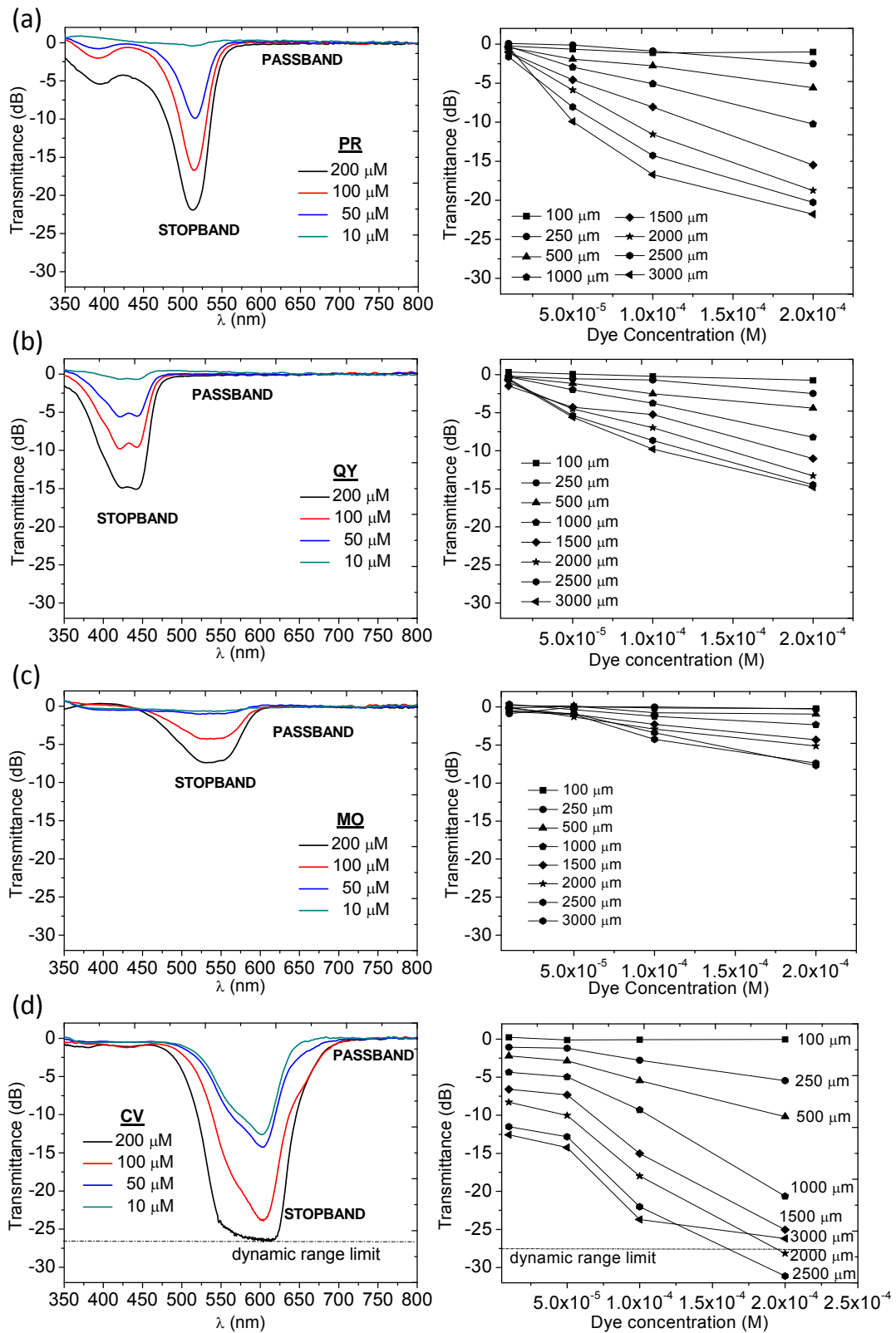


Figure 9. Left column: transmittance vs. wavelength for the four different 3000 μm wide filters. Right column: minimum transmittance values vs. dye concentration for the eight different filter widths. For: (a) phenol red, (b) quinoline yellow, (c) methyl orange, and (d) crystal violet.

4.7 INTEGRATION OF THE FILTERS IN A PhLoC

Once the viability of developing low-cost absorbance-based microfilters was shown, the following step involved their monolithic implementation in a PhLoC system. For this purpose, the microdevice presented in Figure. 10 was designed and then fabricated using the same soft lithographic approach described above for the development of the filter test microstructures. Rhodamine B ($\epsilon = 106.000 \text{ cm}^{-1}\text{M}^{-1}$) was selected as a model target analyte to be measured in the PhLoC system. The reasons for selecting this target analyte are two-folded. Firstly, the absorption band can be used for calibrating the response of the PhLoC to analytes that have a specific absorption band but do not show photonic re-emission (as could be colorants or indicators).^[17] Secondly, the emission band can also be studied to validate the technological filtering approach presented in this work for measuring analytes with photonic re-emission (as could be quantum dots or fluorophores). The absorption and emission bands of Rhodamine B fluorophore are centered at 540 nm and 616 nm, respectively.

Among the different filters fabricated and characterized, the one that best fits for the measurement of this fluorophore is the PR-doped, which, as shown in the previous section, has a sharp stopband, from 450 nm to 540 nm (with maximum absorption at 515 nm) and an almost zero passband value outside this range. It was also discussed how the wider the filter, the higher the stopband value. Nevertheless, keeping in mind that the aim of this work is to develop a filter suitable to be integrated in a PhLoC, a compromise between the overall dimensions of the filter and the filtering capability has to be reached. In our case, we selected a filter width of 800 μm fabricated with the xerogel material doped with the highest concentration of PR tested. It could be anticipated that this filter configuration would be suitable for our purposes considering the values of the stopband attained with a 1000 μm -wide filter (-10.2 dB@515 nm). Taking into account the previously shown Beer-Lambert behavior of all the filters tested, transmittance values of -8.2 dB at the stopband and almost zero at the passband were expected for this filter width. Two readout channels (for the alignment of the collection optical fiber) located at 90° and 180° from the input channel (injection optical fiber) were included in the microdevice. However, with the aim of performing the test in the less favorable conditions possible, only the most challenging configuration of 180° between injection and collection optical fibers was used.

Eight different solutions of the Rhodamine B fluorophore prepared in deionized (DI) water in a concentration range from 25 μM to 500 μM were sequentially injected into the microfluidic channel (60 μm width). The set-up used is shown in Figure. 11. It included a 100 mW monochromatic green light (532 nm, Laser module NANO 250-532-

100, Linos Photonics, Germany) as light source. The light was coupled into the system by a 230 μm in diameter multimode optical fiber (Thorlabs, Dachau, Germany) and collected by an identical one. The collection fiber was positioned in the self-alignment channel located after the PR filter. Thus, light passed through the filter before reaching the spectrometer. Figure. 10 shows a picture of one of the fabricated microdevices, where several filtering structures can be seen together with self-alignment channels and the microfluidic channel filled with a Rhodamine B solution.

For comparative purposes, two identical systems were measured, the only difference being the presence of either a non-doped or a PR doped xerogel acting as a filter. For each dilution absorbance and fluorescence spectra were recorded. The linear fit was carried out and the limit of detection (LOD) calculated following the IUPAC criteria. This states that the LOD is not the lowest detectable analyte concentration, but also depends on both the sensitivity and the accuracy of the linear fit, thus being determined as the least concentration of analyte for which the signal exceeds by a factor of 3 the relative standard deviation of the background signal divided by the slope of the calibration curve.^[18]

Absorbance vs. Rhodamine B concentration showed in Figure. 12(a) shows the expected linear trend in accordance with the Beer-Lambert law at a wavelength of 540 nm. When compared the results recorded using identical PhLoCs with and without the integrated filter (Table 2), it can be seen that the performance of the former has been significantly improved, with a three-fold increase in sensitivity while the LOD was reduced by 35%. This enhancement can be understood considering that the PR filters eliminates background light that causes random variations of the readout signal.

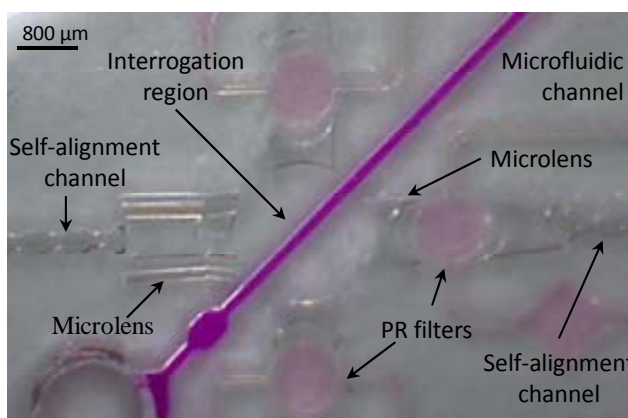


Figure 10. Image of the fluorescence LOC with integrated dye-doped polymeric filters.

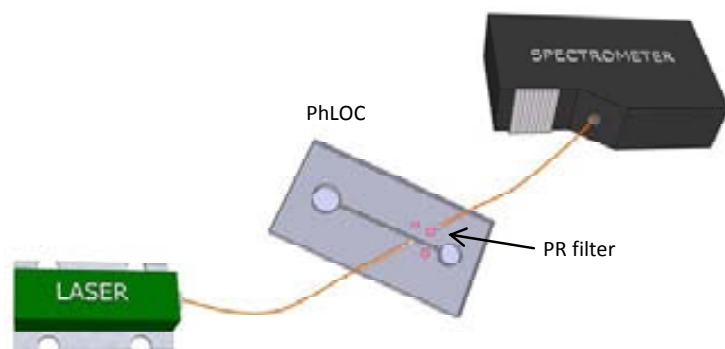


Figure 11. Setup used to carry out the measurements of Rhodamine B target analyte in the PhLOC where the phenol-red based filters were implemented. It comprises a laser working at a wavelength 532 nm, two multimode optical fibers and a spectrometer

Fluorescence vs. Rhodamine B concentration was also studied, and the results are shown in Figure 12(b) and Table 6. It can be seen how the integration of the PR filters is key to carry out fluorescence measurements in the system. When the filters were not included, the sensitivity (slope of the calibration curve) can be considered to be zero, and the LOD has a value higher than the concentration range measured, which basically means that it is not possible to determine the fluorescence emission of the target analyte. By contrast, when the PR-doped xerogel filter was included, a linear trend between Rhodamine B concentration and fluorescence measured at 616 nm was clearly obtained in a concentration range between 25 μM and 350 μM , the estimated limit of detection being $29 \pm 1 \mu\text{M}$. This value compares well with the ones reported by Yamakazi *et. al.*,^[8] who positioned 500 μm path-length cuvettes containing different concentrations of Rhodamine 6G on top of different absorbing layers. They reported LODs of 1.9 μM and 2.5 μM , similar to the one we obtained taking into account the difference in path lengths and the slightly higher extinction coefficient of Rhodamine 6G ($\epsilon = 116.000 \text{ cm}^{-1}\text{M}^{-1}$). When comparing these results with these previously reported, it can be seen that these xerogel-based absorbance filters outperform our previous ink-doped PDMS absorbance filters, while retaining the easy integration and the low cost issues.^[7] Other contributions regarding optical filters for PhLoC applications can be highlighted, as could be Pais *et. al.*,^[19] who reported a 0.1 μM LOD measuring Rhodamine 6G in a disposable lab-on-chip including a cross polarization scheme, and Yao *et. al.*^[20] who reported a 13-fold increase in sensitivity for a 300 μM Rhodamine 6G solution by implementing an interference filter in a microfluidic device. Nevertheless, both approaches rely on either expensive technological steps and/or the alignment of several elements, which hampers the filter applicability in disposable microsystems. By contrast, in the approach presented in this work, the validity of the proposed xerogel-based absorbance filters was assessed as suitable low-cost optical components that are inherently self-aligned and can be incorporated into disposable fluorescence-based photonic lab on chip system.

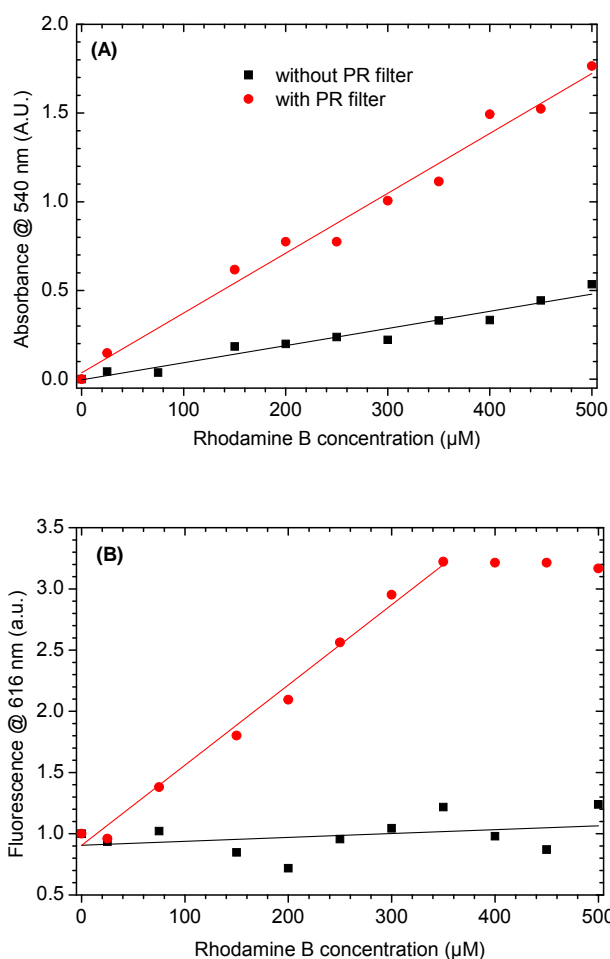


Figure. 12 (a) Absorbance as a function of Rhodamine B concentration measured at 540 nm. (b) Fluorescence emission as a function of Rhodamine B concentration measured at 616 nm. Fluorescence values were normalized considering fluorescence to have a unity value when the microchannel was filled with DI water.

Table 2. Linear fits, R^2 and LOD of the PhLoC with and without Phenol red filter used during the Rhodamine B calibration

	Linear fit	R^2	LOD (μM)
Abs ₅₄₀ without PR filter	$\text{Abs}_{540} = (9.7 \pm 0.7) \times 10^{-4} C - (3.4 \pm 0.1) \times 10^{-3}$	0.95	65 ± 4
Abs ₅₄₀ with PR filter	$\text{Abs}_{540} = (3.4 \pm 0.1) \times 10^{-3} C - (3 \pm 4) \times 10^{-2}$	0.98	42 ± 2
Fluo ₆₁₆ without PR filter	$\text{Fluo}_{616} = (3 \pm 3) \times 10^{-4} C - (9.0 \pm 0.8) \times 10^{-1}$	0.03	763 ± 658
Fluo ₆₁₆ with PR filter	$\text{Fluo}_{616} = (6.5 \pm 0.3) \times 10^{-4} C - (9.0 \pm 0.6) \times 10^{-1}$	0.99	29 ± 1

4.8 CONCLUSIONS

It has been demonstrated that low-cost absorption micro-filters could be easily fabricated using a dye-doped xerogel hybrid polymer material with a simple soft-lithographic approach. The presented tailor-made hybrid organic-inorganic polymeric material is compatible with several dyes, which enables the development of filters covering a wide wavelength range of the visible spectrum. The fabricated micro-filters showed low transmittance values at the stopband, reaching the dynamic range limit of the spectrometer in some cases. Passband transmittance values are close to zero in all cases. Filtering capacity of these filters was consistent with the Beer-Lambert law in all cases and strongly depends on the nature of the dye. The successful integration of these polymeric absorbance micro-filters in a fluorescence based disposable PhLoC was also demonstrated by carrying out calibration studies using Rhodamine B as model fluorophore target analyte and showing the performance enhancement of the system as compared to an identical PhLoC without xerogel filters. In addition, it has been shown that this filtering approach outperforms other previously reported structures considering the attained stopband (as compared to existing high-pass absorbance filters) as well as the ease of their fabrication and integration in analytical microsystems.

References

1. Borisov, S.M. and O.S. Wolfbeis, *Optical biosensors*. Chemical Reviews, 2008. **108**(2): p. 423-461.
2. Dandin, M., P. Abshire, and E. Smela, *Optical filtering technologies for integrated fluorescence sensors*. Lab on a Chip, 2007. **7**(8): p. 955-977.
3. Macleod, H.A., ed. *Thin Film Optical Filters*. 2001, Institute of Physics Publishing: London.
4. Chabinyk, M.L., et al., *An integrated fluorescence detection system in poly(dimethylsiloxane) for microfluidic applications*. Analytical Chemistry, 2001. **73**(18): p. 4491-4498.
5. Mahan, A.H., et al., *On the influence of short and medium range order on the material band gap in hydrogenated amorphous silicon*. Journal of Applied Physics, 2004. **96**(7): p. 3818-3826.
6. Hofmann, O., et al., *Monolithically integrated dye-doped PDMS long-pass filters for disposable on-chip fluorescence detection*. Lab on a Chip, 2006. **6**(8): p. 981-987.
7. Llobera, A., et al., *Monolithic PDMS passband filters for fluorescence detection*. Lab on a Chip, 2010. **10**(15): p. 1987-1992.
8. Yamazaki, M., et al., *Non-emissive colour filters for fluorescence detection*. Lab on a Chip, 2011. **11**(7): p. 1228-1233.
9. Richard, C., et al., *An integrated hybrid interference and absorption filter for fluorescence detection in lab-on-a-chip devices*. Lab on a Chip, 2009. **9**(10): p. 1371-1376.
10. Llobera, A., R. Wilke, and S. Buttgenbach, *Poly(dimethylsiloxane) hollow Abbe prism with microlenses for detection based on absorption and refractive index shift*. Lab on a Chip, 2004. **4**(1): p. 24-27.

11. Llobera, A., et al., *Multiple internal reflection poly(dimethylsiloxane) systems for optical sensing*. Lab on a Chip, 2007. **7**(11): p. 1560-1566.
12. Jo, B.H., et al., *Three-dimensional micro-channel fabrication in polydimethylsiloxane (PDMS) elastomer*. Journal of Microelectromechanical Systems, 2000. **9**(1): p. 76-81.
13. Ulrich, R. and R. Torge, *MEASUREMENT OF THIN-FILM PARAMETERS WITH A PRISM COUPLER*. Applied Optics, 1973. **12**(12): p. 2901-2908.
14. Glaser, R.H., G.L. Wilkes, and C.E. Bronnimann, *Solid-state ²⁹Si NMR of TEOS-based multifunctional sol-gel materials*. Journal of Non-Crystalline Solids, 1989. **113**(1): p. 73-87.
15. Lacan, P., C. Guizard, and L. Cot, *CHEMICAL AND RHEOLOGICAL INVESTIGATIONS OF THE SOL-GEL TRANSITION IN ORGANICALLY-MODIFIED SILOXANES*. Journal of Sol-Gel Science and Technology, 1995. **4**(2): p. 151-162.
16. Pang, L., et al., *Photosensitive quantum dot composites and their applications in optical structures*. Journal of Vacuum Science & Technology B, 2005. **23**(6): p. 2413-2418.
17. Llobera, A., R. Wilke, and S. Buttgenbach, *Optimization of poly(dimethylsiloxane) hollow prisms for optical sensing*. Lab on a Chip, 2005. **5**(5): p. 506-511.
18. Thomsen, V., D. Schatzlein, and D. Mercurio, *Limits of detection in spectroscopy*. Spectroscopy, 2003. **18**(12): p. 112-114.
19. Pais, A., et al., *High-sensitivity, disposable lab-on-a-chip with thin-film organic electronics for fluorescence detection*. Lab on a Chip, 2008. **8**(5): p. 794-800.
20. Yao, B., et al., *A microfluidic device using a green organic light emitting diode as an integrated excitation source*. Lab on a Chip, 2005. **5**(10): p. 1041-1047.

Appendix

Table A1. Spectral properties of phenol red filters. Positive values for transmittance shown in this table and the following ones may be associated to small misalignments when measuring the reference test structure (non-doped xerogel filter structures).

Dye concentration (μM)	Thickness [μm]	Stopband region		Passband region		$T_s - T_p$
		λ [nm]	Transmittance (T_s) [dB]	λ [nm]	Transmittance (T_p) [dB]	
10	100	515	-0.2	570	-0.2	0.0
	250		0.1		0.2	-
	500		-0.4		0.0	-0.4
	1000		-0.3		0.0	-0.3
	1500		-1.0		-0.1	-0.9
	2000		-1.1		0.0	-1.1
	2500		-1.6		-0.2	-1.4
	3000		-0.4		0.3	-
50	100	515	-0.6	570	-0.4	-0.2
	250		-0.1		0.2	-
	500		-1.9		-0.3	-1.6
	1000		-3.0		-0.1	-2.9
	1500		-4.6		0.0	-4.6
	2000		-5.9		0.1	-
	2500		-8.0		-0.2	-7.8
	3000		-9.9		0.1	-
100	100	515	-1.1	570	-0.4	-0.7
	250		-0.9		0.0	-0.9
	500		-2.7		-0.1	-2.6
	1000		-5.1		0.3	-
	1500		-8.1		0.1	-
	2000		-11.6		0.4	-
	2500		-14.2		-0.1	-14.1
	3000		-16.7		0.0	-16.7
200	100	515	-1.0	570	-0.3	-0.7
	250		-2.5		0.2	-
	500		-5.6		0.3	-
	1000		-10.2		0.2	-
	1500		-15.5		0.1	-
	2000		-18.7		0.1	-
	2500		-20.3		-0.1	-20.2
	3000		-21.8		-0.2	-21.6

Table A2. Spectral properties of quinoline yellow filters.

Dye concentration (μM)	Width [μm]	Stopband region		Passband region		$T_s - T_p$
		λ [nm]	Transmittance (T_s) [dB]	λ [nm]	Dye concentration (μM)	
10	100	420	0.3	530	0.2	-
	250		-0.2		-0.1	-0.1
	500		-0.3		0.0	-0.3
	1000		-0.3		0.1	-
	1500		-1.5		-0.3	-1.2
	2000		-1.0		0.0	-1.0
	2500		-0.5		0.3	-
	3000		-0.7		0.4	-
50	100	420	0.1	530	0.1	-
	250		-0.6		-0.1	-0.5
	500		-1.2		-0.1	-1.1
	1000		-2.0		0.1	-
	1500		-4.3		-0.3	-4.0
	2000		-4.5		0.0	-4.5
	2500		-5.4		-0.2	-5.2
	3000		-5.6		0.0	-5.6
100	100	420	-0.2	530	0.1	-
	250		-0.7		0.1	-
	500		-2.5		-0.1	-2.4
	1000		-3.8		0.0	-3.8
	1500		-5.2		0.0	-5.2
	2000		-7.0		-0.1	-6.9
	2500		-8.6		-0.1	-8.5
	3000		-9.8		-0.1	-9.7
200	100	420	-0.7	530	0.2	-
	250		-2.5		0.0	-2.5
	500		-4.4		0.0	-4.4
	1000		-8.2		0.0	-8.2
	1500		-11.0		0.1	-
	2000		-13.2		0.0	-13.2
	2500		-14.4		0.0	-14.4
	3000		-14.7		-0.2	-14.5

Table A3. Spectral properties of methyl orange filters.

Dye concentration (μM)	Thickness [μm]	Stopband region		Passband region		$T_s - T_p$
		λ [nm]	Transmittance (T_s) [dB]	λ [nm]	Transmittance (T_p) [dB]	
10	100	530	-0.1	650	-0.1	0.0
	250		0.9		0.1	-
	500		0.2		0.1	-
	1000		0.3		0.3	-
	1500		-0.2		-0.1	-0.1
	2000		0.0		0.1	-
	2500		-0.5		-0.1	-0.4
	3000		-0.6		-0.1	-0.5
50	100	530	0.1	650	0.0	-
	250		0.0		0.0	0.0
	500		0.1		0.0	-
	1000		-0.4		0.0	-0.4
	1500		-1.0		-0.1	-0.9
	2000		-1.3		-0.1	-1.2
	2500		-1.0		0.1	-
	3000		-1.0		0.1	-
100	100	530	-0.1	650	0.0	-0.1
	250		0.0		0.1	-
	500		-0.7		-0.2	-0.5
	1000		-1.2		0.1	-
	1500		-2.3		-0.1	-2.2
	2000		-2.9		0.0	-2.9
	2500		-3.4		0.0	-3.4
	3000		-4.3		0.0	-4.3
200	100	530	-0.2	650	-0.2	0.0
	250		-0.3		0.0	-0.3
	500		-0.9		0.1	-
	1000		-2.3		0.2	-
	1500		-4.3		-0.1	-4.2
	2000		-5.1		0.3	-
	2500		-7.7		-0.2	-7.5
	3000		-7.4		-0.1	-7.3

Table A4. Spectral properties of crystal violet filters.

Dye concentration (μM)	Thickness [μm]	Stopband region		Passband region		$T_s - T_p$
		λ [nm]	Transmittance (T_s) [dB]	λ [nm]	Transmittance (T_p) [dB]	
10	100	600	-0.5	700	0.0	-0.5
	250		-1.0		0.0	-1.0
	500		-2.2		0.0	-2.2
	1000		-4.4		0.1	-
	1500		-6.6		0.0	-6.6
	2000		-8.3		-0.1	-8.2
	2500		-11.5		0.2	-
	3000		-12.6		0.1	-
50	100	600	-0.9	700	-0.1	-0.8
	250		-1.2		0.1	-
	500		-2.8		-0.2	-2.6
	1000		-5.0		0.2	-
	1500		-7.3		0.1	-
	2000		-10.0		-0.1	-9.9
	2500		-12.8		0.4	-
	3000		-14.2		-0.2	-14.4
100	100	600	-1.5	700	0.0	-1.5
	250		-2.8		0.0	-2.8
	500		-5.5		-0.1	-5.4
	1000		-9.3		0.1	-
	1500		-15.0		-0.3	-14.7
	2000		-18.0		-0.3	-17.7
	2500		-22.0		0.5	-
	3000		-23.7		-0.6	-23.1
200	100	600	-2.5	700	-0.1	-2.4
	250		-5.5		0.1	-
	500		-10.2		0.0	-10.2
	1000		-20.6		0.2	-
	1500		-25.0		-0.2	-24.8
	2000		out of range (- 28.1)*		-0.6	-27.5
	2500		out of range (- 30.7)*		0.9	-
	3000		out of range (- 31.9)*		-0.5	-25.7

* Estimated theoretical values.

Chapter V

SOLID-STATE LIGHT EMITTER BASED ON A FLUOROPHORE-DOPED XEROGEL MATERIAL

5.1 SUMMARY

This chapter is focused towards the development and characterization of a solid-state light emitter (SSLE) based on a fluorophore-doped xerogel. The shape of the SSLE is defined by filling a hollow pear-like PDMS with an organic-inorganic polymeric material doped with a fluorophore organic dye ($\lambda_{abs} = 390 \text{ nm}$; $\lambda_{abs} = 470 \text{ nm}$). In addition, two air mirrors were implemented at both sides of the SSLE to redirect the emitted light.

The formulation of the nondoped xerogel studied in this chapter is identical to that employed in chapter IV. New doping possibilities and applications for this phenyltrimethoxy based hybrid polymer were explored in this chapter due to its proven outstanding optical properties and performance. In addition to the structural analysis carried out in chapter IV, a characterization by confocal microscopy and photostability were accomplished taking into account the nature of the new doping agent. The even dispersion of the fluorophore and high photostability were demonstrated by these studies. Also a spectral study with doped-xerogel waveguides was carried out confirming the suitability of the proposed material for the fabrication of low-cost SSLEs.

5.2 INTRODUCTION

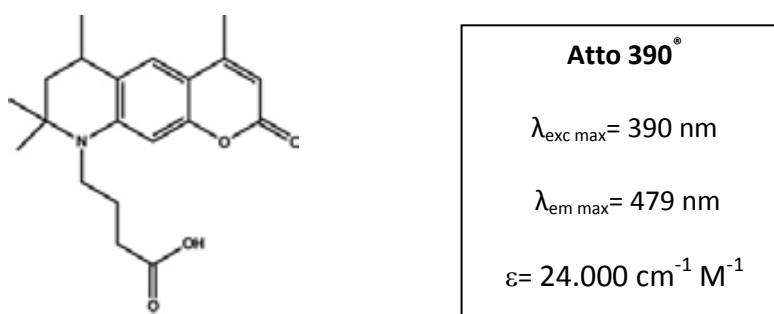
During the last two decades a myriad of photonic lab-on-chip (PhLoC) systems for analytical applications have been presented.^[1] Nevertheless, the number of commercialized devices is still quite low. One of the major impediments to the massive implantation of PhLoC systems is the in/outcoupling of the signals. When coupling external light to an arbitrary system, insertion losses occur. Generally, such insertion losses are strongly alignment-dependant, causing a dramatic degradation of the PhLoC performance for relatively small misalignments.. Alternatively, integrated light sources in combination with passive photonic components and microfluidical structures may allow overcoming these issues. In this context, devices containing (O)LEDs,^[2,3] or liquid laser dye^[4] as integrated light sources were yet presented, although addressing some of the issues, they also present several challenges, as can be complicated multilayer configurations and fast aging.

For bringing systems to market, fabrication costs need to be reduced to a minimum, resulting in the demand of low-cost materials and a fabrication process suitable for mass production. Polymer photonics has been gaining interest in this respect as they offer a high potential to fulfil these requirements. In this context, hybrid organic-inorganic hybrid polymers have played an important role.^[5] One of the main advantages of hybrid sol-gel materials is that they provide the appropriate solid matrix into which different optically active chemical species, even from biological origin, can be easily incorporated^[6] preserving their functionality. In this context waveguides,^[7, 8] microlenses,^[9] and many other photonic components have been reported. Hence, first steps towards advanced photonic materials and devices based on doped sol-gel materials have already been given. Nevertheless, a light source suitable to be integrated in a PhLoC system is yet to be presented.

5.3 FABRICATION

The disposable micro-optical component consists in a PDMS/glass platform filled with a blue light (450 nm) emitting fluorophore-doped polymeric. It was fabricated following the protocol described in Chapter IV (more detailed description can be found in ref [11]). In general terms, the fabrication consisted in two different steps: fabrication of the PDMS/glass device by soft-lithography^[12] and the synthesis of the light emitting polymer by the sol-gel method.^[13]

The prepolymeric sol was synthesized by vigorously mixing 500 μl of phenyltrimethoxysilane (PhTMOS) (Sigma-Aldrich Co., St Louis, MO, USA) monomer with 300 μl of a pH 3 (adjusted with diluted HCl) Atto 390 (Atto-Tec GmbH, Siegen, Germany) H_2O : DMSO 5:1 (v/v) solution in four different concentrations: 500, 100, 50 and 10 μM .



Scheme 1. Atto 390 fluorophore chemical structure and optical characteristics

Once the emitter microstructure was filled, the device was shielded from light and left undisturbed to cure and dry at room temperature. Hydrolysis and polycondensation reactions crosslinked the sol into a polymeric matrix and Atto dye was physically trapped inside this network. Figure 3 illustrates a picture of the resulting fluorophore-doped SSLE.

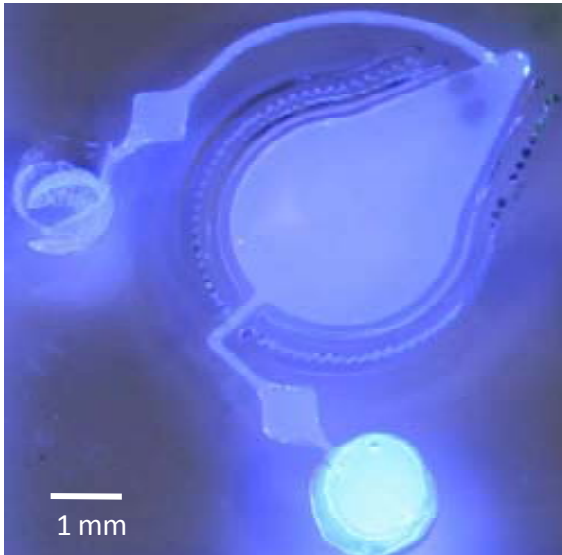


Figure 3. Picture of the presented fluorophore-doped xerogel emitter (500 μ M Atto loaded).

Initially, to validate the optical properties of the doped xerogel, multimode waveguides were fabricated by using the previously discussed MIMIC technique. Thus, waveguides with perfectly defined dimensions (facets defined in the mold) were fabricated on Si/SiO₂ chips (Si substrate with 400 nm-thick thermally grown SiO₂ layer). Four different waveguides were defined in the same chip all being 35 μ m in high, having four different widths 25, 50, 75, and 100 μ m. Three different waveguide lengths were also studied (1, 1.5, and 2 cm). This fabrication process was repeated for the four different Atto concentrations. SEM images in Fig. 7 shows the good definition of the Atto-doped xerogel waveguides. For emissivity measurements of the waveguides the set up employed was the same described in Chapter II but using the 405 nm blue laser as excitation wavelength.

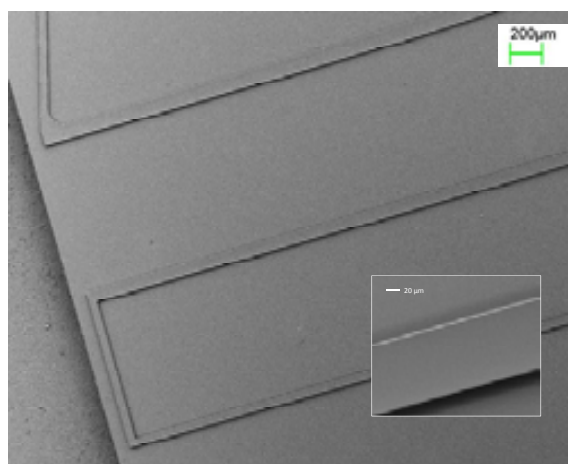


Figure 7. SEM images of the fabricated waveguides.

5.4 SPECTRAL RESPONSE OF ATTO DOPED-XEROGEL WAVEGUIDES

It has to be noticed that for the two lowest concentrations (25 and 50 μM) a filter was included in the setup so as to block the excitation wavelength. The spectra obtained (shown in figure 8) present the expected down conversion (in wavelength) typical from fluorophores. Noticeable is also that as the fluorophore concentration increases, decreases the excitation intensity peaks detected at the output, which is also in agreement with the fluorophore response. Here, it can be concluded that the atto-doped xerogel possess the adequate properties so as to be used in a monolithically-integrated SSLE.

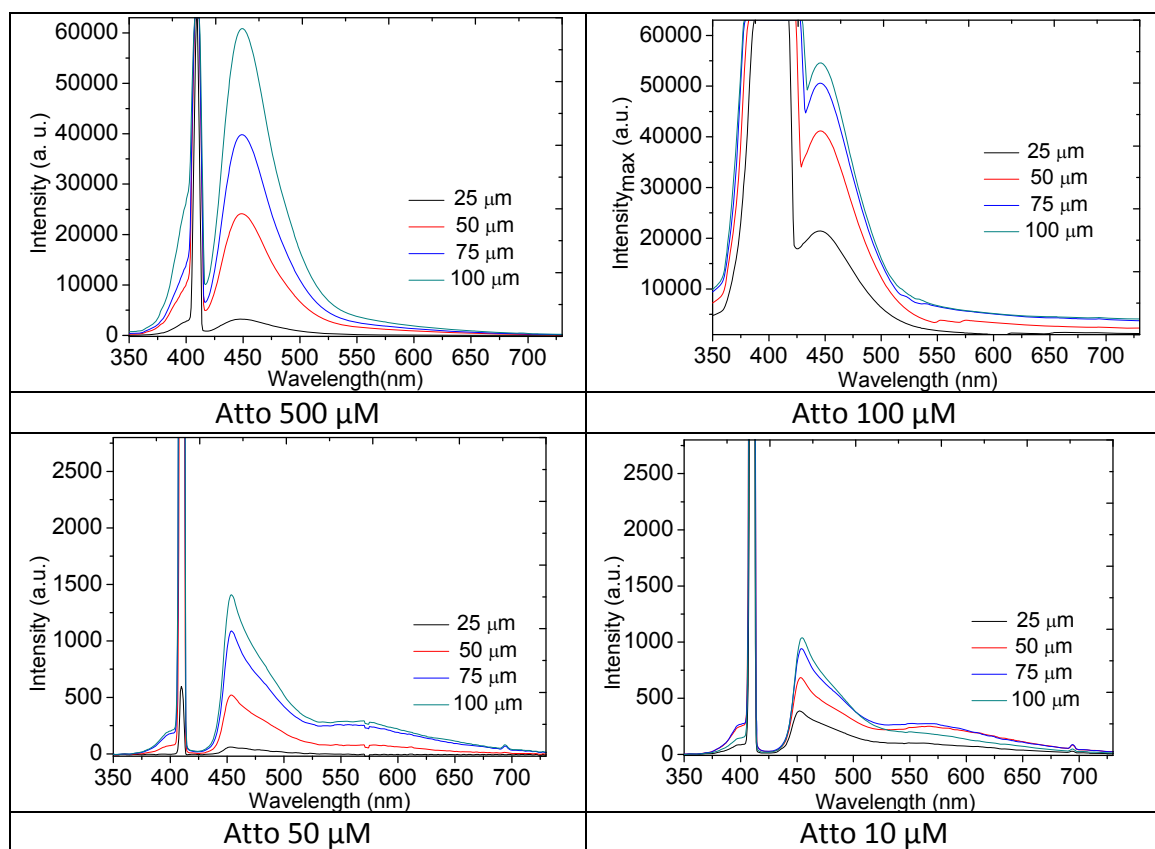


Figure 8. Transmission spectra recorded for Atto doped-xerogel waveguides.

5.5 DESIGN OF THE SSLE

The design of the emitter microstructure is shown in Figure 1; its architecture is composed of a pear-shaped reservoir (high: 230 μm , area: 14 mm^2) connected to microfluidic inlet/outlet ports including diamond-shaped reservoirs. Identical in behaviour than the other fluorophore-based light sources, when externally excited, light from these structures is emitted in $4\pi\text{Sr}$ (solid angle of a sphere measured from a point in its interior). Therefore, only a small fraction of the emission wavelength may be coupled to the system that it would be implemented. To address this issue, two

teeth-shaped air mirrors have been implemented at both sides of the emitter. Such air mirrors were described in [10] and are based on total internal reflection principles.

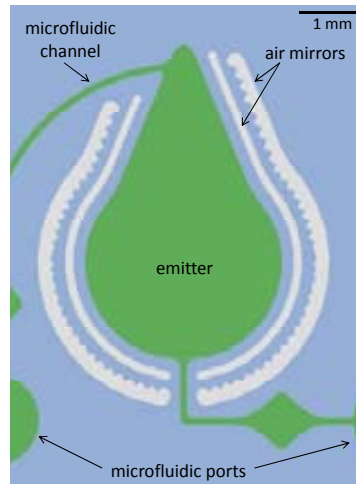


Figure 1. Design of the mask employed to fabricate the emitter microstructure.

The working principle of the air mirrors is illustrated in Figure 2. Considering the refractive indices of PDMS ($n=1.41$) and air ($n=1.00$), if the light falls on the air mirror#1 at an angle higher than 45° , it undergoes total internal reflection (TIR), see Fig. 2(a). Lower angles are able to transmit through this air mirror according to the Fresnel laws. At this point, light reaches the teeth-shaped mirror#2, which consists in two coupled air mirrors. Each part of the teeth works jointly, as they are able to reflect angles smaller than 45° . In this case, the first part of the teeth air mirror is tilted so as to ensure TIR at the light incidence point. The second part of the teeth has a double role. From one side, it also matches with the TIR conditions. From the other side, it is tilted in such a way that redirects the reflected light beam towards the thinner part of the emitter (right hand side in figure 2). Working jointly both the simple and the teeth-shaped air mirror assures that a significant amount of the emitted light is directed towards the microlens defined at the rightmost part of the emitter (Fig. 2 (b)).

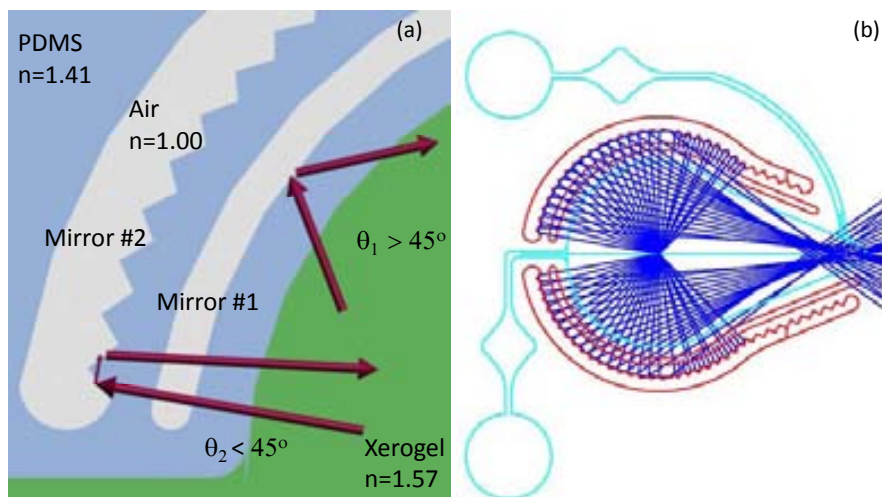


Figure 2. (a) Working principle of the air mirrors (b)General scheme of the operation principle of the presented micro-optical component. In cyan: emitter microstructure, in red: air mirrors, and in dark blue light paths.

5.6 MATERIAL AND STRUCTURAL CHARACTERIZATION

Atto 390 was selected because its high molecular absorption ($24.000\text{cm}^{-1}\text{ M}^{-1}$) and quantum yield (0.90) as well as a large Stokes shift ($\lambda_{\text{abs}} = 390\text{ nm}$, $\lambda_{\text{fl}} = 479\text{ nm}$, in water). It is characterized by a high photostability and thermostability. It is slightly hydrophilic, and solubility in polar solvents as DMF or DMSO is high. High solubility is important to ensure compatibility with different chemical environments, crucial to obtain a homogeneous dispersion of the fluorophore molecules into the hosting medium. A confocal microscopy analysis was carried out to assess the homogeneity of fluorophore dispersion in the material and also to check the quality of casting process. Photostability assumption has also been tested by irradiating with UV-light at controlled irradiation doses a doped material sample. All these studies were performed only with $500\text{ }\mu\text{M}$ Atto-doped xerogel. This corresponds to the highest fluorophore content (52:1, silane: fluorophore molar ratio in the initial *sol* solution), which was chosen to assess influence that the fluorophore may have on the polymeric structure and possible aggregation issues.

5.6.1 Confocal microscopy analysis

Confocal microscopy studies (Leica TCS SP5 confocal microscope equipped with a HC PL APO CS 10.0 \times UV objective with a 0.40 numerical aperture and a diode UV 405-nm laser as light source) were carried out in order to reveal the nature of the fluorophore dispersion in the resulting doped xerogel. For the Lambda study, the scanned area was $1.55\text{ mm} \times 1.55\text{ mm}$ (width \times length) and $0.2\text{ }\mu\text{m}$ in depth, with a scan speed of 400 Hz and a total of 46 exposures (1 channel, 46 frames) to different lambdas in the range from 425 to 650 nm. The projections of the picture series were generated with Leica LAS AF software. Different emission spectra at thirteen arbitrary points of the

microstructure were also recorded and shown in Fig. 3. The mean values for the maximum fluorescence emission intensity and wavelength were 219 ± 6 (3%coefficient of variation, number of spectra =13) and 450 ± 1 nm respectively. These results indicate that the fluorophore is homogeneously dispersed in the polymeric material.

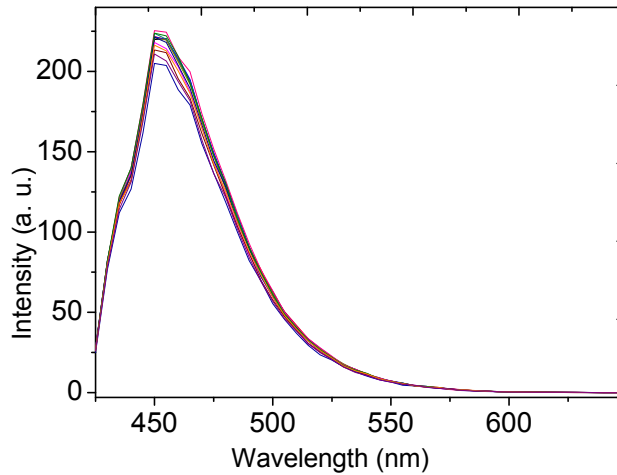


Figure 4. Emission spectra recorded at different points of the emitter microstructure.

A xyz study was also performed to test the quality of the casting process; it consisted of taking images at different depths by varying the focal plane allowing obtaining three-dimensional information of the sample. The isosurface module of Imaris v. 6.1.0 software (Bitplane, Zürich, Switzerland) was used to reconstitute the three-dimensional (3D) models shown in Fig 4. This analysis revealed that during drying step it has been a reduction of the material dimensions. It was due to the relatively high volume of the mold cavity (3.22 mm^3); with the result that the material on the diamond-shaped reservoirs and in the external drops located at the input/output microfluidic ports were not enough to replace the volume left behind by the evaporated solvents. This fact is also noticed in the picture shown in Fig. 3 where two dark spots can be seen in the narrow part of the emitter surface due to the partial emptying of the mold cavity.

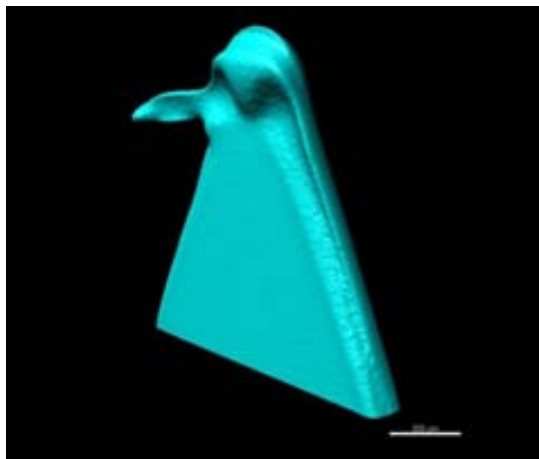


Figure 5. Emission spectra recorded at different points of the emitter microstructure.

5.6.2 Photostability of the fluorophore

The experiment to test the photostability of embedded Atto 390 consisted of irradiate the doped xerogel material with UV-light at controlled irradiation doses, while acquiring emission spectra. The registered spectra were then compared with the reference spectrum and the percentages of initial emission intensity at the maximum (450 nm) were calculated.

The setup included a mask aligner as light source (MA1006 contact mask aligner equipped with a 350 watt mercury lamp, 2 μm resolution, and a split field microscope with 5x and 10x objectives, exposure dose 9 mJ/scm^2 ($\lambda=365$ nm), Suss MicroTec, Munich, Germany), 230 μm diameter multimode optical fiber (Thorlabs Inc., Dachau, Germany) for collecting the light, completed with a microspectrometer (QE 65000-FL, Ocean Optics, Dunedin, FL, USA). Each spectrum was acquired with the average of 10 scans and integration time was fixed to 100 ms. Since the exposure dose is fixed by the equipment, different irradiation doses were achieved by irradiating the sample at different exposure times (t_E) at different time intervals (t). Table 1 lists the employed t intervals and t_E and also the total luminous density corresponding values.

Table 1. Total exposition time, t , and exposure times, t_E , employed in the photostability study.

t (s)	0-60	60-120	120-180	180-600	600-900	900-1500	1500-2700
t_E (s)	10	20	30	60	300	600	1200
Acquired spectra	6	3	2	7	1	1	1
Total luminous energy density (J/cm^2)	0.54	1.08	1.62	5.40	8.10	13.50	24.30

At low exposure times/radiation doses there was some instability with random increases/decreases in the intensity signal; it was stabilized after 15 minutes of total exposition time. With a total dose of 24.3 J/cm^2 the decay in emission was only 4.1 % of the initial value. As expected from flurophore behavior, the emission loss was higher with the initial irradiation with a 4 % loss at 8.1 J/cm^2 , and then it was stabilized with only a 0.1 % intensity loss during 30 min of UV-light exposition, see Fig.6. These results corroborate the high photostability of Atto 390 and, straightforwardly, of the SSLE here presented.

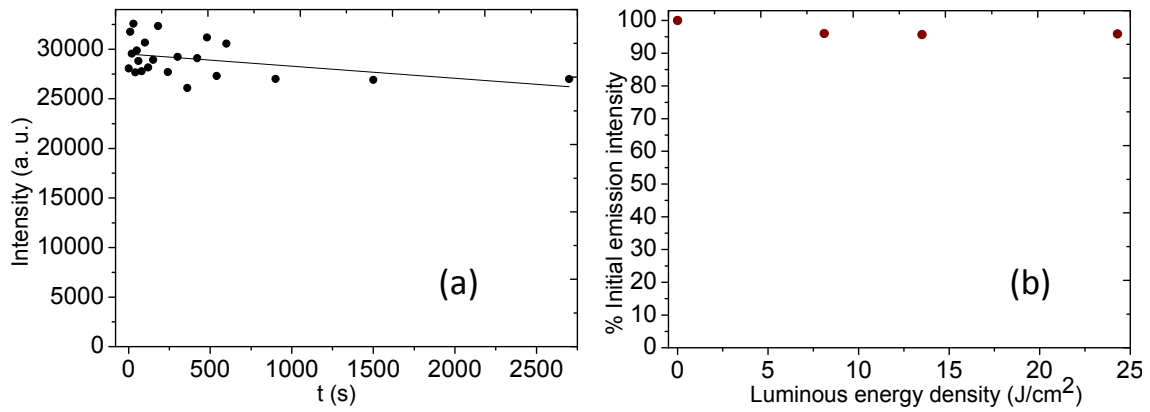


Figure 6.(a) Maximum emission intensity vs. total exposition time. (b)% initial emission intensity vs. luminous energy density.

5.7 MAPPING EMISSION INTENSITY

A study of the emission intensity as a function of the excitation point was performed in order to test the validity of the working principle of the air mirrors and emitter design, as well as to confirm the homogeneity of the material. Fluorescence intensity of the light emitted from Atto dye molecules entrapped in the polymeric matrix as a function of the excitation point position was studied defining a matrix of 7000 x 5000 μm (wide x length) recording a spectrum (integration time 250 ms) every 150 μm using an automated step motor xyz stage (see Fig. 7). Light emitted from the previously mentioned 405 nm blue laser was coupled into a multimode 230 μm fiber optic, which was positioned in a 90° out-of-plane configuration at a working distance of 1 mm with the help of a Micos VT80 micropositioner (PI Micos GbmH, Eschbach, Germany). The readout comprised an identical fiber optic which was inserted into the output self-alignment channel at the end of the emitter microstructure, and connected to the same microspectrometer used in previous characterization experiments. The mapping surface experiment was carried out with the four different Atto concentrations.

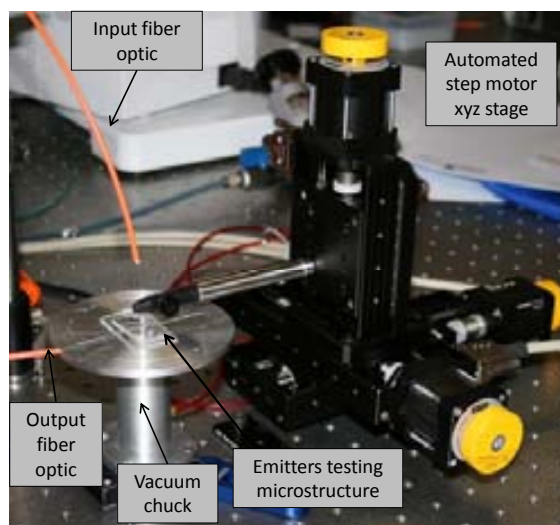


Figure 7. Picture of the setup used for the mapping emission intensity experiment.

The resulting map of maximum intensities as a function of external excitation point is shown in Fig. 8. Graphs #1 and #2 are the profiles of the longitudinal and transverse cross-sections of the intensity map represented by the two green lines. The intersection of these lines marks the position for externally pumping light where the maximum intensity is obtained. A symmetrical behavior was observed, with the maximum of coupled light obtained when exciting in the central longitudinal axis. These results are in good agreement with the expected behavior, validating the optimal performance of the proposed SSLE.

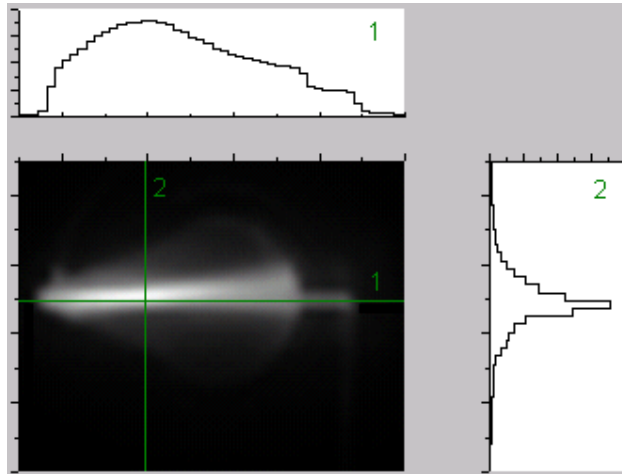


Figure 8. Emission intensity map. Intersection of two green lines marks the optimum position for externally pumping light. Profile #1 intensity longitudinal cross-section, profile #2 intensity transverse cross-section.

Figure 9 shows the spectrum of the Atto-doped xerogel SSLE recorded at the maximum emission point. It emits from 430 nm to 485 nm (FWHM) with a maximum emission at 450 nm. Some residual light from excitation laser can still be collected at 415 nm. The emission intensity as a function of Atto concentration is shown in Fig. 10. A linear trend is followed confirming the good optical properties of the hosting polymeric material.

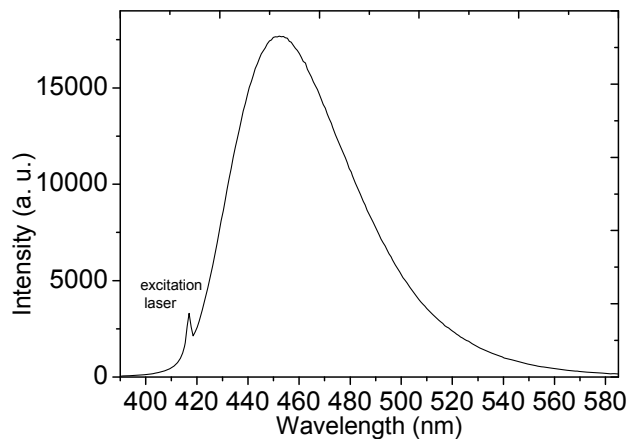


Figure 9. Emission spectrum of the doped xerogel emitter (Atto 500 μM) recorded at the excitation point of maximum emission (integration time 250 ms).

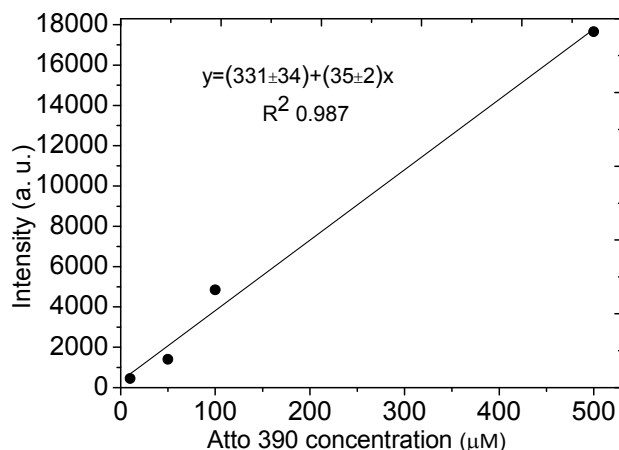


Figure 10. Maximum Intensity recorded at the excitation point of maximum emission vs. Atto concentration.

5.8 CONCLUSIONS

The easy development and successful performance of a xerogel polymeric solid state light emitter including auxiliary micro-optical elements, such as air mirrors, was demonstrated in this chapter. These results show the potential of the presented contribution for the development of disposable photonic components which could be easily implemented in photonic lab-on-chip devices.

References

1. West, J., et al., *Micro total analysis systems: Latest achievements*. Analytical Chemistry, 2008. **80**(12): p. 4403-4419.
2. Pais, A., et al., *High-sensitivity, disposable lab-on-a-chip with thin-film organic electronics for fluorescence detection*. Lab on a Chip, 2008. **8**(5): p. 794-800.
3. Edel, J.B., et al., *Thin-film polymer light emitting diodes as integrated excitation sources for microscale capillary electrophoresis*. Lab on a Chip, 2004. **4**(2): p. 136-140.
4. Balslev, S., et al., *Lab-on-a-chip with integrated optical transducers*. Lab on a Chip, 2006. **6**(2): p. 213-217.
5. Lebeau, B. and P. Innocenzi, *Hybrid materials for optics and photonics*. Chemical Society Reviews. **40**(2): p. 886-906.
6. Zaggout, F.R., *Entrapment of phenol red pH indicator into a sol-gel matrix*. Materials Letters, 2006. **60**(8): p. 1026-1030.
7. Llobera, A., et al., *Fluorophore-doped xerogel antiresonant reflecting optical waveguides*. Optics Express, 2011. **19**(6): p. 5026-5039.
8. Yang, P.D., et al., *Mirrorless lasing from mesostructured waveguides patterned by soft lithography*. Science, 2000. **287**(5452): p. 465-467.
9. Zhang, X.H., et al., *Fabrication of micro-lens arrays built in photosensitive hybrid films by UV-cured imprinting technique*. Journal of Sol-Gel Science and Technology, 2011. **60**(1): p. 71-80.
10. Llobera, A., R. Wilke, and S. Buettgenbach, *Enhancement of the response of poly (dimethylsiloxane) hollow prisms through air mirrors for absorbance-based sensing*. Talanta, 2008. **75**(2): p. 473-479.

11. Llobera, A., R. Wilke, and S. Buttgenbach, *Poly(dimethylsiloxane) hollow Abbe prism with microlenses for detection based on absorption and refractive index shift*. *Lab on a Chip*, 2004. **4**(1): p. 24-27.
12. Xia, Y.N. and G.M. Whitesides, *Soft lithography*. *Angewandte Chemie-International Edition*, 1998. **37**(5): p. 551-575.
13. Hench, L.L. and J.K. West, *THE SOL-GEL PROCESS*. *Chemical Reviews*, 1990. **90**(1): p. 33-72.

Chapter VI

INTEGRATION OF A POLYMERIC SOLID STATE LIGHT EMITTER IN A BIOFUNCTIONALIZED DISPOSABLE PHOTONIC LAB ON CHIP

The work included in this chapter has been reported in one paper entitled “*Disposable photonic lab-on-chip with integrated polymeric light emitter for biosensing*”, by Ester Carregal-Romero, Bergoi Ibarlucea, Andreu Llobera, and César Fernández-Sánchez, which has been submitted to Analytical Chemistry journal as a technical note.

6.1 SUMMARY

Taking the next step from individual functional components to higher integrated devices, this chapter shows the successful monolithic integration in a PDMS-based PhLoC of the SSLE described in chapter V and a biofunctionalized optofluidic MIR system. The SSLE successful integration and performance was assessed by measuring quinolone yellow dye ($\lambda_{\text{abs}} = 440 \text{ nm}$) as a model target analyte, attaining a sensitivity of $0.0208 \text{ A.U.}\mu\text{M}^{-1}$ and a limit of detection (LOD) of $0.60 \mu\text{M}$. In order to demonstrate the potential of the presented approach for the development of cost-effective disposable PhLoCs for biosensing applications, the MIR inner walls were selectively modified with a peroxidase enzyme for the measurement of hydrogen peroxide (H_2O_2). Absorbance detection of the corresponding catalytic reaction was possible using an appropriate colorless redox mediator whose colored product showed an intense absorption band between 390-445 nm. Working in this way, sensitivity and LOD values of $0.0119 \text{ A.U.}\mu\text{M}^{-1}$ and $0.73 \mu\text{M}$ for H_2O_2 , respectively, were achieved. This detection strategy could be applied to other enzyme- or immunoassay- based analytical tools for the measurement of a wide range of target analytes. The results presented here evidenced that a disposable cost-effective PhLoC could be fabricated and implemented into compact analytical systems with the potential to be applied to decentralized point-of-care diagnostic or environmental applications.

6.2 INTRODUCTION

Cost-effective disposable biosensors are required for many applications in different fields such as biomedicine for point-of-care diagnostics or *in-situ* environmental monitoring. These devices should also be easy to use and amenable to be applied under different experimental conditions and for a variety of target analytes. The cost issue should be carefully taken into account considering that many of them show an

irreversible sensor response due to the interaction of the analyte with the corresponding recognition element and the possible contamination that can take place specially when working with complex sample matrices. All these requirements can be fulfilled by developing fully integrated compact and inexpensive PhLoCs fabricated by inexpensive techniques and including the appropriate components for each specific application. To the best of our knowledge, the work presented here describes for the first time such an analytical approach.

The low-cost issue in PhLoCs can be tackled by using polymer fabrication approaches, such as the well-known (PDMS)-based soft lithographic techniques. PDMS has been widely applied in the development of PhLoCs due to its outstanding structural and optical properties. Due to its hydrophobic character, this material shows high non-specific absorption of different organic molecules and biomolecules, this being a severe drawback for real applications of PDMS-based PhLoCs to biochemical analysis. A surface modification process is required to tune the surface properties of the material and to provide it with the capacity to selectively answer to specific target analytes while keeping the optical properties unaltered.^[1] Different surface modification protocols have been described for PDMS, such as oxygen plasma^[2] or UV/ozone treatments,^[3] which produce silanol groups (Si-OH) on the surface. These groups can chemically interact with other functional groups, enabling further modification steps, but they are dynamic and the surface recovers its hydrophobicity with time.^[2] In addition, special instrumentation is required for these processes, and in the case of plasma treatment, it cannot be applied in microfluidic channels that are embedded in PDMS matrices.^[4] For this reason, a previously developed liquid-phase modification protocol was applied, which consists in the introduction of hydroxyl (-OH) groups by physisorption of polyvinyl alcohol (PVA)^[5] and further silanization^[6] of the resulting surface with a silane molecule that introduces aldehyde groups to which proteins and other amino-containing biomolecules can be covalently attached.^[7]

The PhLoC presented herein includes different microoptical components, among them the polymeric SSLE described in the previous chapter, together with a MIR, which was modified with a peroxidase enzyme in order to provide the system with the required functionality to selectively detect H₂O₂. This work benefits from the merits of a PDMS-based LoC and the easy fabrication and the monolithic integration of the polymeric SSLE together with a simple biofunctionalization approach to develop a low-cost PhLoC, which could be easily integrated into compact user-friendly analytical systems.

6.3 EXPERIMENTAL SECTION

6.3.1 Chemicals

The PDMS Sylgard 184 elastomer kit was purchased from Dow Corning (Midland, MI, USA) and used according to the datasheet. 99% PVA, 99% triethylamine (TEA), Tween 20, phenyltrimethoxysilane (PhTMOS), dimethyl sulfoxide (DMSO), horseradish peroxidase (HRP type VI), 2,2'-azino-bis(3-ethylbenzthiazoline-6-sulfonic acid) (ABTS), mixture of the mono- and disulfonic acids of quinoline yellow dye and hydrogen peroxide were purchased from Sigma-Aldrich Co. (St Louis, MO, USA). 90% 11-tiethoxysilyl undecanal (TESU) was from ABCR GmbH & Co. KG (Karlsruhe, Germany). Atto 390 fluorophore dye was from Atto-Tec GmbH (Siegen, Germany). All other chemicals were of analytical grade.

6.3.2 Design

The design of the PhLoC with integrated polymeric SSLE is illustrated in Fig. 1. It includes the emitter pear-shaped structure, a MIR optofluidic system, together with other micro-optical components. The integrated emitter architecture was extensively described in Chapter IV. In general terms, the joint performance of both the simple and the teeth-shaped air mirrors included in the emitter architecture, induce an enhancement of the light coupled into the optofluidic system. An additional air mirror was designed at the MIR channel end coupling point to correctly direct the light coming from the emitter to the system.

The MIR structure (ref. [8], in cyan in Fig. 1) consisted of an 11.25 mm-long zigzagging channel containing two concave air mirrors located at the channel vertices to direct the light from the integrated emitter to the opposite end of the channel. There, transmitted light was collected with the help of two microlenses and a fiber optics positioned in a self-alignment microchannel. The microlenses were implemented to correct the numerical aperture of the used fiber optic.^[9]



Figure 1. Design of the mask employed to fabricate the presented PhLoC. In red: emitter microstructure; in orange: air mirrors; in cyan MIR optofluidic system; in dark blue: microlenses; and in violet: self-alignment microchannel.

6.3.3 Fabrication

The PhLoC structure was fabricated using PDMS and bonded to a glass substrate. The fabrication of the PhLoC comprised two main steps, that is the fabrication of the PhLoC by the protocol described in Chapter IV and the implementation of the light emitter based on the fluorophore-doped organic-inorganic polymer presented in Chapter IV by the sol-gel technology.^[10] Briefly, the PDMS top part with the microfluidic channels including the emitter structure and the microoptical elements described above, was fabricated by standard master-replica molding,^[11] and bonded to a glass substrate by exposition to oxygen plasma. The emitter structure was filled with the fluorophore-doped pre-polymerization solution by an adaptation of the micromolding in capillaries soft-lithographic technique.^[11] The pre-polymerization solution (*sol*) was prepared by vigorously mixing 500 μL of PhTMOS monomer with 300 μL of a 500 μM Atto 390 solution in H_2O : DMSO 5:1 (v/v) at pH 3.

6.3.4 Enzyme immobilization

A previously published method for protein immobilization onto PDMS microchannels was used^[7] here. Horseradish Peroxidase (HRP) enzyme was covalently attached to the inner walls of the MIR and applied as a biological recognition element in the PhLoC. The proposed modification protocol is shown in Figure 2.

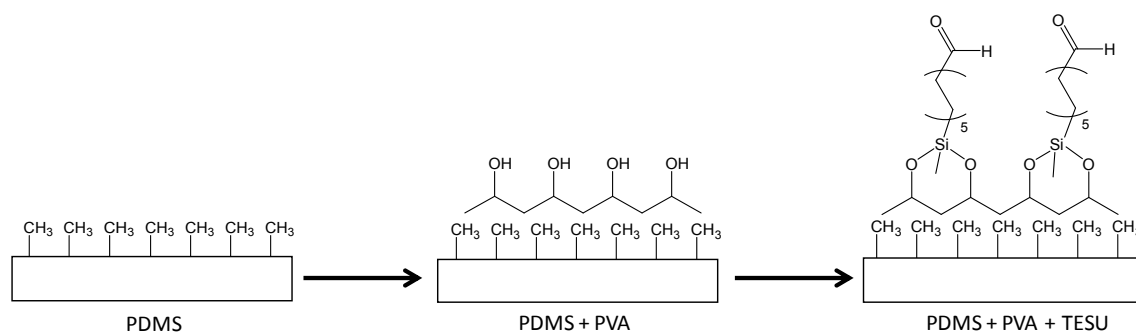


Figure 2. PDMS surface modification steps.

Prior to their modification, the PDMS was cleaned with ethanol and deionized water (DI water). Then a 1 mg ml^{-1} solution of PVA in DI water was pumped through the microchannel and it was left to react for 1h. After this step, they were rinsed in water and dried under a N_2 stream. Next, a silanization process was carried out by incubating the PVA-modified microchannels in a 99.5% ethanol solution containing 2% TESU and 2% TEA for 1h at room temperature (RT). Then they were rinsed with 99.5% ethanol and dried at 80°C for 2h. TESU presents an aldehyde group that can be used as anchoring point for proteins. The immobilization of the enzyme was done by filling the aldehyde-modified PDMS microchannels with a 0.05 M carbonate buffer solution pH 8 that contained 1 mg ml^{-1} HRP type II and 5 mM $\text{NaBH}_3(\text{CN})$ for 1h at RT. $\text{NaBH}_3(\text{CN})$ stabilized the attachment of the enzyme to the silane by reducing the formed Schiff base (imine linkage) to a more stable secondary amine. Finally, a phosphate buffered saline solution pH 7.0 containing 0.02% (v/v) Tween 20 (PBST) was pumped inside the microchannels in order to remove the non-specifically adsorbed HRP molecules. The PhLoCs were filled with PBS and kept at 4°C until their application in the detection of H_2O_2 .

5.3.6 Experimental setup and protocol for absorbance measurements

Light emitted from a blue laser ($\lambda = 405 \text{ nm}$, Laser module NANO 250-532-100, Linos Photonics, Germany) was coupled into a multimode $230 \mu\text{m}$ fibre optic (Thorlabs Inc., Dachau, Germany). This was positioned off-axis (90° , working distance 1 mm) with the help of micropositioners at the maximum emission region of the polymeric emitter, determined in Chapter V to be in the central region of the structure. The readout comprised an identical fibre optic, which was inserted into the output self-alignment channel at the end of the MIR system, and connected to a microspectrometer (QE 65000-FL, Ocean Optics, Dunedin, FL, USA).

Performance studies were firstly carried out with PhLoCs where the MIR structure was not biofunctionalized and using aqueous solutions containing quinoline yellow dye (QY) in a concentration range from $1 \mu\text{M}$ to $25 \mu\text{M}$. For that, $10 \mu\text{L}$ of each solution were cast at the input fluidic port of the MIR with the aid of a micropipette and

injected into the microchannel by applying a slight negative pressure at the output fluidic port using a vacuum pump. The volume of the MIR structure was 1.4 μL . Then, the spectral response was recorded. Integration time was set to 400 ms. For each concentration of the target analyte, the mean value of 10 absorbance spectra was taken. DI water was used as reference and injected in the system in between measurements to clean the channel. All measurements were carried out at room temperature.

In order to assess the performance of the PhLoC biosensor approach, 0.1 M acetate buffer pH 5.5 solutions, containing 0.5mM ABTS and increasing concentrations of H_2O_2 in a range from 1.4 μM to 27.5 μM were sequentially injected into the system, in a similar fashion as above. The same solution without containing H_2O_2 was initially measured and used as reference. Measurements were made under quiescent fluid conditions (absence of flow) in all cases. The spectral response required 10 min to stabilize, after that the readout signal was recorded. In both cases, absorbance measurements were plotted against the target analyte concentration. A linear fit was carried out and the limit of detection (LOD) calculated following the 3σ IUPAC criteria. It states that the LOD is not the lowest detectable analyte concentration, but also depends on both the sensitivity and the accuracy of the linear fit, thus being determined as the lowest concentration of analyte for which the signal exceeds by a factor of 3 the relative standard deviation of the background signal divided by the slope of the calibration curve.^[12]

6.4 ANALYTICAL PERFORMANCE OF THE PhLoC

In previously reported works, our group showed the performance of the MIR structure. Scattering measurements were carried out for cell screening.^[13] Also, absorbance measurements were reported for the detection of L-lactate^[14]. In both works, light from an external light source was coupled into the system by using fiber optics and self-alignment channels defined in the same PDMS structure. Here, the monolithic integration of a polymeric SSLE together with the MIR optofluidic structure in a single PhLoC is demonstrated. The aim was to make the system more user-friendly without compromising its fabrication costs and amenable to be easily integrated in compact optical analytical systems. Also, the inner walls of the MIR structure were selectively modified with a biomolecule, thus implementing a biosensor approach, which provided the system with the adequate selectivity for the detection of a model target analyte.

First, the SSLE performance in the PhLoC was assessed with a non-biofunctionalized device and using solutions of a dye molecule. QY dye was selected because the maximum absorption wavelength ($\lambda_{\text{max}}=440\text{ nm}$) lies within the region of

the emission spectrum of the integrated emitter (Fig. 3). The absorption of the emitter light due to QY dye was successfully recorded and is shown in Fig. 4. The corresponding calibration plot carried out with solutions containing increasing concentrations of QY, as described in the experimental section, is depicted in Fig. 5 and showed a linear increase in the measured absorbance between 1 μM -14 μM QY. The sensitivity and limit of detection were calculated to be $(2.08 \pm 0.05) \times 10^{-2} \text{ A.U.}\mu\text{M}^{-1}$ and $0.60 \pm 0.01 \mu\text{M}$ ($R^2 = 0.995$, $N=9$), respectively. These results demonstrate the good performance of the presented device for sensing in the absorbance regime.

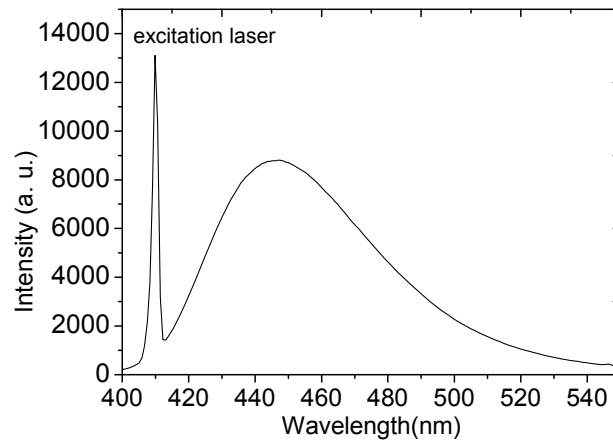


Figure 3. Emission spectrum of the integrated emitter collected at the end of the interrogation region channel containing DI water, reference signal (integration time 400 ms).

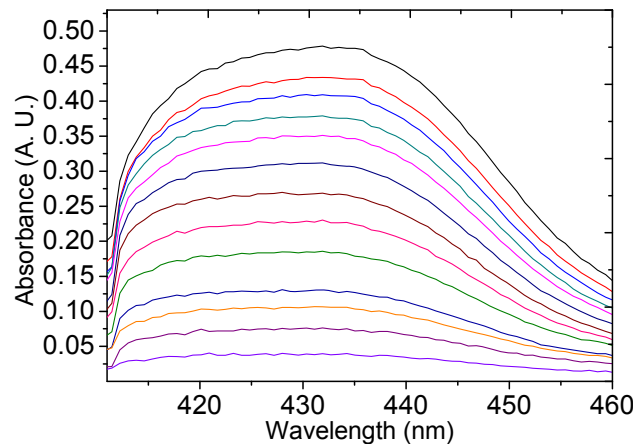


Figure 4. Absorbance spectra for different QY aqueous solutions measured with the presented PhLoC. Concentrations: 1, 2, 3, 4, 6, 8, 10, 12, 14, 16, 18, 20, 25 μM .

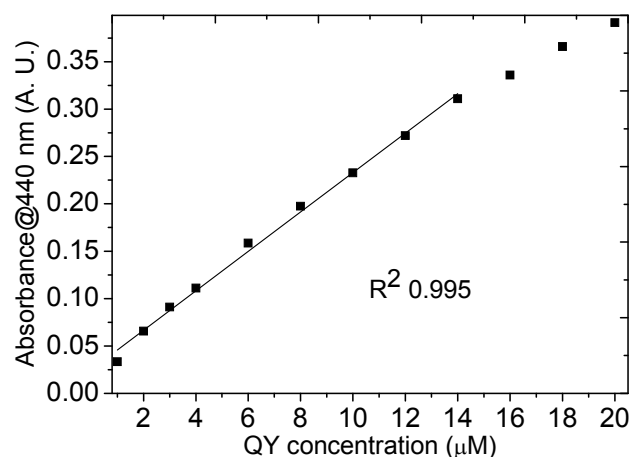


Figure 5. Calibration plot of the absorbance as a function of QY concentration measured at 440 nm.

Similar measurements were carried out with the functionalized PhLoC., A picture of the final device is shown in Figure 6. The surface modification process carried out in the MIR system provided the material with the capacity to selectively answer to the target analyte while keeping the optical properties of the material intact. HRP enzyme catalyzed the reduction of H_2O_2 in the presence of colourless 2,2'-azino-bis(3-ethylbenzthiazoline-6-sulfonic acid) (ABTS) charge transfer mediator, which is concomitantly oxidized to the green-coloured $ABTS^+$ radical cation. This redox specie shows an intense absorption band from 390 nm to 445 nm (FWMH) as it can be seen in Figure. 7. The absorbance value at 435 nm was chosen for the detection of H_2O_2 based on the colored conversion of ABTS mediator that takes place during the peroxidase enzymatic reaction.

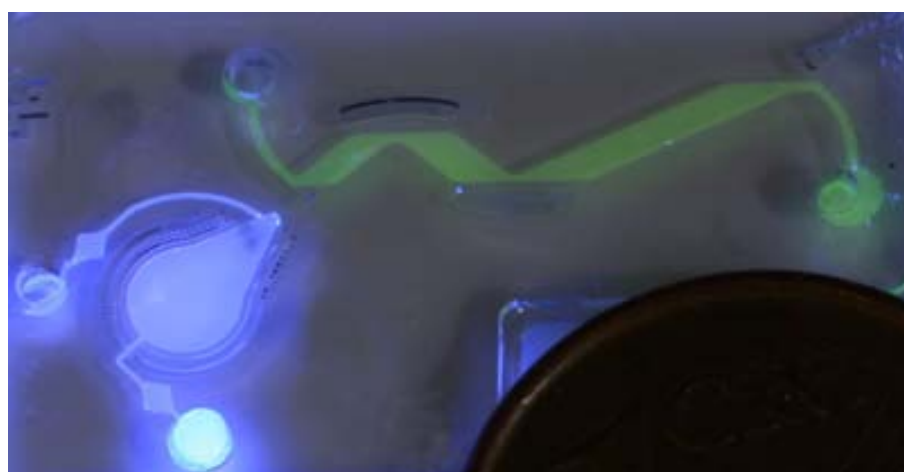


Figure 6. Picture of the PhLoC device. It comprises the different microoptic elements, that is microlenses, air mirrors and alignment microchannels together with the polymer solid-state light emitter and the MIR device. All this components were identified in Figure 1. A 1 cent euro coin is shown as size reference.

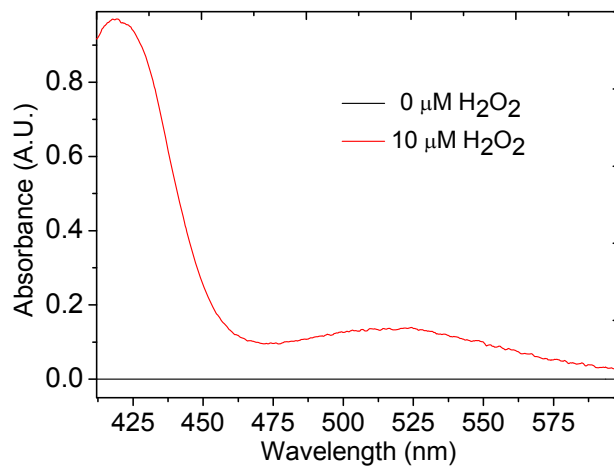


Figure 7. Absorbance spectra of HRP-ABTS reaction medium containing 0 μM and 10 μM of H_2O_2 .

The calibration curves presented in Fig. 8 showed a linear increase in the absorbance at 435 nm from 1.4 μM up to 8.2 μM , which is similar to the one observed using the previous presented PhLoC with an external excitation light source.^[7] A linear fitting was carried out in this range and the estimated analytical parameters are shown in Table 1. The mean sensitivity and limit of detection were calculated to be 0.0119 A.U. μM^{-1} and 0.73 μM for H_2O_2 , respectively. The limit of detection was around 20-fold lower than that of other previously reported optical biosensors for H_2O_2 ,^[15, 16] these devices making use of external light sources.

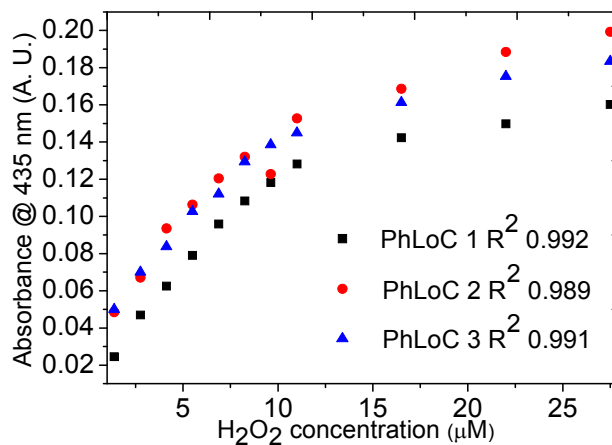


Figure 8. Absorbance as a function of H_2O_2 concentration measured at 435 nm.

Table 1. Analytical data extracted from the H₂O₂ calibration curves carried out with the presented PhLoC.

Device	Sensitivity/A.U. μM^{-1}	LOD [*] / μM	R ²
1	0.0121 \pm 0.0005	0.64 \pm 0.02	0.992
2	0.0125 \pm 0.0006	0.88 \pm 0.09	0.989
3	0.0112 \pm 0.0005	0.67 \pm 0.02	0.991

* LOD calculated following the 3 σ IUPAC criteria using the linear concentration range from 1.4 μM to 8.2 μM for H₂O₂ detection. Absorbance recorded at 435 nm.

6.5 CONCLUSIONS

The work presented in this chapter demonstrates the easy integration and successful performance of a xerogel polymeric light emitter in a PhLoC that also included auxiliary microoptical elements, such as air mirrors, and a MIR optofluidic component, which was bio-functionalized for the selective detection of a model target analyte. Despite its high level of integration, the resulting photonic approach can be fabricated at low cost. The results presented herein show the potential of the presented contribution for the development of disposable photonic lab-on-chips, which could be implemented in compact analytical systems for a variety of applications.

References

1. Bai, Y., et al., *Surface modification for enhancing antibody binding on polymer-based microfluidic device for enzyme-linked immunosorbent assay*. Langmuir, 2006. **22**(22): p. 9458-9467.
2. Bodas, D. and C. Khan-Malek, *Hydrophilization and hydrophobic recovery of PDMS by oxygen plasma and chemical treatment - An SEM investigation*. Sensors and Actuators B-Chemical, 2007. **123**(1): p. 368-373.
3. Berdichevsky, Y., et al., *UV/ozone modification of poly(dimethylsiloxane) microfluidic channels*. Sensors and Actuators B-Chemical, 2004. **97**(2-3): p. 402-408.
4. Sui, G., et al., *Solution-phase surface modification in intact poly(dimethylsiloxane) microfluidic channels*. Analytical Chemistry, 2006. **78**(15): p. 5543-5551.
5. Yu, L., et al., *Poly(vinyl alcohol) functionalized poly(dimethylsiloxane) solid surface for immunoassay*. Bioconjugate Chemistry, 2007. **18**(2): p. 281-284.
6. Sandison, M.E., et al., *On-chip immunoprecipitation for protein purification*. Lab on a Chip, 2010. **10**(20): p. 2805-2813.
7. Ibarlucea, B., et al., *Selective functionalisation of PDMS-based photonic lab on a chip for biosensing*. Analyst, 2011. **136**(17): p. 3496-3502.
8. Llobera, A., et al., *Multiple internal reflection poly(dimethylsiloxane) systems for optical sensing*. Lab on a Chip, 2007. **7**(11): p. 1560-1566.

9. Llobera, A., R. Wilke, and S. Buttgenbach, *Poly(dimethylsiloxane) hollow Abbe prism with microlenses for detection based on absorption and refractive index shift*. *Lab on a Chip*, 2004. **4**(1): p. 24-27.
10. Hensch, L.L. and J.K. West, *THE SOL-GEL PROCESS*. *Chemical Reviews*, 1990. **90**(1): p. 33-72.
11. Xia, Y.N. and G.M. Whitesides, *Soft lithography*. *Angewandte Chemie-International Edition*, 1998. **37**(5): p. 551-575.
12. Thomsen, V., D. Schatzlein, and D. Mercurio, *Limits of detection in spectroscopy*. *Spectroscopy*, 2003. **18**(12): p. 112-114.
13. Ibarlucea, B., et al., *Cell Screening Using Disposable Photonic Lab on a Chip Systems*. *Analytical Chemistry*, 2010. **82**(10): p. 4246-4251.
14. Ordeig, O., et al., *Dual Photonic-Electrochemical Lab on a Chip for Online Simultaneous Absorbance and Amperometric Measurements*. *Analytical Chemistry*, 2012. **84**(8): p. 3546-3553.
15. Llobera, A., et al., *Full-field photonic biosensors based on tunable bio-doped sol-gel glasses*. *Lab on a Chip*, 2008. **8**(7): p. 1185-1190.
16. Ho, W.-J., et al., *Fabrication of a miniature CMOS-based optical biosensor*. *Biosensors & Bioelectronics*, 2007. **22**(12): p. 3008-3013.

Chapter VII

OTHER DOPED SILICON-BASED POLYMERIC MATERIALS AND MICROFABRICATION TECHNIQUES EXPLORED

7.1 QUANTUM-DOTS DOPED HYBRID ORGANIC-INORGANIC POLYMER

Different strategies for the inclusion of CdSe/ZnS core/shell quantum-dots (QDs) into hybrid organic-inorganic polymers were investigated in this section. Two sol-gel formulations were studied in order to obtain a transparent polymer with well dispersed QDs showing no aggregation. The results from transmission electron microscopy, confocal microscopy and spectral characterization confirmed the successful doping of CdSe QDs into hybrid organic-inorganic xerogels. The aim of these studies was to develop a material that could be applied in photonics, which showed a higher photostability than those ones developed using organic fluorophores.

7.1.1 INTRODUCTION

QDs are fluorescent semiconductor nanoparticles, which have attracted much attention because of their potential applications in, nanophotonics,^[1] nonlinear optical devices^[2] and fluorescence probes.^[3-4] The application of QDs in the fields of photonics, optoelectronics and biondiagnosis requires the combination of the QDs with polymers. Thus the development of methods to obtain well-defined polymer-QD hybrid materials with tunable optical properties is an active field of research.^[5] However, the incorporation of QDs into a thick bulk polymer matrix has remained challenging due to aggregation issues.

A large number of complicated synthesis techniques have been investigated to prevent aggregation of QDs during the polymerization process. Some of these methods are briefly described below. Gao *et al.*^[6] used Pb methylacrylate to make PbS QDs, then polymerized the vinyl moieties to form a solid polymer composite. Frog *et al.*^[7] incorporated QDs within a polymer containing phosphine donors attached to the polymer backbone to form a polymerized QDs composite film. Lee *et al.*^[8] used the same phosphine ligand covering QDs to prevent the QDs from phase separating during polymerization to form a solid composite polymer. Zhang *et al.*^[9] employed the polymerizable surfactant to transfer QDs to styrene solution and polymerized to solid polymer composite. To prevent the QDs from leaching off the polymer matrix, Pang L. *et al.*^[10] described a simple method that consisted of pre-polymerizing PMMA in solution containing QDs. The pre-polymerized polymer could be then casted onto various molds and fully polymerized to form solid-state polymer-QD composites.

How the nanocrystals incorporate themselves into a polymer in these bulk processes is the result of delicate balance of enthalpic and entropic effects.^[11] In the enthalpic balance, compatibility between the QDs capping layer and the polymer must be achieved. Configurational entropic factors associated with the bending of the polymer chains around the nanoparticles are also important.^[12] Thus linear polymers consisting of chains which have a radius of gyration much larger than the nanoparticle radius, when blended with nanoparticles, form a uniformly dispersed nanoparticle/polymer composite.

In the approach presented herein QDs were dispersed in a hybrid organic-inorganic viscous *sol* solution. The assumption was that chemically compatible water dispersed QDs will accommodate into the nanoporous formed in a highly crosslinked *sol* network thus avoiding entropic issues related with the polymeric chains. This *sol* was also soft lithographically processed to construct microstructures for the development of photonic devices.

7.1.2 EXPERIMENTAL DETAILS

Different compositions were studied but the best results were obtained with the two formulations listed in the table below. With these formulations, transparent materials with no aggregated QDs were obtained.

Xerogel 1 composition was the same used in the previous section. Xerogel 2 composition is similar to that one but with slight variations. A silane modified with a N-trimethoxysilylpropyl-N,N,N-triethylammonium chloride, 50% ethanol (AB 111493, ABCR GmbH & Co. KG, Karlsruhe, Germany) surfactant, was included in the xerogel formulation in an attempt to stabilize the nanoparticles and obtained a more homogeneous QDs dispersion.

	Composition	Loss of weight
1	615 μ l MTMOS + 75 μ l PhTMOS+ 60 μ l TMOS + 280 μ l H ₂ O + 900 μ l EtOH	60%
2	600 μ l MTMOS + 28 μ l AB111493 + 75 μ l PhTMOS+ 60 μ l TMOS + 280 μ l H ₂ O + 900 EtOH + 25 μ l HCl (0.1 M)	60%

The *sol* solutions were prepared at room temperature in a beaker and left it under thorough magnetic stirring until it lost around 60 % of their initial weight. The lower the solvent content in the *sol* solution, the higher is the crosslinking degree and also, the faster is the formation of the xerogel network, and the greater the likelihood of preventing the particles from segregating. Then 50 μl of these *sol* solutions were mixed with aqueous solutions containing commercial CdSe/ZnS core/shell QDs that included a capping polymer layer with surface carboxylic moieties (Ocean NanoTech, Springdale, Arkansas, USA) in a concentration range from 0.09 to 0.18 μM and vigorously stirred in a vortex. Monoliths for the material structural analysis were fabricated. Also, patterned 80 μm x 100 μm (height x length) waveguides on Si/SiO₂ chips were fabricated by micromolding in capillaries soft lithographic technique (MIMIC) following the protocol described in Chapter 2. They were used to carry out the material spectral analysis and assessed the fabrication process of photonic components. Here, the spectral characterization is qualitative because the chips were manually cleaved to get roughly 1 cm-long structures, and thus, the dimensions of the waveguides were not perfectly defined.

7.1.3 CHARACTERIZATION

The following studies were carried out with 0.18 μM QDs doped xerogel materials, unless stated otherwise. This corresponds with the material with the highest content of nanoparticles.

Transmission electron microscopy (TEM) analysis (JEM-2011, resolution 0.18 nm at 200 kV, acceleration voltage 80 - 200 kV) was carried out to assess the dispersion of the nanoparticles in the polymers. Confocal microscopy studies (Leica TCS SP2 confocal microscope equipped including a HC PL APO CS 10.0x UV objective with a 0.40 numerical aperture and a diode UV 405 nm laser as light source) were carried out in order to elucidate QDs aggregation that would affect their luminescent properties in the resulting doped polymer matrix.

Results obtained from these studies are shown in Figure 1. TEM pictures revealed that in xerogel 1 a homogeneous dispersion of the QDs was achieved. Xerogel 2 TEM pictures showed that QDs were segregated in certain regions. This is likely to be related to an incompatibility between the surfactant chemically bonded to the hybrid network (introduced by the AB111493[®] silane) and the QDs carboxyl surface groups.

The above mentioned results were confirmed by the confocal microscopy analysis. QDs doped xerogel waveguides were scanned in this study. 3D reconstructions of the microstructures were made, as described in the experimental section, and results recorded with 100 μm -wide QDS-doped waveguide structures for both compositions

are shown in Figure 1. Xerogel 1 showed similar luminescence intensities along the structure (3D model). For xerogel 2, 3D model shows that the luminescence is reduced to some regions of the waveguide thus revealing that the QDs were not well dispersed. Nevertheless, the luminescence is not quenched those indicating that there were not aggregation. Different emission spectra at ten arbitrary points of the microstructures were also recorded. The spectra and the mean values for the maximum emission intensity and wavelength are shown in Figure 1. These results are a good indication of the homogeneous dispersion of the QDs into the xerogel 1 host matrix that is of key importance to control the optical properties of the resulting material. Bad dispersion but not aggregation in xerogel 2 was also confirmed by the fact that when recording a spectrum in one of the QDs filled regions, the emission intensity is similar to the one recorded in xerogel 1.

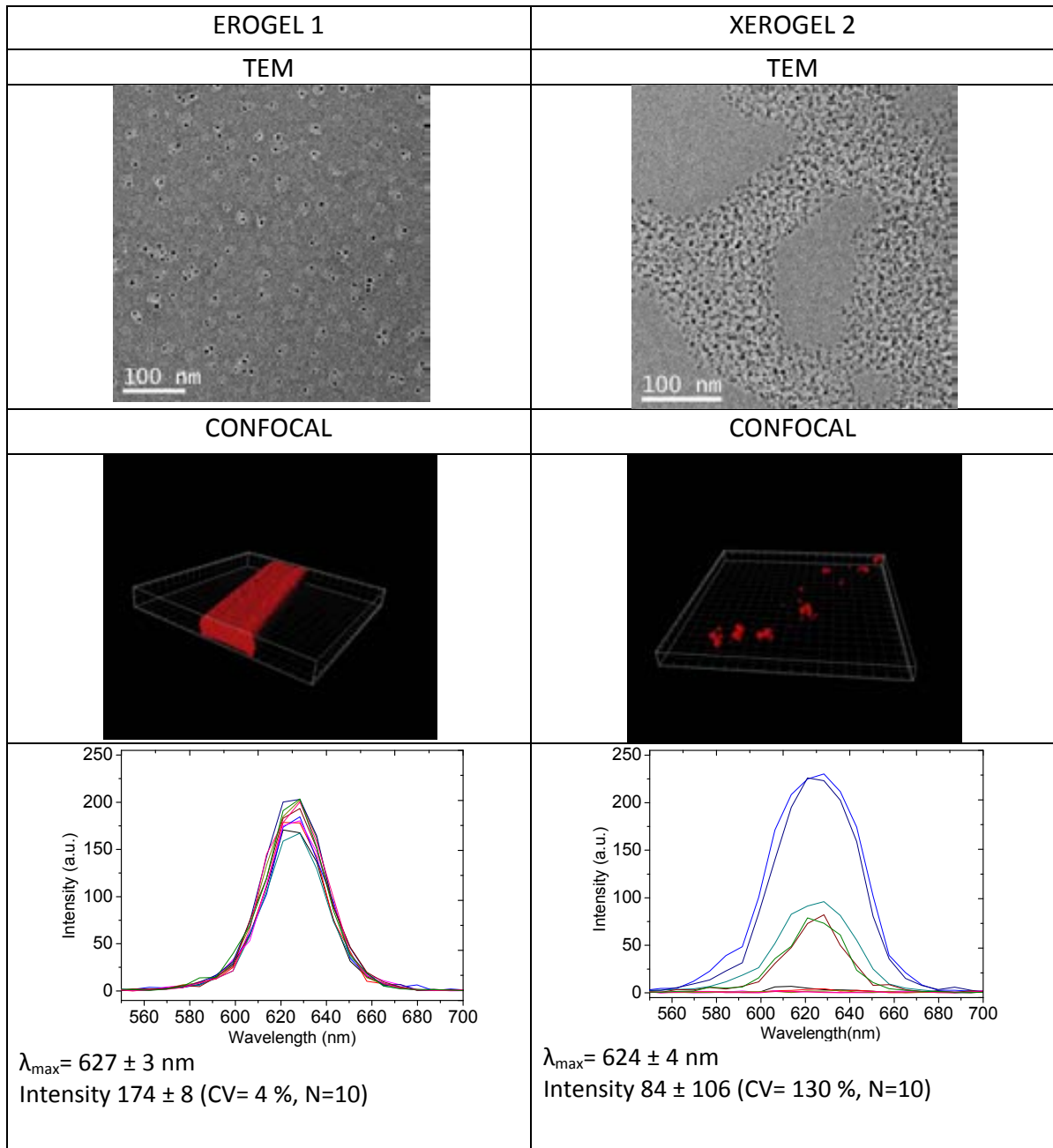


Figure 1. Results from the material characterization for the both QDs-doped xerogels: TEM images, confocal 3D models, and confocal lambda study.

In order to demonstrate the potential of those QDs doped xerogel materials for the development of photonic components, the optical characterization of the waveguides fabricated with the xerogel was carried out. The setup was similar to the ones employed in Chapters III and V.

Figure 2 shows the spectra recorded with a 100 μm -wide, QDs doped xerogels 1 and 2 waveguides in three different concentrations. A strong emission at 600-650 nm is observed in both cases. This wavelength matches with the maximum emission of the CdSe/ZnS core/shell QDs ($\lambda_{\text{emission}}=623$ nm). In Figure 2 the signal at lower wavelengths corresponds to the recorded output light from the excitation blue laser. With both xerogel formulations, the studies carried out with the waveguides fabricated with different QD concentrations showed that the emission intensity was proportional to the QDs content in the xerogel materials. However, those ones performed with the xerogel 2, where the QDs were not evenly dispersed were non-reproducible, these being directly related to the lack of control over the real QD amount that was trapped in the waveguide polymer backbone.

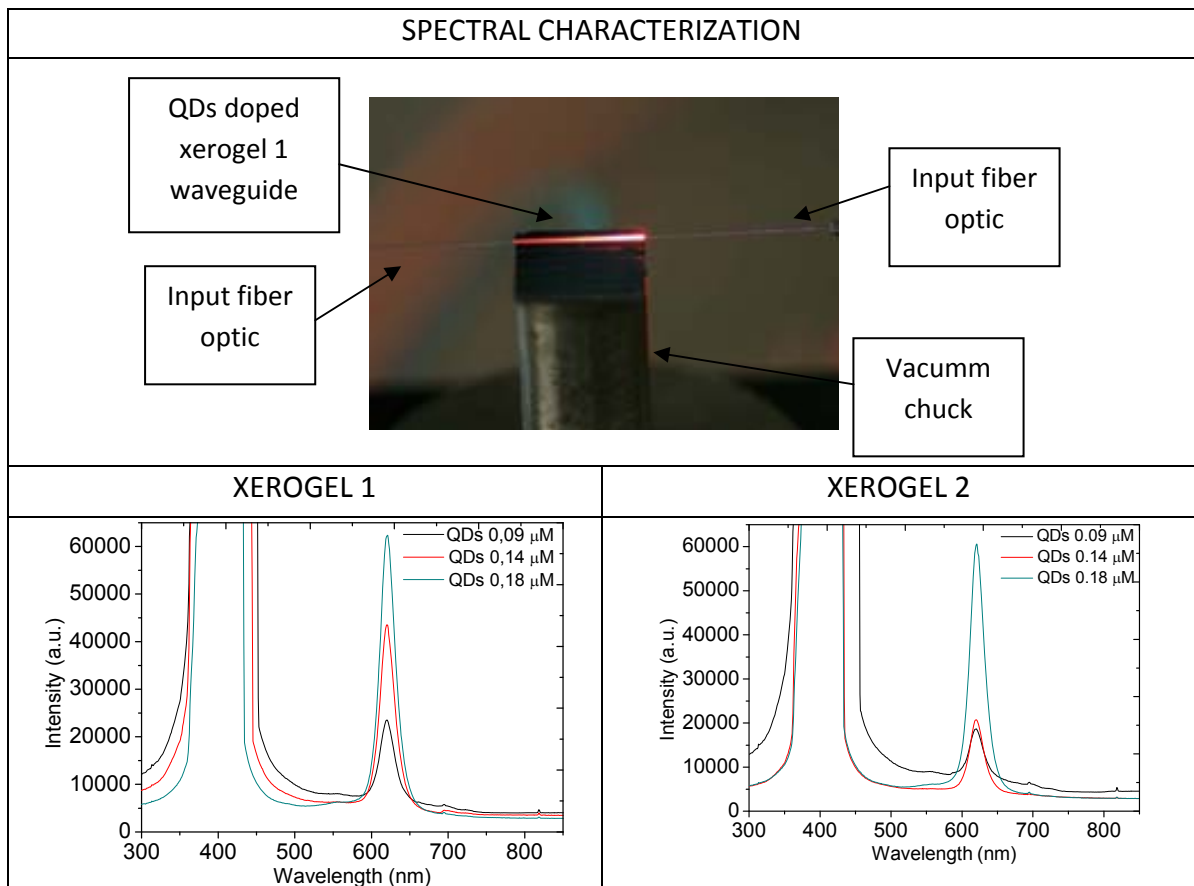


Figure 2. Results from the spectral characterization of the QDs doped xerogels waveguides.

7.1.4 CONCLUSIONS

A simple approach for the inclusion of QDs into a hybrid organic-inorganic material is shown in this section. Two different compositions were tested and transparent materials conserving the luminescent properties of the QDs were obtained. Even dispersion of nanocrystals was achieved for one of the studied compositions.

Waveguides of the xerogel materials containing different QDs concentrations were easily fabricated and optically characterized with good results. From the work shown in this section it can be anticipated that these materials are a suitable approach for the fabrication of disposable photonic devices. Work is in progress in order to develop QDs based solid state light emitters for low-cost photonic lab on chip systems.

References

1. Gong, C., K.-L. Wong, and M.H.W. Lam, *Photoresponsive molecularly imprinted hydrogels for the photoregulated release and uptake of pharmaceuticals in the aqueous media*. Chemistry of Materials, 2008. **20**(4): p. 1353-1358.
2. Zhou, W., et al., *Controllable fabrication of high-quality 6-fold symmetry-branched CdS nanostructures with ZnS nanowires as templates*. Journal of Physical Chemistry C, 2008. **112**(25): p. 9253-9260.
3. Mamedov, A.A., et al., *Nanorainbows: Graded semiconductor films from quantum dots*. Journal of the American Chemical Society, 2001. **123**(31): p. 7738-7739.
4. Ruan, G., et al., *Imaging and tracking of tat peptide-conjugated quantum dots in living cells: new insights into nanoparticle uptake, intracellular transport, and vesicle shedding*. Journal of the American Chemical Society, 2007. **129**(47): p. 14759-14766.
5. Tomczak, N., et al., *Designer polymer-quantum dot architectures*. Progress in Polymer Science, 2009. **34**(5): p. 393-430.
6. Gao, M.Y., et al., *SYNTHESIS OF PBS NANOPARTICLES IN POLYMER MATRICES*. Journal of the Chemical Society-Chemical Communications, 1994(24): p. 2779-2780.
7. Fogg, D.E., et al., *Fabrication of quantum dot/polymer composites: Phosphine-functionalized block copolymers as passivating hosts for cadmium selenide nanoclusters*. Macromolecules, 1997. **30**(3): p. 417-426.
8. Lee, J., et al., *Full color emission from II-VI semiconductor quantum dot-polymer composites*. Advanced Materials, 2000. **12**(15): p. 1102-+.
9. Zhang, H., et al., *From water-soluble CdTe nanocrystals to fluorescent nanocrystal-polymer transparent composites using polymerizable surfactants*. Advanced Materials, 2003. **15**(10): p. 777-+.
10. Pang, L., et al., *PMMA quantum dots composites fabricated via use of pre-polymerization*. Optics Express, 2005. **13**(1): p. 44-49.
11. Mackay, M.E., et al., *General strategies for nanoparticle dispersion*. Science, 2006. **311**(5768): p. 1740-1743.
12. Gupta, S., et al., *Entropy-driven segregation of nanoparticles to cracks in multilayered composite polymer structures*. Nature Materials, 2006. **5**(3): p. 229-233.

7.2 XEROGEL DIFFRACTION GRATINGS FABRICATED BY NANOIMPRINT LITHOGRAPHY (NIL)

The preliminary work carried out on the development of patterns of a hybrid sol-gel polymer at the sub-micrometer and nanometer scale is described in this section. The final aim was to implement one-step fabrication processes that were simple to carry out and cost-effective in order to be able to develop photonic components of highly added value. In this context, this work was focused on exploring the feasibility of applying thermal nanoimprint lithography to pattern the hybrid sol-gel polymer and fabricating diffraction gratings, which could be integrated on waveguides for the development of ultracompact sensor devices.

7.2.1 . INTRODUCTION

Since the pioneering work of Chou et al.,^[1] nanoimprint lithography (NIL) has emerged as a promising parallel (possibility of simultaneous fabrication of devices at wafer level) and low-cost technique for defining periodic patterns on a surface, which could be applicable to numerous applications ranging from nanophotonics to microfluidics^[2,3].

NIL has been demonstrated to be a high volume and cost-effective patterning technique with sub-10 nm resolution and has great potential for next generation lithography^[4]. The principle of NIL is quite simple. As shown in Figure 1, a mold containing nanoscale or sub-microscale features is pressed into a thin film of a polymeric material (resist) or a spin-coated film of a pre-polymerization solution under controlled conditions of pressure and temperature. These conditions should be chosen so that, in the first case the process induces a deformation of the film and generates a replica of the mold on the thin polymer film. In the second approach, the experimental conditions induce the filling of the features on the mold by the pre-polymerization solution and the polymerization process itself, so that a polymer replica of the mold is also formed.^[5] Various types of resist materials can be applied, from thermoplastics to UV cross-linked polymers. When working with thermoplastics the process is controlled by temperature in order to generate the patterns (thermal NIL).^[6] Working with UV curable polymers requires the application of UV light for the polymer generation process and the use of transparent molds at the required working wavelengths (UV NIL).^[7] Both approaches left a residual layer of the patterned material, which can be removed by a dry or wet etching post-process (last step, Figure 1).

While both techniques have been widely applied for the patterning of different resist polymeric materials, used as masks for further nanofabrication processes, they have also been applied to the direct imprinting of sol-gel polymeric films for the straightforward fabrication of different optical components such as diffraction

gratings, waveguides or photonic crystals^[8-10]. In this context, the results on the fabrication of an ultracompact polymeric sensor approach that comprises a micrometer-scale waveguide onto which sub-micrometer diffraction gratings were defined for the in-coupling and out-coupling of the light into the waveguide, together with a sensing area, are presented. The entire structure is fabricated in a single step using a thermally cured hybrid sol-gel material with a similar composition to the one shown in Chapter II.

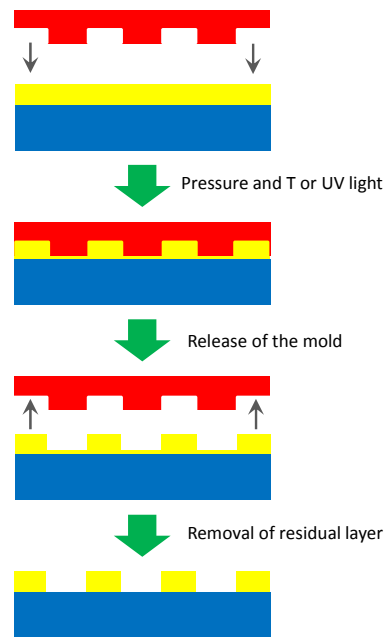


Figure 1. Illustration of the NIL process. In red – mold; yellow – polymer (resist); blue – substrate.

7.2.2. EXPERIMENTAL DETAILS

The xerogel polymer was similar to the one synthesized in Chapter II, with slight variations. Some 615 μL MTMOS, 75 μL PhTMOS and 60 μL TMOS were also mixed. The solvent was a hydroalcoholic solution containing 280 μL DI water and 900 μL Ethanol instead of the water solution applied in the other polymer preparation. The amount of water was set so that the water to silane molar ratio was 3:1, this being the minimum amount of water required to get the complete hydrolysis of all the silane molecules. The *sol* solution was prepared in this way at room temperature in a beaker and left it under thorough magnetic stirring until it lost around 55 % of its weight. At this point, the *sol* solution showed the adequate viscosity required for the NIL process. Under these experimental conditions, the resulting xerogel material showed a refractive index of 1.465

The fabrication of the xerogel structures was carried out at the École Polytechnique Fédérale de Lausanne (EPFL). A Thermal NanoImprinter EHN-3250, thermal imprint

system purchased from Engineering System Co., Ltd. (ESCO Sasaga 5652-83, Matsumoto, Nagano, Japan) was used.

First, the fabrication of the mold was carried out on a silicon substrate following the steps depicted in Figure 2. Alignment marks were firstly defined by standard UV lithography using a positive tone photoresist followed by a fluorine plasma reactive ion etching (RIE) process to transfer the photolithographic patterns into the Si substrate. This was followed by the definition of the gratings by a combined electron beam lithography using a 100 keV beam using hydrogen silsesquioxane (HSQ) resist. Three different grating periods were defined, that is 200, 300 and 500 nm. The HSQ pattern was transferred into the Si substrate using a chlorine RIE process. Then a 11 μm -thick film of SU-8 resist was spin-coated on the substrate and patterned to define the waveguides and the sensing area by direct writing laser technique. The thus fabricated stamps were vapor coated with an anti-adhesion layer of trichloro(1H,1H, 2H, 2H-perfluorooctyl) silane.

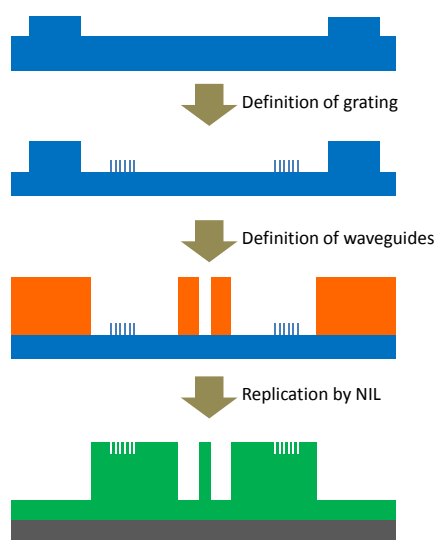


Figure 2. Mold fabrication and replica by NIL. In blue- Silicon substrate; orange – SU8; green – xerogel material showing the fabricated structures and residual layer.

Second, the thermal nanoimprint process was carried out on silicon substrates with a 0.4 μm -thick layer of thermally grown silicon oxide. These substrates were chemically activated by an O_2 plasma process in order to improve the adhesion of the sol-gel material. A layer of the pre-polymerization solution was spin-coated at 750-1000 rpm in order to get a thickness between 12-14 μm .

Third, the coated substrates were introduced in the NIL equipment and the patterning process carried out (last step, Figure 2). The experimental conditions were: Imprinting at room temperature for 10 min, by applying a pressure of 0.5 MPa and a temperature of 40 $^\circ\text{C}$ for 5-10 min. A scheme of the fabricated xerogel structures is depicted in Figure 3.

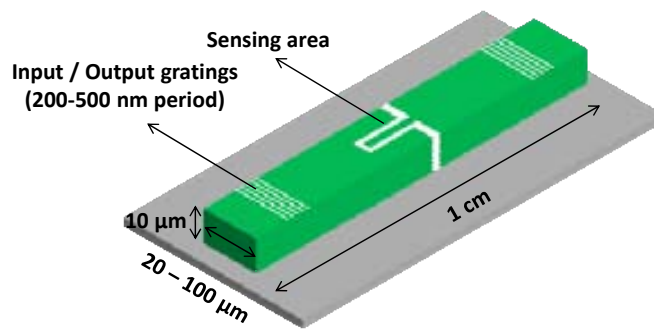


Figure 3. Fabricated structures and corresponding dimensions.

The resulting microstructures show the dimensions depicted in Figure 3, the residual layer being less than 1 μm thick. This has not been removed, since it could be anticipated that its optical behavior would be not relevant on the overall performance of the sensor device.

7.2.3 CHARACTERIZATION

A structural characterization of the xerogel structures was firstly carried out by optical, scanning electron and atomic force microscopies.

Optical images in Figure 4 show well-defined structures of the xerogel material. Up to now, the fabrication yield has been low and the imprinting process often failed. This occurs due to a lack of control on the viscosity of the *sol* solution, the time and T of the NIL process itself or the sticking between the mold and the xerogel material. Work is in progress in order to increase the fabrication yield and get a better control over the entire imprint process.



Figure 4. Optical images of waveguides of different widths. The light dark area at one side of each waveguide is the defined grating. Also, the sensing area of the 75 μm -wide waveguide is shown.

SEM images of these structures are shown in Figure 5.

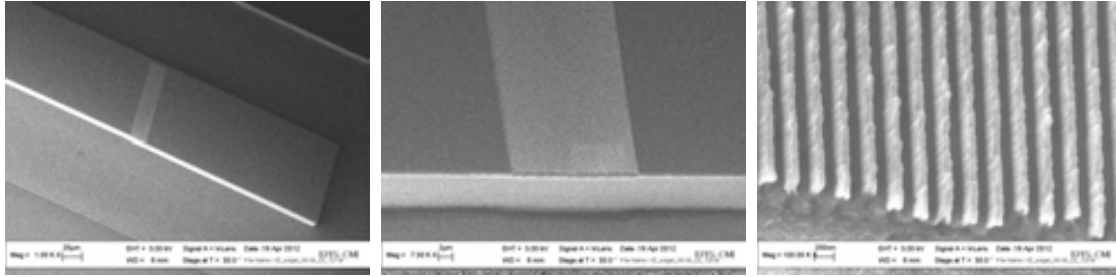


Figure 5. SEM images of a 50 μm wide waveguide, incorporating a 300 nm period 100 nm- thick grating. The area of the grating is 25 μm long having the width of the waveguide.

SEM images show the good definition of the structures and the lack of inhomogeneities on the xerogel surface. It also demonstrate that with the chosen xerogel material and using this simple NIL approach, structures in the submicrometer and nanometer scale can be fabricated.

Figure 6 includes AFM images of the actual gratings, which also show the good definition of the gratings and their period. The estimated roughness is around 0.6 nm.

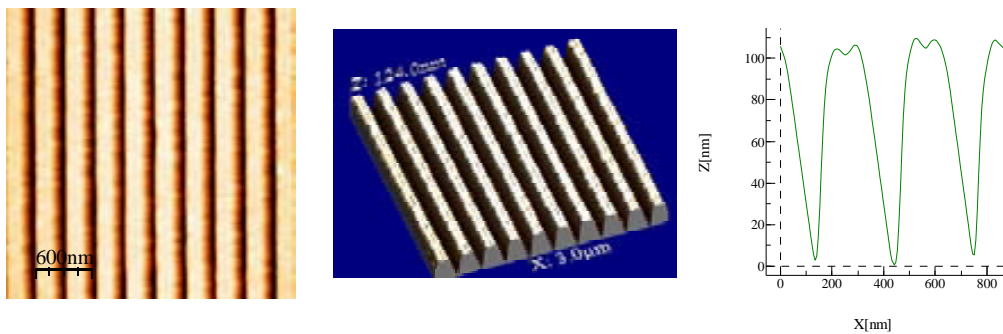


Figure 6. Topographic AFM image, 3D reconstruction and profile of the gratings defined on a 75 μm wide waveguide.

The optical performance of the gratings was assessed. These are preliminary measurements and were carried out just to demonstrate the in coupling of light into the waveguide using the grating. Figure 7 shows a picture of the set-up used to carry out the measurements, which includes a laser source, to which a fiber optics was connected. A lens was also included to correct the numerical aperture of the fiber optics and also focus the light on the grating structure. In the picture on the right hand side the coupling of the light and guiding of it into the waveguide can be distinguished.

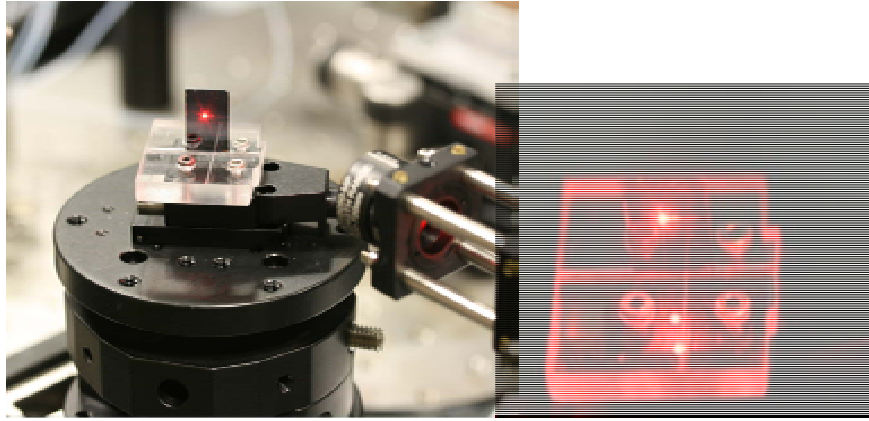


Figure 7. Pictures of the set-up used for the grating characterization and light coupling through the grating.

The experimental excitation angles of the grating showing a period of 300 nm (Λ) defined on a 100 μm -wide waveguide was measured in the transverse electric (TE) polarization mode, for three wavelengths: 405, 633 and 658 nm. The values were compared with the theoretical ones, which were calculated using the following equation.

The resonant coupling between the guided mode and a diffraction order of the grating is governed by the phase matching condition

$$\sin \theta = n_{\text{eff}} + m \frac{\lambda}{\Lambda}$$

with θ as the incident angle of light, n_{eff} as the effective refractive index of the guided mode, m as the diffraction order (here $m = -1$), λ as the wavelength in air and Λ as the grating period. The effective index depends on the wavelength, the material and the dimensions of the waveguide. It was considered that for the TE mode the $n_{\text{eff}} \approx 1.465$.

Results are shown in Table 1, and show the good correlation between the theoretical and the experimental values. The excitation angles are negative due to the very small period of the grating, which should be corrected in the next fabrication process.

λ (nm)	θ_{theory}	θ_{exp}
405	6.6°	7°
633	-40°	-40.5 °
658	-47°	-47°

The coupling efficiency of the grating was also estimated and the maximum value was $\eta = 0.2\%$ for a grating of $\Lambda = 300$ nm, at 658 nm and in TE polarization. This value is very low and it is representative of the different issues that have to be worked out before achieving high quality structures and that were highlighted above.

Work is in progress in order to get suitable structures, thoroughly assessed the efficiency of the gratings not only for in coupling the light but also for out coupling it at the end of the waveguide. Additionally, the performance of the sensor area is yet to be evaluated.

7.2.4 CONCLUSIONS

The feasible fabrication of patterns of a hybrid xerogel polymer in the nanometer and submicrometer scale has been shown by developing an ultracompact sensor structure that includes gratings for light coupling and a waveguide, which in turn integrates a sensing area, as the transducer element of the sensor approach. The fabrication yield is quite low and the performance of the gratings is quite limited. Several issues related to the NIL process and the design of the gratings on the waveguide is going to be tackled in order to improve the efficiency of the fabrication process and the performance of the polymer structures.

Reference

sS. Y. Chou, P. R. Krauss, P. J. Renstrom, *Science* 1996, 272, 85.

1. W. Wu, Z. Yu, S. Y. Wang, R. S. Williams, Y. M. Liu, C. Sun, X. Zhang, E. Kim, Y. R. Shen, N. X. Fang, *Appl. Phys. Lett.* 2007, 90, 063107.
2. C. Peroz, J. C. Galas, J. Shi, L. Le Gratiet, Y. Chen, *Appl. Phys. Lett.* 2006, 89, 243109.
3. Y. Xia, J. A. Rogers, K. E. Paul and G. M. Whitesides, *Chem. Rev.* 1999, 99, 1823–1848.
4. L.J. Guo, *J. Phys. D: Appl. Phys.* 37 (2004) R123–R141.
5. M.-G. Kang, L. J. Guo, *Adv. Mater.* 2007, 19, 1391–1396.
6. L. H. Thamdrup, A. Klukowska, A. Kristensen, *Nanotechnology* 19 (2008) 125301.
7. W.-S. Kim, K. B. Yoon, B.-S. Bae, *J. Mater. Chem.*, 2005, 15, 4535–4539.
8. C. Peroz, V. Chauveau, E. Barthel, E.lin Søndergård, *Adv. Mater.* 2009, 21, 555–558.
9. D. J. Kang, J.-K. Kim, B.-S. Bae, *Opt. Express*, 2004, 12, 3947-3953.

CONCLUDING REMARKS

The development of low-cost miniaturized analytical devices is demanding for obtaining disposable devices. Having this aim in mind, we combined simple microfabrication technologies with easy to obtain polymeric materials for developing low-cost photonic components and achieve their integration on polymer/glass photonic lab on chip platforms.

The main results of this work are the following:

1. A simple approach for the low-cost fabrication of polymeric photonic components based on fluorophore-doped hybrid organic-inorganic polymers has successfully been developed. A thorough characterization of the material has been carried out demonstrating its good structural and optical properties. Different microstructures have been fabricated by micromolding in capillaries soft lithography technique with high repeatability, reproducibility and reliability in the replication of the master dimensions. Waveguides with different widths and lengths have been fabricated and optically characterized.
2. It has been demonstrated that low-cost absorption micro-filters can be easily fabricated using a dye-doped xerogel hybrid polymer material with soft-lithographic approach. The successful integration of these polymeric absorbance micro-filters in a fluorescence based disposable PhLoC has also been demonstrated by carrying out calibration studies using Rhodamine B as model fluorophore target analyte and showing the performance enhancement of the system as compared to an identical PhLoC without xerogel filters .
3. The design, development and successful performance of a fluorophore-doped xerogel polymeric solid state light emitter (SSLE) including auxiliary micro-optical elements, such as air mirrors, have been demonstrated. They have shown interesting properties, such as good light directionality and adequate down conversion (excitation to emission) efficiency. The successful integration of a SSLE with a bio-functionalized MIR optofluidic component, has allowed obtaining a true PhLoC. It has been applied to the selective detection of a model target analyte . Despite its high level of integration, the resulting photonic approach has been fabricated using a single mask technology and at low cost. Yet, the obtained PhLoC presents an outstanding analytical performance.
4. The synthesis of additional hybrid organic-inorganic xerogel materials doped with QDs inorganic nanoparticles has been explored. Two different compositions have been tested and transparent materials conserving the luminescent properties of the QDs have been obtained. The application of these materials in photonics has required the even dispersion of the nanocrystals, these being achieved with just one of the studied compositions.

5. The feasible fabrication of patterns of a hybrid xerogel polymer in the nanometer and submicrometer scale has been explored by applying NIL technique. An ultracompact xerogel sensor structure that includes diffraction gratings for light coupling and a waveguide, which in turn integrates a sensing area, has been designed and fabricated. The fabrication yield currently is quite low and the performance of the gratings is quite limited. Several issues related to the NIL process and the designs of the gratings on the waveguide are going to be tackled in order to improve the efficiency of the fabrication process and the performance of the polymer structures.

